2014

CNT MEMBRANE PLATFORMS FOR TRANSDERMAL DRUG DELIVERY AND APTAMER MODULATED TRANSPORT

Tao Chen
University of Kentucky, tao.chen@uky.edu

STUDENT AGREEMENT:

I represent that my thesis or dissertation and abstract are my original work. Proper attribution has been given to all outside sources. I understand that I am solely responsible for obtaining any needed copyright permissions. I have obtained needed written permission statement(s) from the owner(s) of each third-party copyrighted matter to be included in my work, allowing electronic distribution (if such use is not permitted by the fair use doctrine) which will be submitted to UKnowledge as Additional File.

I hereby grant to The University of Kentucky and its agents the irrevocable, non-exclusive, and royalty-free license to archive and make accessible my work in whole or in part in all forms of media, now or hereafter known. I agree that the document mentioned above may be made available immediately for worldwide access unless an embargo applies.

I retain all other ownership rights to the copyright of my work. I also retain the right to use in future works (such as articles or books) all or part of my work. I understand that I am free to register the copyright to my work.

REVIEW, APPROVAL AND ACCEPTANCE

The document mentioned above has been reviewed and accepted by the student's advisor, on behalf of the advisory committee, and by the Director of Graduate Studies (DGS), on behalf of the program; we verify that this is the final, approved version of the student's thesis including all changes required by the advisory committee. The undersigned agree to abide by the statements above.

Tao Chen, Student

Dr. Bruce J. Hinds, Major Professor

Dr. Fuqian Yang, Director of Graduate Studies

CNT MEMBRANE PLATFORMS FOR TRANSDERMAL DRUG DELIVERY AND APTAMER MODULATED TRANSPORT

THESIS

A dissertation submitted in partial fulfillment of the requirements for the degree of Master of Science in Materials Science and Engineering in the College of Engineering at the University of Kentucky

By

Tao Chen

Lexington, Kentucky

Director: Dr. Bruce J. Hinds, Professor of Materials Engineering

Lexington, Kentucky

2014

ABSTRACT OF THESIS

CNT MEMBRANE PLATFORMS FOR TRANSDERMAL DRUG DELIVERY AND APTAMER MODULATED TRANSPORT

CNT membrane platforms are biomimetic polymeric membranes imbedded with carbon nanotubes which show fast fluid flow, electric conductivity, and the ability to be grafted with chemistry. A novel micro-dialysis probe nicotine concentration sampling technique was proposed and proved *in vitro*, which could greatly improve the efficiency and accuracy of future animal transdermal studies. To enhance the scope of transdermal drug delivery which was limited to passive diffusion of small, potent lipophilic drugs, a wire mesh lateral electroporation design was also proposed which could periodically disrupt the skin barrier and enhance drug flux.

It was shown that AMP binding aptamer at the tip of carbon nanotubes may act as gatekeepers and regulate ionic transport through CNT membrane. Multiple cycle gating of ionic transport upon AMP binding/unbinding which changes the aptamer conformation was displayed. This CNT membrane-aptamer system closely mimics how protein ion channels modulate ion flow by responding to stimuli, which may have significant impact on active membrane transport.

Finally an enhanced electroosmosis concept by “ratchet” functionalization at both ends of carbon nanotubes in was discussed. Direct observation of water transport by electroosmosis was made possible through enhanced flow in vertically aligned high flux CNT membranes.

KEYWORDS: CNT membrane, transdermal drug delivery, electroporation, aptamer, electroosmosis

Signature Tao Chen

Date_____

CNT MEMBRANE PLATFORMS FOR TRANSDERMAL DRUG DELIVERY AND APTAMER MODULATED TRANSPORT

By

Tao Chen

Dr Bruce Hinds
Director of Thesis

Dr. Fuqian Yang
Director of Graduate studies

14th July 2014

ACKNOWLEDGEMENTS

I would like to thank my advisor Dr. Bruce Hinds for introducing me to CNT membranes, continuous guidance during my graduate research and thesis preparation. I am thankful for NIH for providing financial support. I would like to thank Dr. Thomas Dziubla, Dr. Brad Berron for being on my master's committee, and Dr. Fuqian Yang as the director in my graduate studies.

I would like to thank Brian Wajdyk, Dr. Jia Ye, Dr. Dali Qian for help in electron microscopy and training in Center for Nanoscience and Engineering (CeNSE). I would like to thank Larry Rice and Jerry Rougeux for help in lab maintenance and supplies. I would also like to thank past and present group members, Dr. Ji Wu, Dr. Xin Su, Dr. Xin Zhan, Jingyuan Yao, Zhiqiang Chen, Nick Linck, Gaurav Gulati, Rupam Sarma for collaboration on research and helpful discussions.

Thanks to my great friends Di Liang, Yun Bai, Yucong Sang, Yitian Zhang, Yan Jin, Jie Pan in Lexington who has made my life exciting. Finally thanks to my parents and relatives who are always behind me.

Table of Contents

List of Tables

List of Figures

Chapter 1 Introduction

The world has seen remarkable advances in nanotechnology in both academia and industry in the last decade. Between 2001 and 2008, it is reported that the number of inventions, discovery, ideas, funding, and job market related to nanotechnology have increased by 25% annually.[1] The worldwide market for products incorporating nanotechnology reached about $254 billion in 2009 and is expected to reach $3 trillion in 2020. Carbon nanotubes are amongst one of the fascinating nanotechnology discoveries that continues to attract interest today, being first reported in 1991 when Ijima discovered multi-walled carbon nanotubes by using an arc discharge method.[2] Carbon nanotubes (CNTs) are rolled-up tubes made of graphite (Figure 1.1)**;** depending on which direction along the lattice vector graphite is rolled either armchair (n=m), zigzag (n, 0), or chiral (n, m) type carbon nanotubes are formed. They are allotropes of carbon with a nanostructure that can possess an aspect ratio greater than 1 million.[3] According to the number of layers of graphite, CNTs can be classified into single-walled (SWCNT), double-walled (DWCNT), or multiwalled carbon nanotubes (MWCNT), with diameters ranging from 0.8nm-30nm, and differing properties based on their structure.

1.1 General properties of Carbon nanotubes

Carbon nanotubes have been prepared using various methods including electrolysis, arc discharge, laser ablation, sono-chemical/hydrothermal, and chemical vapor deposition

(Figure 1.2). Higher temperature synthesis techniques such as arch discharge or laser ablation were first used to produce CNTs, but chemical vapor deposition became the prevalent technique since the alignment, length of nanotube, diameter, and purity of a nanotube can be controlled by the latter.[4] CNTs exhibits fascinating electronic, thermal, and mechanic properties: depending on the way it is rolled up, CNT can be either metallic or semiconducting; they can carry current density of up to $4*10^9$ A/cm^2, which is more than 1000 times greater than that of metals such as copper.[5] The theoretical thermal conductivity of a carbon nanotube can be up to 6600 W/ (m*K), which is 5 times higher than that of diamonds. Carbon nanotubes are also the strongest materials to be found in terms of tensile strength and Young's moduli, as they can go up to 63 GPA and 1 TPA respectively,[6] the strength resulting from the sp^2 bonding between carbon atoms. The high aspect ratio (up to 1.36×10^8) and surface area (up to 1315m^2/g) of a carbon nanotube provided abundant active surface area for functionalization, which makes it an ideal platform for catalysis and energy storage.[7]

1.2 Functionalization of Carbon Nanotubes

Carbon nanotubes are nanomaterial with fascinating properties; however pristine carbon nanotubes are insoluble in aqueous and organic solvents due to their easy aggregation into bundles under large van der Waals force, severely hindering its usage. Uniform and stable dispersion by functionalization is critical to CNTs' performance in various applications.[8] Functionalization also generate active sites on carbon nanotube

surface which becomes available for further grafting with desired chemical moieties, opening up a broad spectrum of grafting possibilities. Depending on the interaction mechanism with the functional group, CNT functionalization can be classified as either covalent (sidewall derivatization and tip openings) or non-covalent (π- π interactions).

1.2.1 Covalent functionalization

Covalent functionalization of carbon nanotubes mainly includes the use of oxidation, reduction, acid cutting, and CNT-metal complex to modify carbon nanotube sidewall and tip structure (Fig 1.3). A widely used approach of CNT covalent functionalization is the treatment by strong oxidizing agents, although it is aggressive in nature and usually leave defects on CNT surface.[9] J. Liu and R.E. Smalley et al. used concentrated sulfuric and nitric acids (3:1) to treat CNTs with sonication, which produced local high temperature domains that attacked the surface of CNTs. [10] The prolonged sonication of CNTs in strong oxidative environment opens up their previously closed ends and introduced oxygen moieties such as carboxyl group at the ends, which could be used to attach further functional groups. Lieber et al. covalently linked primary amine to the carboxylate groups on the end of CNTs using carbodiimide chemistry, which is practical and popular in the linkage of two protein molecules, between a peptide and a protein, and between oligonucleotides and proteins.[11] Furthermore, the carbodiimide chemistry which forms an amide bond could be carried out in aqueous solutions and room

temperature, which allowed the attachment of chemistry to CNTs and the attachment of CNTs to a substrate surface under mild conditions. The ability to functionalize CNTs with carboxylate groups and primary amine groups allowed its manipulation and processing with various biomolecules.

Diazonium salt reactions could be used to introduce desired moieties onto carbon nanotube surface by the in situ reduction of a diazonium compound which form an aryl radical that can further interact with carbon atoms on carbon substrate (Figure 1.4). Compared to other surface modifications, diazonium chemistry offers several advantages:[12] 1) it offers an array of functionalities (-NO2,-COOH,-SO3H, etc.) since aryl diazonium with different functionalities could easily be synthesized in the lab by demand; 2) the modification method shows stronger stability compared to thiol modification due to the covalent bonding;[13] 3) it is a mild functionalization method that avoids detrimental damage to the CNT being functionalized. Our group prefers the use of diazonium salt reduction over other functionalization methods to treat CNTs because the above stated advantages.

1.2.2 Non-covalent functionalization

CNTs could be non-covalently functionalized with aromatic molecules and surfactants to break CNT bundles formed by strong adhesive forces, enabling an uniform dispersion of

CNTs. Non-covalent functionalization methods of CNTs includes π-π stacking, Van der Waals force, hydrogen bonding, and electrostatic forces.[8,14] Figure 1.5 shows the absorbance of three types of surfactants (NaDDBS, SDS, and Triton X-100) onto nanotube surface, which all serves to separate CNTs from each other in solution. Chen et al. first reported the irreversible attachment of pyrenyl to SWCNT sidewall via π-π stacking,[15] which functionalized SWCNTs with succinimide ester groups that are highly reactive with primary and secondary amines, which existed in abundance in various biomolecules. Non-covalent functionalization also uniformly disperse CNTs in aqueous solutions and organic solvents by spatial separation and charge repulsion from the amphiphilic nature of surfactants. Islam Et al. compared the dispersion of CNTs in SDS (sodium dodecyl sulfate), Triton-X, NaDDBS (sodium dodecylbenzene sulfonate) and showed that uniform dispersion of CNTs with concentration up to 20mg/ml could be achieved with surfactants. The uniform dispersion of CNTs allowed its application in deposition, microfluidics, fabrication of nano-based fibers, and composites where previously bundled CNTs showed inferior properties.

Both non-covalent and covalent functionalization of CNTs are equally important for fabrication of a CNT based membrane and its activation into a fully functional one. For example, the non-covalent dispersion of CNTs are important for uniform dispersion in polymer, and covalent functionalization allows the grafting of dyes/ aptamers onto the

CNT membrane for gatekeeping. The details of CNT functionalization will be discussed in detail in chapter 2.

1.3 General Applications of Carbon Nanotubes

The functionalization of CNTs has opened opportunities for numerous potential applications. Due to their capability of being semiconducting (SWCNT) and conducting (MWCNT), CNTs was utilized for either FET-based sensors or electrodes for electrocatalysis.[16] Their high aspect ratio allows them to be fabricated into ropes analogous to spinning yarns with 2% the diameter of a human hair, which possess strength, toughness, mechanical energy damping capability, and resistance to knot-induced failure.[17] The properties of CNTs also gives an advantage in electrocatalysis where expensive catalysts are required to be utilized with highest possible surface to mass ratio. It should be noted that the purity of CNTs is of critical importance in its performance as catalyst support, while usually commercially made CNTs usually contain metal catalyst particles, ash, and other residues. The residue catalyst particles contained in the commercially received CNTs can contribute toward the total observed catalytic behavior, causing confusion in the overall observed result.[18] Described here in short are some previously developed applications of CNTs in catalysis, sensors, biomedics, and membranes which is most relevant to the topic of this thesis.

1.3.1 CNT as catalyst support

CNTs are considered an ideal platform for catalysts due to their high surface to mass ratio, electric conductivity, and facile functionalization ability to provide catalytic sites.[16] They have been involved in development for better fuel cells, organic reaction catalysis, and platform for biomacromolecule immobilization. In the interest of developing clean, sustainable, and mobile power sources, much attention is given to proton exchange membrane fuel cells (PEMFCs) and direct methanol fuel cells (DMFCs).[16,19] A practical problem associated with the realization of cheap fuel cells is the high cost of Pt catalysts. By depositing Pt catalyst on the surface of CNTs, reduced amounts of Pt is needed to reach the same catalytic activity. Some attempts have been made to anchor Pt catalysts on MWCNT to improve catalytic activity, which relies on strong oxidation to treat CNT surface to allow Pt deposition. Shown in Figure 1.6 is the schematic for Pt deposition on SWCNT and TEM image showing Pt on SWCNT in detail.[20,21] Later X. Su, B.J. Hinds deposited ultrathin film of Pt on CNT functionalized by diazonium chemistry, where the electrochemically induced diazonium salt reduction allows uniform thin layer Pt deposition.[22] Metal-modified SWCNTs and MWCNTs has also shown to exhibit organic reaction catalyzing abilities. The aldehyde group in prenal (3-methyl-2-butenal) has been hydrogenated using a Pt/SWCNT system yielding the unsaturated alchohol prenol (3-methyl-2-butenol). CNT supported group 9 and 10 metal catalysts has also been investigated for the hydrogenation of aromatic molecules with partial success,[23]

and the enhancement brought by CNT support maybe due to the low steric hindrance of catalysts mounted on sidewalls of CNTs, the authors conclude.

1.3.2 CNTs in sensors

CNTs are also viewed as ideal platforms for sensors due to their electric conductivity and large area available for functionalization. Due to their conductivity, electrical-based sensors are ideal due to easy electrochemical measurements, integration in electric circuits, and low costs. Pristine SWCNT can be used as wires to connect two electrodes, and the conductance between the electrodes can be easily measured as a function of the gate bias voltage. By the induction of gases with concentration as low as 200 ppm into contact with SWCNTs, conductance change of up to 2 orders of magnitude maybe observed.[24] This change of conductance is due to the binding of gas molecules on to SWCNT surface through its defects and dramatically changing its electronic energy states, thus changing its conductivity. Comparing to conventional solid state sensors, SWCNT sensors hold the advantage that they are fast in response (2min) and could be operational at room temperature.

CNT may also be made into electromechanical sensors.[25] In a study from T.W. tumbler, an individual SWCNT was suspended over cliffs, where AFM force on the side of the SWCNT caused it to bend into a v-shape and elongates reducing its diameter. Results

show that under AFM tip force conductance drops and when the AFM force is released the measured conductivity reversibly increase. This is due to the band-gap increase corresponding to metal-semiconductor change and deformation increases. Furthermore, either macromolecules or small molecules maybe functionalized onto CNTs allowing sensor in various environments.

Electrochemical sensors based on CNT and aptamers will be discussed in more details in Chapter 3.

1.3.3 CNTs for drug delivery

CNTs are considered promising nano-carriers which were utilized in diagnostics or drug delivery.[26] Via CNT functionalization, they become soluble in aqueous solutions and turn biocompatible for drug delivery *in vitro* and *in vivo* thanks to its uniform distribution.[27] Functionalized CNTs has been used for the delivery of drug molecules and larger biomolecules, such as proteins, DNA, and small iRNA *in vitro* and *in vivo*. Shown in Figure 1.7 is the delivery of siRNA into cells by a covalent linkage onto CNTs which could later be reversibly cleaved and the siRNA released. Although previously viral-based siRNA delivery has shown great promise, the safety concern of viral vectors is significant which hampered its realization. In this regard CNTs emerged as a replacing carrier and successfully delivered siRNA into cells upon cleavage of a cleavable bond between

SWCNTs and siRNA, most importantly, arguably safer than viral vectors.[28] One of the first works in the area was the use of carbon nanotubes as drug delivery vehicles for PTX in cancer treatment.[29] PTX, paclitaxel is a widely used cancer chemotherapy drug. H. Dai et al. showed *in vivo* that PTX conjugated to a PEG (polyethylene glycol) chained SWCNT offered over 10-fold higher PTX tumor uptake than clinical Taxol in a 4T1 breast cancer model. In comparison, SWCNT-PTX showed a high tumor suppression efficacy of 59.4% compared to 27.7% from Taxol on Day 22. The much higher uptake of PTX by tumor and the increased drug efficacy owes to the prolonged blood circulation time and EPR effects brought by the SWCNT-PTX.

CNT have shown their potential in biomedical applications. However, biocompatibility and toxicity of CNT is still in debate.[28] It is therefore reasonable and much needed for a platform that harnesses the advantages of CNT for biomedical applications while avoiding their potential dangers in humans. CNT based membranes which controllably delivers drugs outside the body maybe such a solution.

1.4 CNT Membrane: a versatile fast flow platform

Cell membranes are amazing natural structures that demonstrate selective permeability and are critical to maintaining normal biological functions. The embedded proteins in the membranes acts as the gatekeepers that control flux in and out of membranes and

determines which substances are granted access. X-ray structures indicates that the conformation of ion channels can be controlled under voltage bias, which can open and close the controlled ion channels, and determine which ions are transported.[30] Recent research has been trying to mimic the fascinating working principles of these membranes and their gatekeeping abilities.

CNTs are structurally similar to proteins in biological membranes due to their tubular shape and hydrophobic graphitic inside wall. Hummer's molecular simulations envisions the formation of ordered water molecule column through the inside core of a CNT,[31] where the pulse transport of water through the near friction-less core allowed enhanced water flow. Crooks et al. reported the flow of polystyrene through a membrane containing only a single 150 nm diameter carbon nanotube,[32] which confirms that transport through CNT inner core is valid experimentally, while previous reports show nano-pore transport with results averaged from an array of nano-pores. Later B.J. Hinds et al. reported a CNT membrane with well aligned multi-walled carbon nanotube formation shown in Figure 1.8.[33] Aligned MWCNT were first grown vertically on quartz substrate by chemical vapor deposition method (CVD), then the MWCNT were embedded in polystyrene to make the membrane. Follow-up water plasma treatment not only cleared residue polymer at tips of membranes, excess Fe catalysts, they also oxidized carbon on the CNT and generated carboxylate groups, which could be used to covalently functionalize the tip of CNT for gate keeping chemistry. B.J. Hinds et al.

demonstrated that bulky molecules functionalized at the entrance of CNT can sterically hinder ion flux, similar to when a protein channel in the "closed" gating state. Majumder et al. further studied the gate keeping effects with respect to ion transport,[34] where the anionic dye molecules were attached to the carboxylate groups at the tip of CNT tip as gate keeper. It was seen that due to charge attraction cationic molecule transport through the CNT membrane is greatly enhanced, which outlined the importance and viability of various gate keepers at CNT membrane to make it a biomimetic membrane. B.J. Hinds group also found that fluid flow through CNT membrane is 4-5 orders of magnitude faster than conventional fluid flow in 2005,[35] resulting from the atomically flat core of the MWCNT and molecules being transported slipping through nearly frictionless. The similar results of fast transport in CNT membrane was also observed by the Holt group in 2006.[36] Both the results from Hinds group and Holt group confirmed the Hummer group's molecular dynamics simulations,[31] which seted the possibility of the CNT membrane as a fast fluid and gas transport/separation platform.

There are merits to the CNT membrane that makes it ideal for transport/separations applications. First, they offer an amazing 4-5 magnitude higher fluid/gas flow that is comparable to biological membranes. Secondly, the CNT membranes are fabricated by embedding CNT in polymer, so they offer robustness which biological membranes lacks. Thirdly, the unique shape and chemistry of CNT allows functionalization at the tips allowing gatekeeping actions mimicking biological membranes. At last carbon nanotubes

are conductive allowing for electrochemical functionalization, control of gatekeeping by electric bias and energy efficient electroosmotic pumping. Modest regulation of ion transportation through the CNT membrane is seen with steric hindrance and electrostatic effects with functionalization at the tip. More pronounced regulation of ion transportation was seen with voltage bias controlling the anion tethered molecules shown in Fig 1.9.[37] Although the overall trend of positive and negative bias on MV^{2+} and $Ru(bpy)_3^{2+}$ transport rate is similar, the steric hindrance of the dye allowed the smaller permeate to transport at a higher rate thus resulting in a separation factor of 22 at -130 mV bias.

It should be noted that in the above report negatively charged dye molecules were functionalized to the CNT tip via two step functionalization chemistry. First the carboxylate group density on the tips of CNT is increased by electrochemical diazonium grafting. The second step is amide coupling of charged dye molecules to the carboxyl groups at the tip. Specifically, Electrochemical grafting of 4-carboxylphenyl diazonium is used to increase the carboxyl density. However simulations and experimental results show that by a normal electrochemical diazonium functionalization, carboxyl groups can also be created deeper down the CNT entrance, which disrupts the smoothness of the CNT wall and induce unwanted charge repellence.[38] In order to reduce the unwanted functionalization deep down the CNT which reduces ionic flux, a flow grafting method was improvised. Specifically during flow grafting of diazonium, 10 cm water column on

the opposite side of the membrane is maintained so that a constant pressure flow keeps diazonium molecules reacting only with CNT surface at the tip, reducing diazonium reactions further down the tube.[39]

Wu et al. used CNT membranes for programmable transdermal drug delivery on human skin *in vitro*.[40] CNT membranes were produced using a method modified from Crooks et al. shown in Figure 1.10. Briefly, CNT-epoxy composite were fabricated by mixing CNT, epoxy, hardener, and surfactant. After curing to appropriate hardness, a microtome cutter is used to cut the CNT-epoxy block into 5 um thick membranes. It is notable that by using this method hundreds of membranes can be made in a short time frame, greatly simplifying the previous vertically aligned CNT membrane method. However by using this method CNTs are randomly dispersed and thus flux/CNT density maybe lower than aligned CNT membranes. Wu et al. also studied efficient electro-osmotic flow in CNT membranes as shown in Figure 1.11.[41] Electro-osmotic flow (EOF) usually comprises only a small portion in the net electro-induced flow made up of electrophoresis and electroosmosis, but in this study CNT membranes made with SWCNT/DWCNT with small inner diameter and densely charged surface greatly enhanced electro-osmotic flow. They showed that the flux of neutral caffeine molecules was greatly enhanced by applying bias to induce electroosmosis, which contributed greatly to total observed flow. Compared to conventional modified anodic aluminum oxide membranes, the electro-osmotic velocities were enhanced by nearly 500 fold and the power efficiency

was enhanced by 19 fold. More importantly the electroosmosis effect is efficient under sufficiently low voltages of (0.3-0.6V), which reduced the energy requirements and allowed the potential applications for EOF effect in portable devices.

1.5 Summary of Research

CNT membranes exhibit amazing properties as a biomimetic membrane that can be used for drug delivery, catalysis, gatekeeping, ion flow regulation, etc. It is the focus of this thesis to contribute to the current applications of CNT membranes: improving its current capabilities in drug delivery, gate keeping, and ion flow mechanism.

The first part of this thesis focus on CNT membrane for programmable drug delivery. Wu et al. shows that CNT membranes can be used for programmable delivery of nicotine *in vitro* and *in vivo* (Figure 1.12).[40,42] Consequent *in vivo* study showed that the detection of small amounts of nicotine and its metabolized product is inaccurate. Also the robustness of the membranes is a concern if nicotine delivery patch devices for humans are to be developed in the future. Therefore in this context new generation CNT membranes was developed that have similar fluxes compared to previous studies yet with better mechanical stability by applying a support membrane below the CNT membrane. Under skin micro-dialysis membrane was used to help analyze nicotine flux as soon as it is permeates through the skin from patch delivery site. By the dialysis

membrane it is possible to use market nicotine cessation patches to gauge nicotine flux and therefore determine the effectiveness of our CNT patches. We may also analyze and measure the nicotine flux and resulting concentration right at the delivery site, before it is circulated through the body and diluted in the various body compartments. This would allow a more precise measurement tool to analyze the on/off and delivery potencies of our membrane, paving the way for future improvements.

A setback for CNT membrane usage in transdermal drug delivery is the low passive flux rates of various important pharmaceutical drugs across skin such as clonidine. In order for the CNT membrane to be the rate limiting factor during delivery, the permeability of the drug through the skin has to be larger than the permeability of the drug through the CNT membrane, otherwise the skin will become the limiting factor. Currently there are numerous methods to improve drug permeability through the skin, such as electroporation, microneedles, iontophoresis, etc. Electroporation was chosen because it can be a non-invasive method to improve skin permeability, and the fact that it uses electric pulses combines well with the electric bias controlled on/off of the CNT membrane. Taking the best from the programmability of CNT membranes and the efficiency of electroporation, we hope to increase the range of drugs capable of being delivered and increasing flux to therapeutically required values.

The second part of the thesis sets to utilize CNT membranes for its gate keeping abilities, as CNT membranes have been demonstrated for ion selectivity and gate keeping abilities mainly due to charge repulsion effect and spatial confinement. In order to push the CNT membrane to be truly biomimetic, an ATP hairpin aptamer that could reversibly change conformation was functionalized onto CNT membrane tips to enable gating of ionic flux through membrane. By functionalizing ATP hairpin aptamers to the tip of CNT, the CNT membrane can be either in the "closed" state or "open" state depending on the target binding state of the aptamers. This is big step forward in CNT membrane technology and a basis for further development of functionalization at the tip that may perform more functions such as molecule grabbing, releasing, separation, or selective trafficking. Further studies also showed that CNT membranes with high ionic flux maybe functionalized to efficiently pump water by enhanced electroosmosis. In the future CNT membranes may rise to compete with conventional membranes in the treatment of water both in micro-environments and on the macroscale.

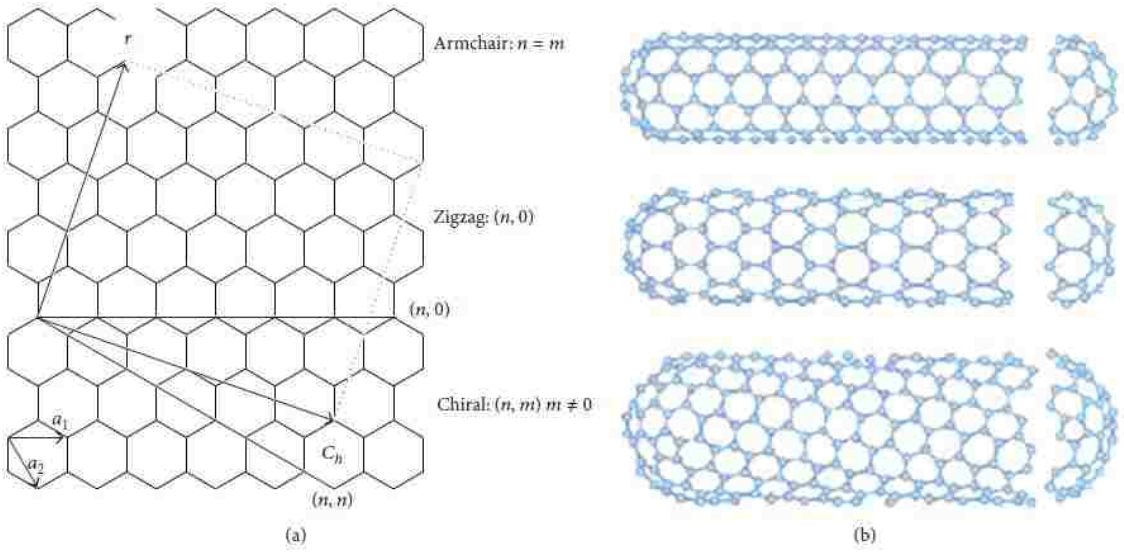

Figure 1.1 Schematic representation of a) formation of single-walled carbon nanotube by rolling up a grapheme sheet and b) three types of carbon nanotubes formed due to different rolling methods. Reproduced from ref.3

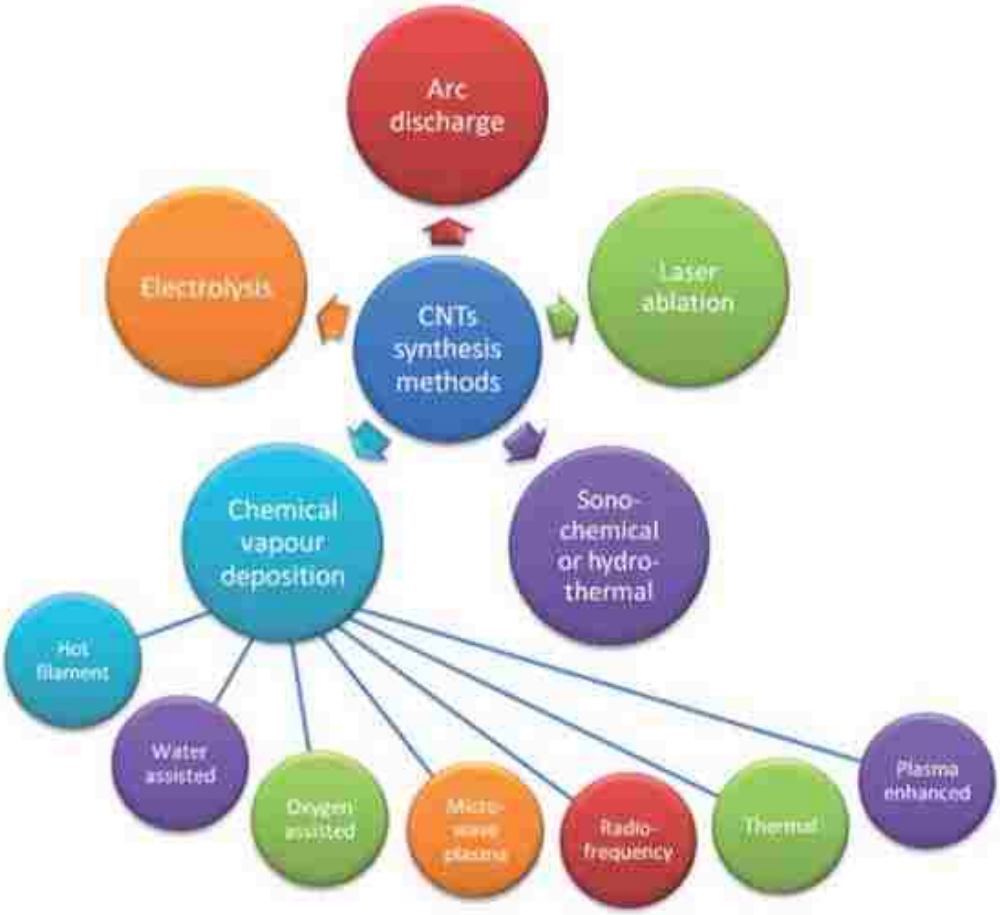

Figure 1.2 Currently used methods for carbon nanotube synthesis. Reproduced from ref.4

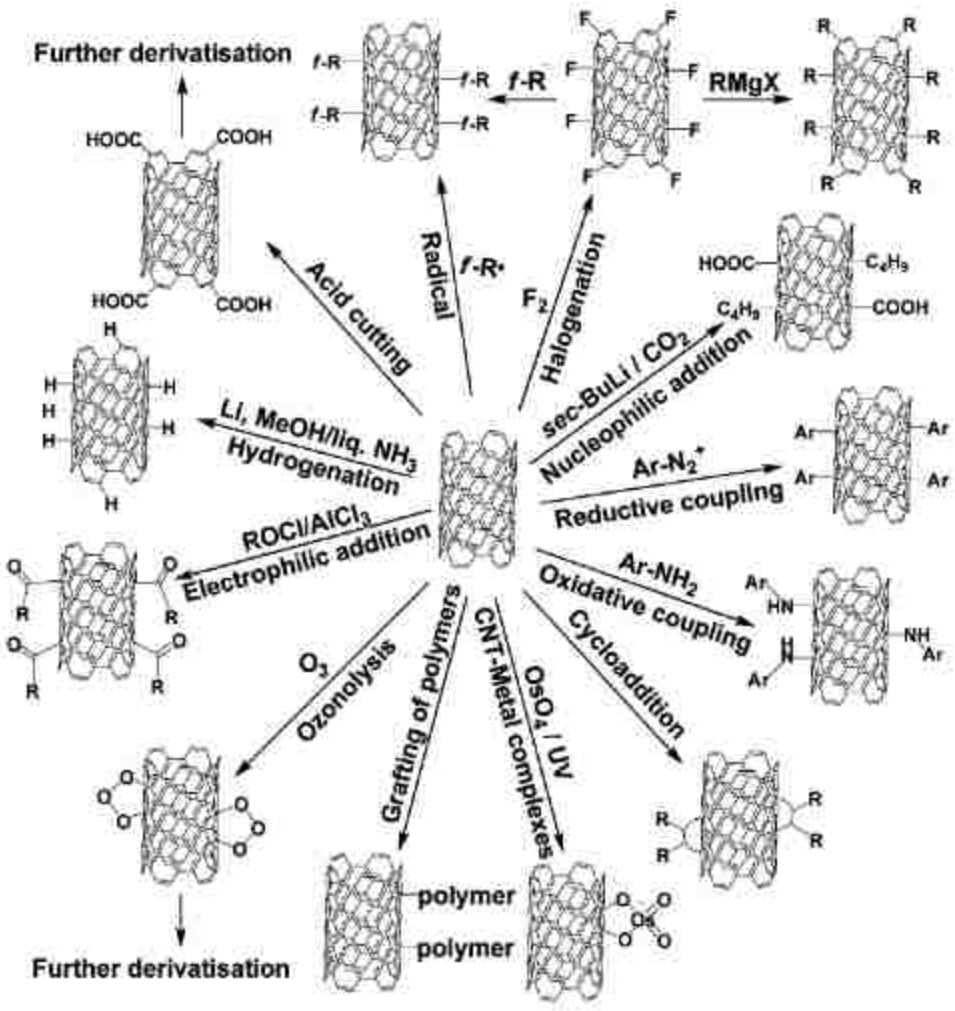

Figure 1.3 Covalent surface functionalization of CNT. Reproduced from ref.9

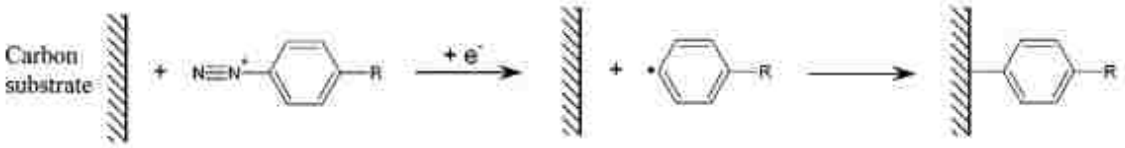

Figure 1.4 Schematic of reduction of aryl diazonium cation and subsequent covalent bonding onto a carbon atom of carbon substrate. Reproduced from ref.12

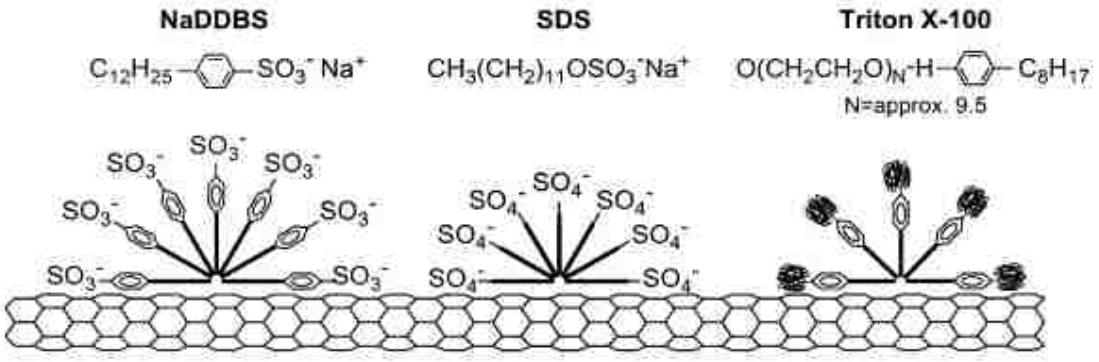

Figure 1.5 Schematic of typical surfactants absorbance onto nanotube surface. Reproduced from ref.8

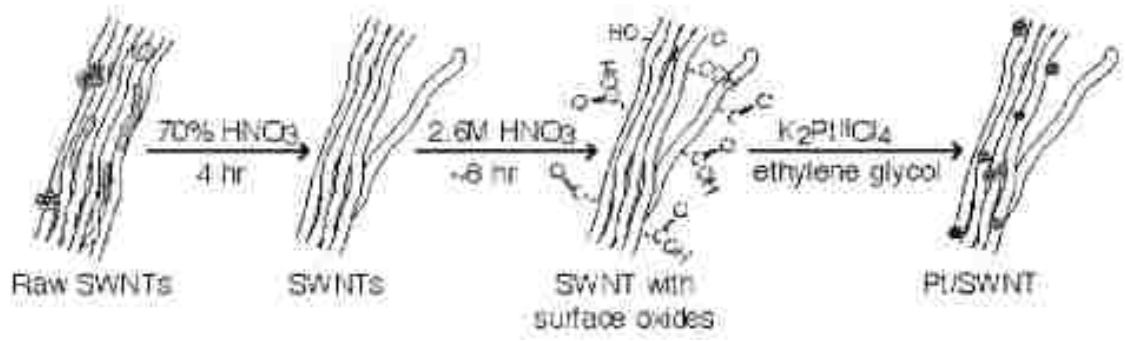

a)

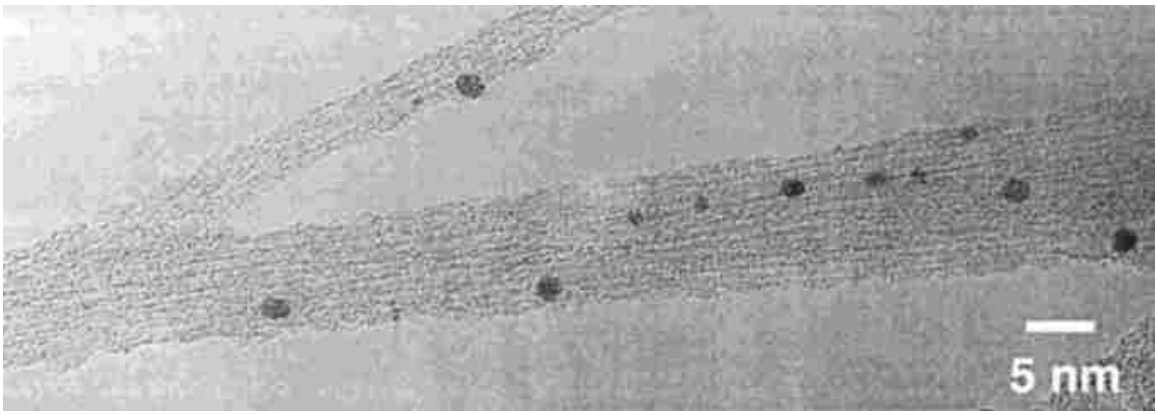

b)

Figure 1.6 a) Purification of SWCNT by concentrated HNO_3, followed by surface oxidation in dilute HNO_3, and then Pt loading by an ion exchange reaction. b) High magnification view of a single bundle showing typical Pt loading and sizes. Reproduced from ref.20

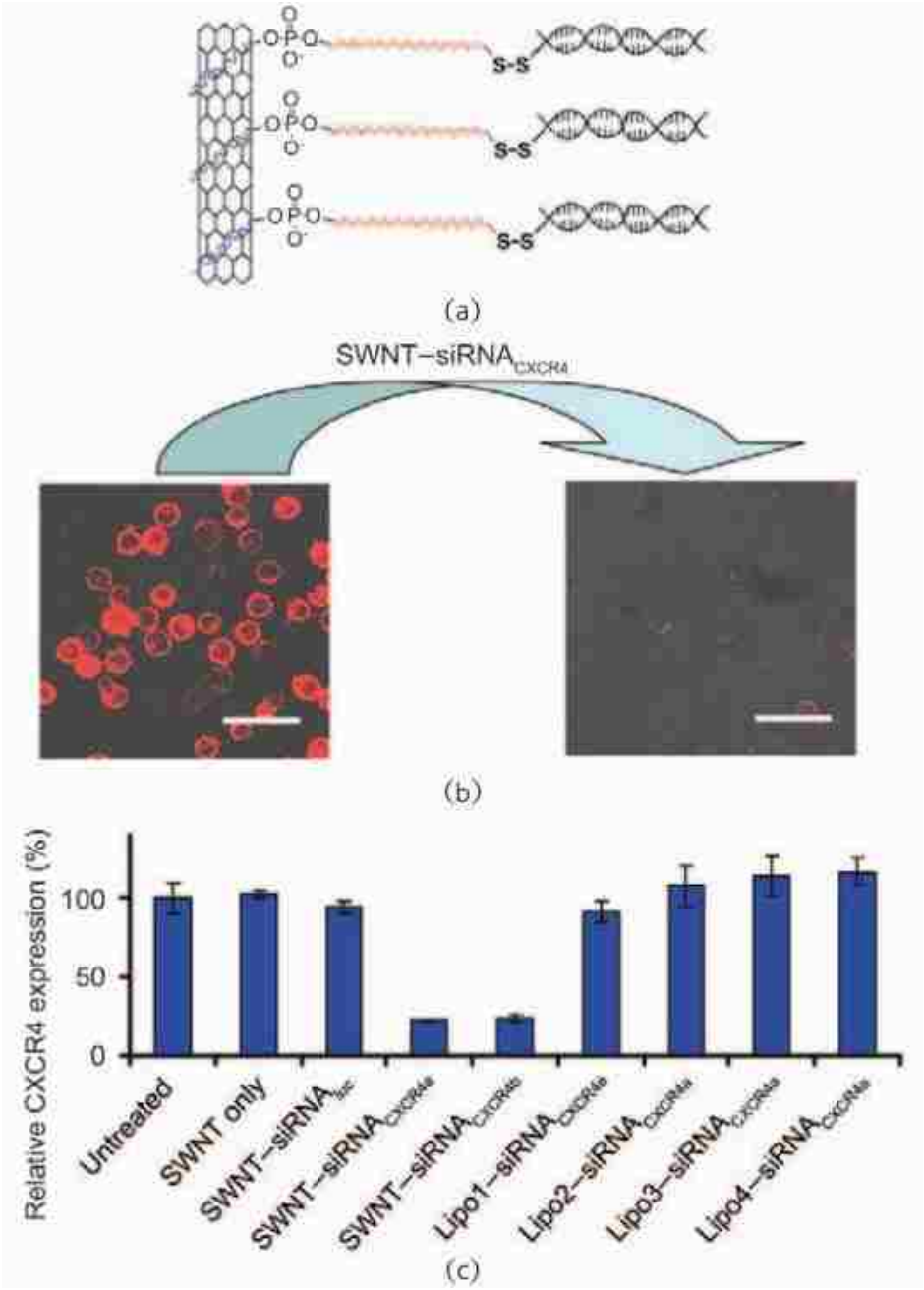

Figure 1.7 (a) A scheme of SWCNT-siRNA conjugation via disulfide linkage. (b) Confocal images of untreated cells (left) and SWNT siRNA$_{CXCR4}$ treated cells (right) after PE-anti CXCR4 staining. (c) CXCR4 expression levels on CEM cells three days after various treatments, including four types of liposomes and Luciferase control. Reproduced from ref.28

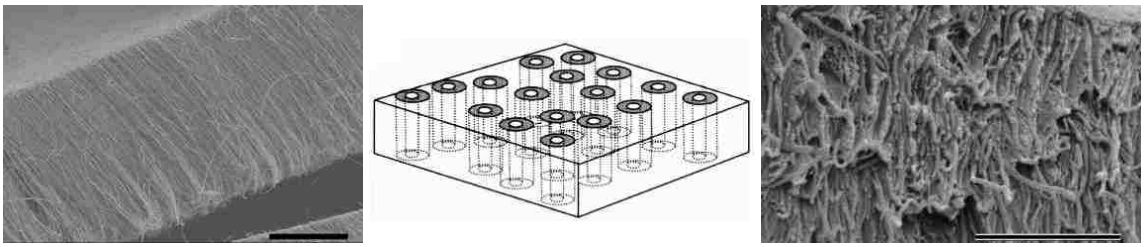

a b c

Figure 1.8 a) As-grown MWCNT array produced by Fe-catalyzed chemical vapor deposition process. Scale bar 50 µm. (b) Schematic of the proposed membrane structure by embedding MWCNT array in polystyrene. (c) Cross section view of the CNT-PS membrane after exposed to H_2O plasma oxidation. Reproduced from ref.33

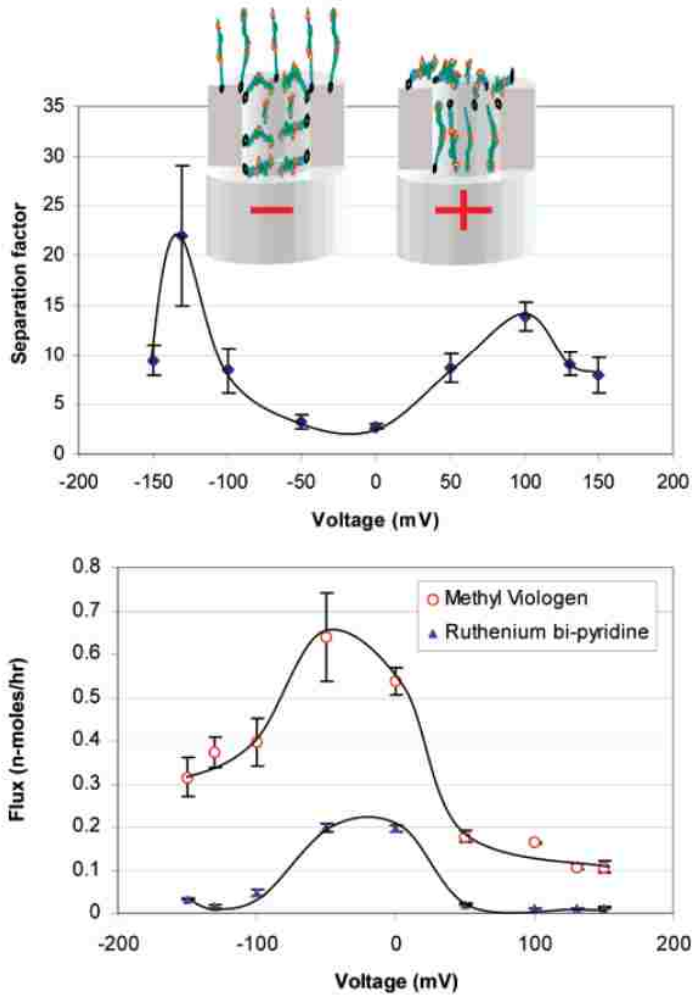

Figure 1.9 (a) Changes in separation coefficient with respect to voltage applied. (b) Fluxes of the two permeates at applied voltages across the CNT-FG membrane. Membrane area is 0.3 cm^2.

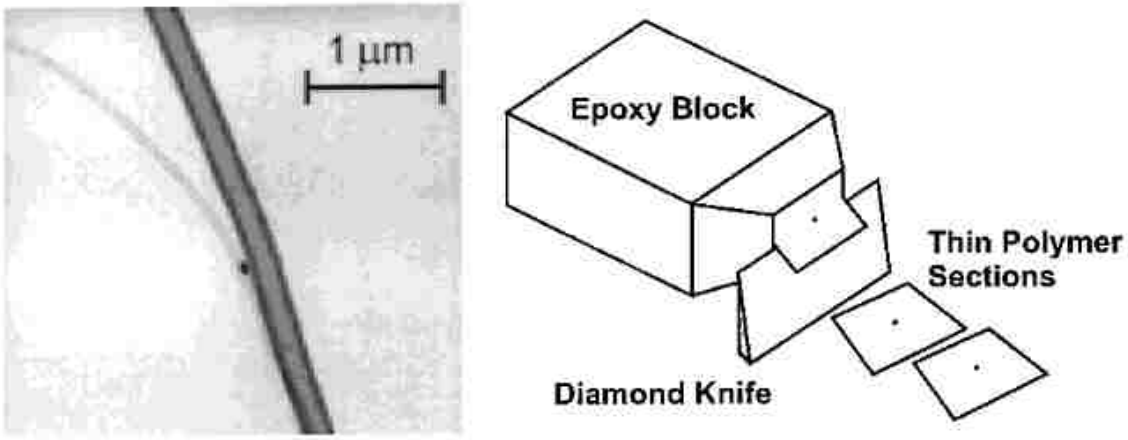

Figure 1.10 (a) A typical multiwalled CNT used to make the single channel imaged by TEM. It has a uniform diameter over a length greater than 100 µm. (b) The single MWCNT embedded in epoxy and cut into sections using microtome. Reproduced from ref.32

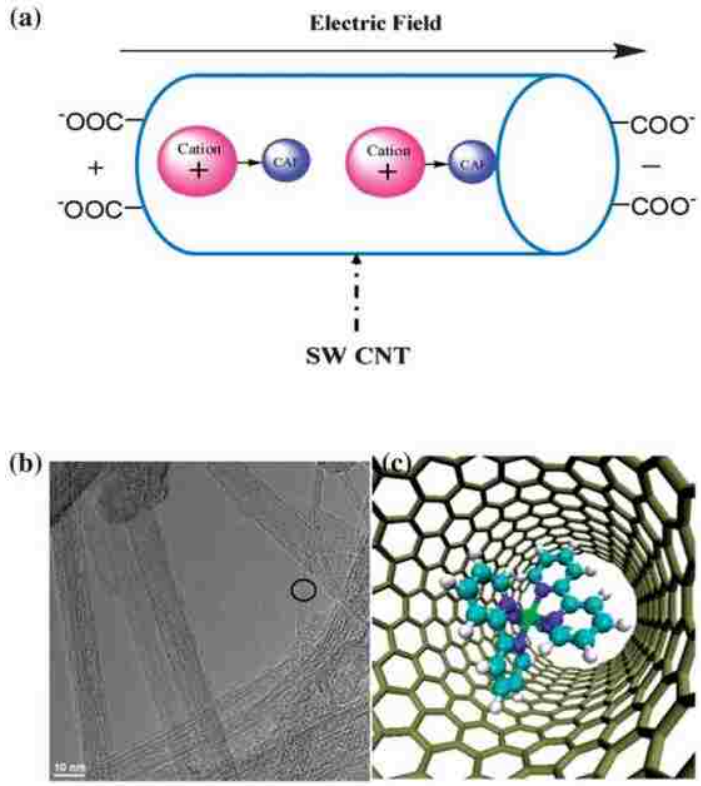

Figure 1.11 (a) Schematic of highly efficient electro-osmotic pumping of neutral caffeine using various cations in SWCNT or MWCNT. The SWCNTs have inner diameter ranging from 0.8-2nm, and MWCNT have ~7 nm inner diameter. CAF (caffeine) with ~0.5 nm diameter (b) TEM of SWCNTs with ~2nm inner diameter. (c) 3 dimensional model of $Ru(bpy)_3^{2+}$ moving in a (12,12) SWCNT. Reproduced from ref.41

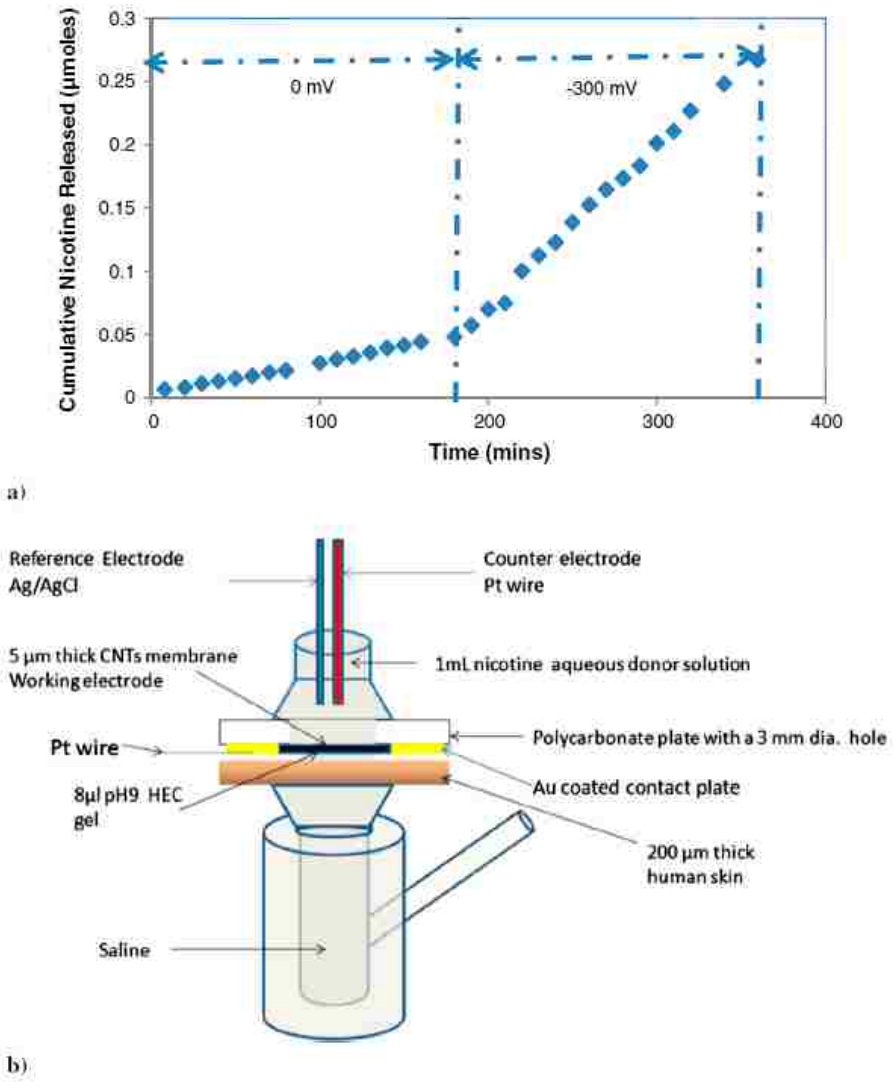

Figure 1.12 (a) Flux of nicotine through CNT membrane with/without applying -300 mV bias. The on/off ratio of high flux to low flux under -300 mV bias and 0 mV bias is 5.5. Donor concentration is pH8 220 mM nicotine aqueous solution. (b) Schematic setup of nicotine delivery device with donor/CNT membrane/skin components. Reproduced from ref.40

Chapter 2 CNT Membranes in programmable nicotine delivery and electroporation enhanced drug delivery

2.1 Introduction

Oral delivery and hypodermic injection are the two most frequently administered drug delivery options in humans. However these two delivery routes are not perfect: patients taking oral drugs may suffer from undesired peaks in drug concentration; first pass effect of the liver can prematurely metabolize drugs administered by the oral route and greatly reduce bioavailability.[43] Transdermal drug delivery emerges as an alternative seeking to overcome these setbacks and bring unique desirability to medical practices. By definition, transdermal drug delivery is "a term that should be restricted to the situation in which a solute diffuses through the various layers of the skin and into the systematic circulation for a therapeutic effect to be exerted".[44]

Transdermal drug delivery is by no means a new concept of the modern society. For over thousands of years man have placed substances on the skin for therapeutic effect and the practice have continued to the modern era. The first modern transdermal delivery system in the United States was approved in 1979- a three day patch that delivers scopolamine to treat motion sickness. In 1991 the approval of nicotine transdermal patches for nicotine replacement therapy (NRT) brought up the profile of

transdermal drug delivery in medical practices and general public. Today there exists a number of patches which delivers c8lonidine, fentanyl, lidocaine, nicotine, nitroglycerin, oestradiol, oxybutynin, scopolamine and testosterone.[45,46] A list of drugs currently proved for transdermal delivery is detailed in table 2.1. With the variety of drugs available, the annual US transdermal market for transdermal patches is more than US $3 billion alone.

Transdermal drug delivery has many advantages compared with the oral route. Besides reducing the first pass effect of oral therapeutics, transdermal patches can also reduce side effects associated with oral delivery. For example, oestradiol patches for hormone replacement therapy are used by more than one million patients annually, and in contrast to oral doses, do not cause liver damage.[45,47] Similarly, transdermal clonidine, nitroglycerin, and fentanyl exhibits less adverse effects than conventional oral dosage. More importantly, transdermal nicotine have helped smokers quit smoking more efficiently than other nicotine replacement therapy (NRT). One study shows that two years after transdermal nicotine patch therapy, patients were four times more likely to have quitted smoking compared to patients that received placebos.[48] Using these experimental data, the time span nicotine patch was approved, and public sells figure of the patch, it was estimated that more than one million US smokers have quitted smoking with the help of nicotine patches.

Transdermal drug delivery also has some advantages compared to the injection route, which is painful and pose risk of disease transmission by needle re-use. Additionally, transdermal patches can be self-administered, which serves to increase patient compliance due to simplicity of use and time efficiency from saving trips to the hospital.[43]

2.2 Structure of the skin

The main barrier to the transdermal route is the skin. As shown in Figure 2.1, the skin can be categorized into three main layers: the epidermis which is the outmost layer that protectively wraps tissue beneath; the dermis which is mainly built of connective tissue, and the hypodermis. The epidermis can be further classified into five sublayers or strata: stratum corneum, stratum lucidum, stratum granulosum, stratum spinosum, and stratum germinativum.

The stratum corneum is comprised of layers of dead cells (corneocytes) surrounded by lipid rich matrix, sometimes the structure is referred to as “brick and mortar”. The lipid is organized in layers and hold tightly to adjacent corneocytes, providing barrier function. It is found that the outmost layer, the stratum corneum, provides almost the entirety of the barrier function of the epidermis due to its lipophilic nature although it is only 10-20 μm thick, quite thin compared to other layers of the skin.[49] The barrier

function of the skin is reflected in its electrical properties, often characterized with impedance spectra.[50] An equivalent circuit model consisting of a resistor (R_S) in series with the parallel combination of a resistor (R_{SC}) and a capacitor (C_{SC}) have been well studied,[51] where R_{SC} and C_{SC} represent properties of the stratum corneum, and R_S the deeper layers (epidermis). Representative values are $R_{SC}=10^4$-10^6 Ω cm^2, C_{SC}= 1-50 nF/cm^2, and R_S=100-200 Ω cm^2.[52] Considering R_{SC} being 2 to 4 magnitudes larger than R_S, it is natural that the stratum corneum is identified as the main layer of resistance to drug delivery in the skin.

2.3 Programmable transdermal delivery using CNT membranes

One of the most important areas of transdermal drug delivery is in addiction treatment, where the overall costs of drug abuse in the United States exceed half a million dollars annually, as reported by the National Institute on Drug Abuse (NIDA).[53] Nicotine transdermal patches has been widely used for treating nicotine addiction as a nicotine replacement therapy. Pain treatment forms another big potion of transdermal market sells, mainly fentanyl and clonidine (analgesic adjuvant). Together they occupy 44% of all transdermal products globally.[54] Current patches on the market can be classified into two types: reservoir type and matrix type. In a reservoir type patch the drug delivery rate is controlled by a rate controlling membrane between the reservoir and skin. In the matrix type patch the drug, adhesive, and mechanical backing is combined into a

simpler design, and rate control is governed by skin permeability. However both membrane designs cannot provide variable delivery rates, lowering addiction cessation efficiency.[55] A number of enhancement techniques has been through development to both enhance delivery rates and provide some rate control, including iontophoresis, electroporation, microneedles, abrasion, ultrasound, etc. Iontophoresis stands out as it can provide programmable and variable delivery rates, however a strong current is required which can cause skin irritation.[56] The complexity of the device and high power requirements is also a concern and have limited its impact. A new transdermal drug delivery technology that provides programmable delivery rates, low power requirements, and simple design is much anticipated.

CNT membranes has attracted much attention and received research focus, especially in gate keeping and controlling molecular flux.[33,34,37] The fast flow, electric conductivity, and chemical versatility of CNT membranes make them ideal components in rate control of diffusing molecules. In 2010 J. Wu, B.J. Hinds published their *in vitro* results on programmable transdermal drug delivery using carbon nanotube membranes,[40] details shown in figure 1.12. The CNT membrane replaces conventional polymer rate control membrane to be placed between the reservoir and skin. As the entire bottom side of the CNT membrane which is mechanically affixed to polycarbonate support is made conductive, counter wires positioned in the reservoir can be easily used to provide electric bias. Under 0 V, nicotine molecules passively diffuse through CNT membrane

and diffuse through the skin, providing the "off" flux. Under negative bias as low as -600mV, cationic nicotine molecules diffuse through CNT membranes at accelerated rates due to combination of passive diffusion, electroporation, and electroosmosis. The result is an "on" nicotine flux, which can be up to 5.5 times the "off" flux, or called the on-off ratio. It should be noted in this case the CNT membrane is the rate-limiting barrier to nicotine flux, as nicotine diffusion coefficient for skin is higher than that of CNT membrane (2.68×10^{-8} cm^2 compared to 1.07×10^{-10} cm^2/s). This is important because if the skin is the rate limiting barrier, the rate control of the CNT membrane would have minor effect on final nicotine that diffuses through the skin. Later *in vivo* experiments on programmable nicotine delivery using CNT membranes was conducted by the same group in hairness guinea pigs.[42] Figure 2.2 shows the schematic of the CNT membrane device and an optical image of the actual device. The device dimensions of the CNT membrane device is only 2.5 cm x 2.5 cmx 1.5 cm, which is quite compact compared to other transdermal rate-control or enhancement techniques. A button battery provided power for the membrane that can last up to 4-6 days without the need of battery replacement.

2.4 New *in vitro* studies using supported fast flow CNT membrane and micro-dialysis sampling

Although initial *in vitro* and *in vivo* studies using the CNT membrane for transdermal drug delivery has shown great results, a few setbacks needs to be solved in order for the

full potential of CNT membranes to be realized. First, data points for the *in vivo* studies is limited due to animal safety concerns and fast animal metabolism forming bi-product without known metabolic conversion rates. Secondly, although moderate flux rates was achieved for nicotine *in vitro* and *in vivo*, higher nicotine delivery rates or clonidine delivery rates is desired to encompass the requirements and open up new possibilities, which required the development of new CNT membranes with faster fluid flow. Thirdly, it is important to support CNT membranes with necessary mechanical backing, as the leak of concentrated nicotine can be dangerous for the test animal or possible later human subjects.

It is part of this thesis that we conducted a series of experiments currently *in vitro* and preparing for *in vivo* to solve the problems described above. To better map time dependent dosage and on/off, a micro-dialysis membrane delivery rate sampling scheme was developed. By implanting the micro-dialysis membrane directly below the epidermis where the CNT membrane is located, drug concentration can be measured without having to frequently draw blood samples and study entire body metabolism or by product. Secondly, both high loading microtome cut CNT membrane and aligned carbon nanotube membrane provided by Porifera was used in the studies in an effort to improve nicotine flux and on/off ratios. Thirdly, membrane support consisting of nylon mesh was positioned below the CNT membrane and polycarbonate support to provide mechanical stability for the membrane. The stabilization can potentially cancel out

pressure from the skin/gel layer and external force applied from the top of the membrane device.

2.4.1 Experimental setup of CNT membrane and micro-dialysis

2.4.1.1 Chemicals and materials

DWCNT with an average core diameter of 1.5 nm was purchased from cheaptubes.com. MHHPA(hexahydro-4-methylphtalic-anhydride, mixture of cis and trans), catalyst (2-ethyl-4-methyl-1H-imidazole-1-propanenitrile, MES(2-[N-morpholino]ethane sulfonic acid), EDC(ethyl-(N',N'-dimethylamino) propylcarbodiimide hydrochloride), sulfo-NHS(N-hydroxysulfosuccinimide), Direct blue 71 dye was purchased from Sigma Aldrich. Epon 862 was purchased from Miller-Stephenson. Filter membranes with pore size 1 µm and 20 µm PTFE unlaminated was purchased from Sterlitech. The micro-dialysis membranes was purchased from BASi Inc. Nylon mesh with 255 µm wire distance and 47% opening was purchased from Component Supply Company.

2.4.1.2 Fabrication of the micro-tome cut DWCNT membrane and mounting

DWCNT with 2% loading was fabricated with modifications from a previous method.[32,40] To describe it briefly 0.1 DWCNTs were first dispersed in 1L DI water with 2g SDS under tip sonication at 10W, 20% magnitude for 2h.(Qsonica, Model S-4000, tip size of 1/8

inch). The solution was filtered through 20 µm PTFE membrane to remove CNT bundles and impurities, then SWCNTs were gathered from the filtered solution on a 1 µm PTFE membrane. Next the purified SWCNTs was mixed with Epon 862, MHHPA, surfactant Triton X-100, and catalyst by a Thinky^{TM} centrifugal shear Mixer, and the mixed CNT-epoxy was degassed through vacuum (Welch 1400B pump) to remove bubbles and then cured under 85^{O}C to appropriate hardness. The cured composite was cut into 5µm thick membranes with a Reichert-Jung microtome, after which the cut membranes (0.6 cm x 0.6 cm) were glued over a 3mm hole in polycarbonate plate to act as mechanical support. The top side of the membrane is in the recess of the hole and the bottom side of the membrane is designated on the bottom plane of the polycarbonate plate. Both sides of the as-prepared SWCNT membrane was treated with water plasma oxidation for 1min to remove extra polymer at CNT tip. As seen in figure 2.3, SWCNT have an average core diameter of ~1.5 nm and length of 5-30 µm as reported by the manufacturer. The thickness of as-microtome cut membranes is ~5 µm subject to some variance in certain areas (figure 2.3b), and no cracks was observed for the membranes fabricated.

The CNT membranes (~0.6x0.6 cm^2) were glued over a 3mm diameter hole in polycarbonate plate (1mm thick) acting as mechanical support. To strengthen the CNT membrane from below, nylon mesh with 255µm openings was first glued onto polycarbonate plate, with the meshes covering the 3mm diameter hole. CNT

membranes was then glued onto the top of the nylon mesh. This stabilized CNT membranes on the nylon mesh plane and greatly reduced force being applied from the skin contact and above the membrane device. The top side of the membrane is in the recess of the whole and the bottom side of the membrane is on the bottom plane of the polycarbonate. The whole bottom side of the CNT membrane received gold coating ~30 nm thick to provide electric conductivity to act as working electrode. The membrane area received less gold coating compared to surrounding polycarbonate support plate to reduce gold coating layer's effect on decreasing membrane flux.

2.4.1.3 Mounting of Porifera CNT membranes

Received Porifera CNT membranes were round discs 12-16 cm in diameter as the aligned CNTs were grown on Si substrate discs. In order to mount them to allow flux test square pieces of 0.7x0.7 cm were cut from the large disc and glued onto the hole of polycarbonate plate (1mm thick) which the microtome fabricated CNT membranes were mounted on. Further gold coating and functionalization processes on the Porifera CNT membranes resembled that of the microtome-cut CNT membranes.

2.4.1.4 Functionalization of CNT membrane

To functionalize the membrane with aptamers, the U-tube setup was used as shown in figure 2.4. First the DWCNT membranes are flow-grafted (FG) with benzoic acid by immersing the top of the membrane in 100 mM 4-carboxy phenyl diazonium tetrafluoroborate and under 2 cm DI water pressure at the bottom of the membrane for 12 h. Flow grafting with 2 cm DI water pressure limits further dye functionalization to the tip of the carbon nanotubes. Immediately following diazonium grafting, 4mL fresh dye solution with 100mg direct blue 71 and 5mg EDC, 5mg sulfo-NHS is prepared. The top of the membrane is again immersed in the direct blue solution for functionalization for 12 hours under 2cm DI water column pressure.

2.4.1.5 Preparation of skin

Fresh porcine pig ear skin was obtained from a local abattoir. Front and back side ear skin was dermatomed to 250-300 µm pieces and kept in -20°C refrigerator until use. Before conducting an experiment the skin was taken out and thawed in 0.9% saline under room temperature. Dermatomed skin of 250-300 µm is preferred over heat separated epidermis as skin with intact epidermis better mimic *in vivo* skin environment.[56]

2.4.1.6 Screening of CNT membranes for nicotine ON/OFF

Either microtomed cut membranes with high loading (2.5% weight) or aligned CNT membranes received from Porifera were screened for nicotine flux and on/off with U-tube KCl screening and flow cell setup prior to *in vitro* micro-dialysis screening over skin because the individuality of CNT distribution and local polymeric conditions means not all membranes possess required flux and on/off. Following membrane fabrication and mounting, they were first screened in U-tube setups shown in figure 2.5. Edaq potentiostat was used to provide constant bias during measurements, and two Ag/AgCl electrodes were placed on the top and bottom side of the CNT membrane acting as working electrode and reference electrode, with distance between electrodes being 10 cm. Following KCl screening experiments, CNT membranes were screened flow cell setup, will fresh PBS solution being supplied by syringe pump which flows into auto sampler. HPLC measurements were then made of the samples and flux and on/off ratios calculated. Membranes with suitable flux and on/off ratios pass to microdialysis flow cell study with skin.

2.4.1.7 Microdialysis and flow cell setup

The microdialysis membrane probe is shown in detail in figure 2.6 as depicted by the manufacturer. It is a hollow dialysis fiber with an outer diameter of 320 µm, length of 5mm, and a MWCO of 30KDA, and hollow plastic tubing with outer diameter of 218 µm was collected on both sides of the probe to provide inlet and outlet. The 30KDA

molecular weight cutoff allowed nicotine molecules in the vicinity of the microdialysis membrane probe to permeate through and carried downstream by the constant PBS flow through probe and its tubing. The microdialysis membrane was implanted into the dermis so measured flux is the localized nicotine flux in the skin prior to systematic circulation or dilution. To prove that microdialysis can be used to sample nicotine concentration and to provide a comparable base line for CNT membrane nicotine delivery, commercial Nicoderm patches was used in a microdialysis study. The microdialysis membrane was implanted into the dermis of the full thickness skin (1.5 mm), then the skin placed above the receptor chamber of a vertical Franz diffusion cell, with the stratum corneum facing the donor chamber. The commercial Nicoderm patch was cut into small size with area comparable to that of our CNT membrane (0.07 cm^2) and fixed onto the stratum corneum. Fresh PBS flowed through the dialysis membrane with a rate of 2µL/min controlled by a syringe pump. The PBS that flows through microdialysis membrane was collected by a fraction sampler collecting at 1 h intervals. The receptor chamber was filled with fresh PBS and stirred with magnetic stir bar to simulate *in vivo* blood circulation to decrease the depot effect.

Nicoderm microdialysis membrane experiments was performed using 200-300µm thin porcine skin. During full thickness skin Nicoderm experiments it was found that due to the strong skin depot ON/OFF ratios was not significant as expected. Even with the magnetic stirred receptor chamber nicotine could not be removed from the skin at a

sufficient rate causing "off" state nicotine concentration to drop very slowly on the measured nicotine profile. The thin skin Nicoderm experiment used a setup which combined the flow cell and the microdialysis is shown in figure 2.7, where the microdialysis probe sits below the thin microtomed skin, which was positioned above the sampling chamber. Phosphate buffer solution was injected by syringe pump into the sampling chamber which was collected by fraction sample collector downstream to simulate blood circulation. Another set of syringe pump and fraction sample collector was used to inject PBS into the dialysis probe and collect PBS solution flowing out of the probe to measure nicotine concentration.

Programmable delivery of nicotine by CNT membrane was measured by the same setup as the Nicoderm experiments except the nicotine source, where in this case the CNT membrane replaced the Nicoderm patch and was positioned above the skin. The reference/counter electrodes shown in figure 2.7 and CNT membrane as working electrode provided bias for the membrane to switch between off state and on state. During OFF state 0 mV bias was applied and ON state -1.2V to -1.5V was applied by Edaq potentiostat, with off state lasting 12h and ON state lasting 12h for 1-3 cycles.

2.4.2 Results and Discussion

2.4.2.1 SEM of Porifera CNT membranes

Aligned CNT membranes from Porifera was preferred due to their large membrane size, mechanical stability, and expected high flux capability. The well aligned growth of vertical CNTs meant the membrane made from impregnating them in polymer would possess a high pore area, as all tubes face vertically. It is also possible then to grow desired length of CNTs and impregnate them with polymer to give the membranes mechanical robustness, the thicker the membrane the higher the robustness. Too long a CNT however means longer travel distance for molecules inside CNT cores and becomes undesirable, thus current Porifera membranes had thickness of 30-50 µm well showing reasonable mechanical robustness and diffusion time.

The CNT membranes were checked for CNT distribution and membrane conditions by SEM with images shown in figure 2.8 (Batch 16 membranes were presented here due to high ON/OFF ratios). In figure 2.8a the surface of the membrane can be observed with an abundance of CNTs protruding out from the embedding polymer which appears as white dots on the SEM image, and no cracks spanning the membrane thickness was observed. In figure 2.8b both the top surface and cross section can be observed with CNTs, the CNTs on top surface appeared as white dots and CNTs from the cross section appeared in strands that protrude from the side. It was likely that during sample preparation the shear force cutting the cross section brought out tubes close to the cross section and appeared as it is on the SEM image, although they were initially vertically aligned. The observed CNTs/polymer surface was similar to the earlier report

by J. Wu, B.J. Hinds, where they observed the top surface of microtomed multi-walled carbon nanotube membrane with CNTs protruding out from embedding polymer.

2.4.2.2 KCl ionic current screening and nicotine ON/OFF results

All batches of membranes received from Porifera were first tested for ionic current flow in U-tube setup with 0.1 M KCl as the ionic species before nicotine flux and ON/OFF studies without skin in the flow cell setup. Table 2.2 shows the typical 0.1 M KCl screening current, nicotine flux and ON/OFF ratios of Porifera batches compared with the typical microtome-cut CNT membrane KCl screening current and nicotine flux. All ON/OFF ratios were calculated by dividing the flux of ON state nicotine flux under -1.5 V negative bias by OFF state nicotine flux under 0 V bias. Batch 13, 16, and 25 of Porifera CNT membranes showed moderate ON/OFF ratios ranging from 3.2 to 4.95, which was higher than reported by J. Wu, B.J. Hinds. However, nicotine ON flux of batch 13 and 25 was below the required therapeutic flux, rendering the two membranes less useful in practice. Batch 16 membranes exhibited ON/OFF ratios of 4.95, with OFF and ON flux respectively being 0.4 µmole/h*cm^2 and 1.98 µmole/h*cm^2, which matched that of therapeutic requirements (0.3 µmole/h*cm^2 and 1.1 µmole/h*cm^2 respectively). Batches such as 46, 47, and 50 did not show noticeable ON/OFF ratios, two of which was less than 1, the notion that KCl screening current of a membrane was generally proportionate to its nicotine flux could not be applied to these membranes. 0.1 M KCl

screening current of these membranes was high compared to batch 16 although their nicotine flux was lower which was unexpected. It is speculated due to the small diameter of the CNTs in the membranes the majority of CNT tips were blocked by polymer reducing porosity, the abnormally high KCl ionic current probably resulting from the high conductivity of the CNTs. Further investigation would be required in the future to identify the exact cause of failure for some of the aligned CNT membranes in order to improve the fabrication process, as aligned CNT membranes are still desirable due to their mechanical stability and expected high flux.

In comparison most microtome-cut membranes with 2.5% weight ratio showed 0.1M KCl ionic current of 8-10μA, high OFF and ON fluxes, and ON/OFF ratios as high as 7.94. Weight ratio of CNTs to embedding epoxy/hardener dictated OFF and ON fluxes: the higher weight ratios resulted in increase in porosity and thus higher OFF and ON fluxes. It should be noted however it is impracticable to significantly raise weight ratios beyond 5%, as CNTs-epoxy composites beyond 5% poses incomplete mixing and difficulty in microtome-cutting due to hardness of CNTs.

2.4.2.3 Microdialysis membrane measurements of Nicoderm released nicotine in full thickness porcine skin

Release profile of nicotine from a 0.07 cm^2 Nicoderm patch (21mg/24h) was measured by a microdialysis membrane implanted inside the dermis shown in figure 2.9. The results show that microdialysis membrane implanted in the skin could successfully detect nicotine that was released by a commercial patch which permeated through stratum corneum into the lower skin layers with measured peak concentration to be ~50 µg/ml. Upon removal of the patch measured concentration correspondingly decreased at a steady rate which lasted into hour 32, which is expected since nicotine would steadily be removed by phosphate buffer solution circulation. It is undesirable however that a lag-time of 26h was observed as high nicotine concentration was detected by the microdialysis membrane even after the Nicoderm patch was removed. The cause of this lag-time was due to nicotine depot effect in the skin and no viable routes of clearance for the trapped nicotine inside skin. This lag-time could be detrimental to our experimental design to show ON/OFF using CNT membranes as measured ON/OFF ratios will be significantly less than actual due to the trapped nicotine. The actual lag-time is expected to be shorter in *in vivo* studies because of blood circulation in the dermis quickly clearing deposited nicotine. To better simulate *in vivo* microdialysis results with sufficient body clearance in preparation for i*n vivo* studies, thin skin microdialysis studies with Nicoderm patch was conducted.

2.4.2.4 Microdialysis membrane measurements of Nicoderm released nicotine in dermatomed (200-300 µm) thin porcine skin

As described in the experimental section and drawn in figure 2.7, a combination of flow cell and microdialysis membrane sampling was used to measure nicotine release by Nicoderm patches. Flow cell provided constant phosphate buffer flow through the sampling chamber beneath the thin skin and microdialysis probe, simulating *in vivo* blood circulation. This served two purposes: 1) To reduce the skin depot effect which resulted in considerable lag-time 2) To compare microdialysis results with conventional flow cell results to better understand nicotine delivery profiles measured by microdialysis and possible *in vivo* behavior. From the results of the thin skin studies which are shown in figure 2.10, it can be observed an initial burst of nicotine concentration measured by the probe in 0-4 h which was expected due to inherent lag-time of nicotine diffusion through skin and the design of the Nicoderm patch. From hour 4 onward until Nicoderm patch removal at hour 12, the nicotine delivery reached a semi-steady state delivery profile which was justified by previous studies by Y.B. Bannon et al.[57] The main difference between thick full skin nicotine release and thin skin release was the fast clearance time demonstrated by the latter: via efficient clearance of the underlying phosphate flow through sampling chamber, a switch from ON state to OFF state was reached within 2 hours compared to that of more than 26 hours in thick skin experiments. The average amount of nicotine measured starting 2 hours after the removal of Nicoderm patch was 0.0016 µmoles, which is 13.75 fold smaller than the mean steady state nicotine concentration of 0.022 µmoles (per 0.07 cm^2 area membrane and per hour), an figure small enough to be considered as residue value since the ON/OFF ratios of current CNT membranes are in the range of 6-13.6. This fast

clearance rate of ~2h indicates the microdialysis probe's potential to accurately map out CNT membrane nicotine delivery ON/OFF profile.

2.4.2.5 Switchable transdermal delivery of nicotine by CNT membrane

Switchable nicotine delivery by CNT membranes was performed on the flow cell/microdialysis system following demonstration of viability and calibration by Nicoderm patches. As shown in figure 2.11, cumulative nicotine release profile from CNT membrane/porcine skin was measured by microdialysis for a total of 3 ON/OFF cycles. For the ON cycle -600 mV bias was applied to electrophoretically and electroosmotically pump nicotine through cores CNTs along with passive diffusion, while for the OFF cycle electric bias was maintained off at 0 mV for nicotine to passively diffuse through CNT membrane into skin, which is mainly governed by the concentration gradient. As discussed previously the diffusion coefficient for nicotine through skin is larger than the coefficient through CNT membrane, so the rate of release through CNT membrane/skin was determined by the CNT membrane. In cycle I OFF flux was 0.01 µmoles/(cm^2*hr), ON flux 0.17 µmoles/(cm^2*hr, which yields an extraordinary ON/OFF ratio of 13.6. In cycle II OFF flux was 0.04 µmoles/(cm^2*hr), ON flux 0.11 µmoles/(cm^2*hr, indicating an ON/OFF ratio of 2.4. In cycle I OFF flux was 0.02 µmoles/(cm^2*hr), ON flux 0.11 µmoles/(cm^2*hr, showing an ON/OFF ratio of 4.8. The first cycle ON/OFF of 13.6 was quite remarkable as previous report by J. Wu and B.J. Hinds showed ON/OFF ranging

from 3.5 to 5.5. We contribute the improvement in ON/OFF ratio the exclusive use of DWCNTs here as compared to the use of both DWCNTs and MWCNTs in their study. DWCNTs with their smaller diameter will improve electroosmosis velocity for fluids presumably due to the smaller diameter forcing larger percentage of the solvent to be pushed by ions, increasing electroosmosis velocity which in turn contributed to the total observed nicotine delivery rate during ON phase.[41]

2.4.3 Conclusions

The preliminary data shows that we have successfully demonstrated multiple cycle ON/OFF nicotine delivery by CNT membrane measured using a microdialysis membrane setup. The measured nicotine profile fits well with previous studies and have shown its potential to map out nicotine concentration profiles *in vivo* with a large amount of data points with short time intervals which the conventional blood draw method could not achieve due to animal safety concerns. Follow up detailed animal protocol using hairness guinea pigs is currently being developed within the group to prove the concept in hairness guinea pigs. Since transdermal drug delivery studies typically last for several days, the regrowth of hair will significantly affect the contact between skin and transdermal patches, resulting in errors in diffusion rates; the use of hairness guinea pigs are ideal in solving this problem. Simplified outline of experimental design is herein given to provide an idea of how the experiments will be carried out: 1) 6 hairness guinea

pigs will be divided into 2 groups of 3. 2) Each group will be anesthetized for implantation of microdialysis setup below skin. Upon successful implantation one end of the microdialysis probe will be connected to a syringe pump supplying fresh phosphate buffer solution and the other end connected to a flow cell collecting nicotine sample data. The animals will be monitored for their health condition. 3) Since no blood draw will be taken on the guinea pigs, commercial nicotine patches (Nicoderm) with 0.07 cm^2 area will be applied to the test subject dorsal area for 1-2 days to calibrate the nicotine permeation behavior of each subject as individuality exists. 4) The commercial nicotine patch will be removed for 1 day prior to CNT membrane nicotine delivery studies to give the animal sufficient recovery time and for the local nicotine concentration to drop below residue values. 5) CNT membranes will be applied to the animals for multiple ON/OFF cycle delivery of nicotine.

One innovative approach to improve addiction treatments efficacy is to couple remote counseling via phone or internet survey to program a delivery device, which has been proven to be more effective than self-administered treatments.[58] Future plans of the group are to continue switchable CNT membrane drug delivery in human subjects after proving it to be effective in animals, as the membrane device is compact, energy efficient, and can be easily coupled with WIFI/ Bluetooth watch to control delivery rates.

2.5 Electroporation in enhancement of drug delivery

Nicotine can permeate through the skin well over therapeutically required rates because of its small size (162 Da). Due to the strong stratum corneum barrier, only a limited amount of drugs can permeate through the skin in significant amounts. The transport of most drugs through skin is slow with long lag-times and suffers from low flux rate, which greatly limits the potentials of transdermal drug delivery. CNT membranes may be the solution as a wide range of drugs such as clonidine and fentanyl could be delivered similarly to nicotine. However their slow permeation rates through the skin means the skin is the rate-controlling component and renders CNT membrane rate control ineffective. To improve drug transport through the skin, enhancement methods therefore are required to step up drug transport through the skin up to therapeutic level. A number of approaches have been developed previously by various groups around the world which seeks to disrupt the skin barrier to allow faster drug transport through the skin, which were detailed in the following sections.

2.5.1 Chemical enhancement methods

Chemical enhancers were a natural approach of enhancement because it can readily be formulated into the drug containing layer of a transdermal patch. Many effective chemical enhancers disrupt the highly ordered structures of the stratum corneum by

inserting amphiphilic molecules into the bilayers to disorganize their packing or by extracting lipids using solvents and surfactants to create packing defects.[59] Hundreds of chemical enhancers were studied, including existing molecules and molecules which were specifically designed for this purpose, such as Azone (1-dodecylazacycloheptan-2-one) and SEPA (2-n-nonyl-1,3 dioxolane). Systematic designing and screening processes of chemical enhancers was also proposed.[60] Although chemical enhancers have seen some success, it did not bring change to the structure of the skin so the key obstacle was not tackled, inherently limiting its effectiveness in most cases.

2.5.2 Iontophoresis

Iontophoresis was an enhancement method seeking to increase the range of drugs available for transdermal drug delivery with reversible mechanisms that poise minimum skin irritation. The delivery of drugs is accompanied by a small constant electric current that drives the drug ion into the skin, which is depicted in figure 2.12. The drug formulation containing the ionized drug molecule (D^+) is placed in the anode compartment.[61] Application of electric potential leads to a flow of electrons in the system. Due to the flow of electric current in the forward direction, D^+ drug ions is electrophoretically delivered into the skin. To compensate for the flow Cl^- ions move from the skin into the anode compartment. One advantage of iontophoresis is the controllability of drug flux: the amount of drug compounds is heavily related to the

quantity of electric charge flow, the duration of the current application, and active area of contact. Improved onset time and also a more rapid offset time also makes iontophoresis desirable. A wide range of drugs used for various purposes were tested for iontophoretic delivery, notably including lidocaine for local anesthetics,[62] fentanyl for pain management,[63] piroxicam (a NSAID),[64] etc. Although iontophoresis have achieved some success, the maximum delivery rate is limited by skin irritation and pain caused inability of electric current confinement in the stratum corneum. Iontophoretic patches devices can also be quite costly because microprocessors were required to control current magnitude.[65] Human trials have gone under way the

2.5.3 Microneedles

A straightforward approach to improve drug flux through skin is simply breaking the stratum corneum structure by punctuation with microneedles. With the micro-sized sharp needles, the stratum corneum barrier could be broken and minimum pain inflected on the paint thanks to the fine geometry of the needles. Both solid microneedles that broke the skin for controlled delivery by a patch and hollow microneedles with drugs directly coated on for rapid release were developed.[66] Although microneedles are desirable due to their low cost and simplicity, a key problem was not well addressed: the number of drugs available for transdermal delivery can be increased by the use of microneedles, yet it still lacks a rate controlling component of

delivery, as typically an external patch was applied to the punctured skin afterwards. The actual delivery rate of drugs still depended on the delivery rate of the polymer rate-controlling membrane in the patch and that rate is typically not switchable.

Another key drawback with microneedles was the self-relaxation and healing of skin overtime after the enhancement was deployed, which rendered long term patch application impossible.

2.5.4 Electroporation

Amongst other active enhancement methods developed to enhance transdermal drug delivery, electroporation stands out due to its long lasting effect, controllable delivery rate, and simplicity of device. Electroporation is the use of short, high-voltage pulses to temporarily disrupt the stratum corneum structure to allow enhanced delivery of molecules of interest. The use of short, high voltage pulses is a well-known method to disrupt cell membrane for gene transfection and other applications.[67] The electroporation of mammalian skin was later studied by M.R. Prausnitz, J.C. Weaver et al. for enhanced drug delivery of calcein.[68] The fluorescent marker calcein with 622 Da, -4 charge that naturally permeates through the skin in very small quantities (less than 10^{-4} $\mu g/cm^2*hr$) was used as the test molecule. By application of a number of electric pulses with voltage from 55-300V on porcine and human skin, enhancement of up to 4 magnitudes and enhancement duration of up to 24 h was seen. Parameters such as

pulse voltage, pulse number, pulse duration, design of electrode, and intrinsic properties of the drug such as charge, lipophilicity, molecular weight, formulation determined the efficiency and magnitude of electroporation assisted transdermal drug delivery. Since then extensive *in vitro* research on transdermal drug delivery by electroporation was carried out by individual groups, including calcein, fentanyl, Lucifer yellow, dextran sulfate, nalbuphine, tetracaine, buprenorphine, etc.[69] Electroporation has also been combined with other enhancement methods such as chemical enhancers, ultrasound, iontophoresis for the combined benefit.

The major current challenge in the clinical acceptability of electroporation is debates of its after effect on the skin, underlying tissue, and human sensations. A number of methods have been used to assess skin's tolerance to electric pulses, including visual examination, measurement of skin electric properties, TEWL (trans-epidermal water loss), as well as clinical studies. A list of electroporation effects on the skin is shown in table 2.3.[69] Although most studies show perturbation to the skin being "reversible" and "minimal", patient pain, sensation, and muscle stimulation is still of the primary concern. As initially the electric field is applied on the high resistance stratum corneum, subsequent lowering of resistance of the stratum corneum will introduce electric field deeper into underlying tissues where nerve endings are more populated, although innovative electrode geometry may help to confine electric field to the surface of skin and reduce associated pain. Shown in figure 2.23 is an illustration of simulated

transverse and lateral electroporation, where the rectangles and their stacking represents idealized stratum corneum layered structure and each rectangle was attributed a resistance value.[70] 50V was applied to the in (a) transverse electroporation and (b) lateral electroporation geometry. The modeling system calculated electric field strength in the vicinity of each rectangle and if the threshold voltage was reached (1V), the block was considered electroporated and its resistance reduced to that of low resistance electrolyte. When a rectangular block is electroporated, electric field and current were redistributed, and the illustration herein represents the final status of the blocks under 50V electric voltage after many redistribution intermediate phases. It could be seen that in the case of transverse electroporation, electric field penetrated all layers of corneocytes and electric field distribution was deep into skin, where in the lateral electroporation electric field was largely confined to the outer surface of stratum corneum. This local confinement limited electric field in the stratum corneum, or at larger voltages, the epidermis, where the lack of nerve endings results in reduced pain and contraction associated with electroporation. K. Sugibayashi et al. studied transdermal drug delivery by combination of electroporation and microneedle array, which is shown in figure 2.14.[71] The microneedle array served two purposes: they either punctured the skin alone, or acted as electrodes of lateral electroporation and the flux enhancement results being studied synergically. The small distance of 0.4 mm and 4.0 mm between positive and negative microneedle electrodes meant large electric field even with a small applied bias. The results showed that a 7-fold increase in the delivery of test molecule FD-4 resulting from microneedle puncture (no electroporation), a 20-

fold increase from electroporation alone (the microneedles contacted skin with no puncture), and 140-fold flux increase when the microneedles punctured the skin with applied voltage also applied. This proves that lateral electroporation alone could provide substantial flux enhancement and benefit controllable drug delivery, from which we gained the evidence to develop a lateral wire-mesh electrode electroporation array.

2.6 Electroporation enhanced CNT membrane transdermal drug delivery

2.6.1 Primary hypothesis

Passive drug flux through skin varies greatly between each individual because of the individuality in pore number/size, hair conduit, skin layer thickness, gender, and health condition. Electroporation may enhance drug flux 1-3 orders of magnitude and thus minimize individual differences so a wider variety of drugs may be delivered and at similar flux rates. As therapeutic needs may change each hour or day of the treatment a rate control system is also greatly desired to be incorporated with electroporation, which the CNT membrane have previously achieved in the delivery of nicotine *in vitro* and *in vivo*. It is proposed that by periodical electroporation of the skin to enhance skin permeability, CNT membrane could be used to control the flux rates of drug molecules through the skin as post-electroporation drug permeability through skin becomes greater than that of CNT membrane. Drugs previously incompatible with transdermal delivery due to their low permeability through skin may now be delivered into skin at

switchable rates. Drugs that demands careful flux regulation such as fentanyl and clonidine may also be delivered now transdermally with reduced side effects compared with oral delivery.

In order for CNT membrane to be the rating controlling component, permeability of the drug through skin has to be greater than the flux though the CNT membrane, otherwise the skin would become the rate limiting component in the system. A special wire mesh electrode would have to be designed to efficiently electroporate the skin while requiring low voltage and power consumption to make the system portable.

2.6.1 Experimental

2.6.1.1 Wire mesh fabrication

Two types of micro array electrodes was fabricated in the lab with insulated aluminum wires because of the unusual case of weaving (Most companies weave bare metal wire mesh for various applications). Figure 2.15(a) shows the freestanding wire mesh type with wires secured in frame on the four sides, with average wire distance between wires being 200-250 µm, which limits electric current to the surface of epidermis and caused less pain in the subject.[72] To fabricate the wire mesh, two combs were mounted on stands with their teeth facing each other and in proximity; notches were cut on the top

of each teeth so they could lock wires in place. A rod was positioned in a plane below the combs being parallel to the combs direction to allow a looming geometry of wires (PAC insulated aluminum wires with outer diameter of 75µm was used for fabricating the wire mesh). The leading wire was locked and tied on the teeth of the first comb, winded down to the bottom plane rod then leaded back to the first teeth of second comb, similar to the conventional fabric weaving mechanism. The wires was locked in place in the teeth along the span of the comb until a minimum of 12-14 vertical wires were weaved. After the vertical wires was spun horizontal wires was added in successively by a repetition of interlocking the combs, placing in a horizontal wire, and then pulling apart the two combs. Glue was used on the sides of the wire mesh to define the edges of the mesh and hold wires in place. In order for the wire mesh junction points to act as electrodes the wire mesh was polished using sandpaper to expose the bottom plane of the wire mesh, the side view of a typical polished wire mesh contacting skin is shown in figure 2.16. Electric field would be confined to the bottom plane of wire mesh and top surface of skin since only the junction points of the wire mesh was polished, preventing discharge in other locations and directions.

A second type of wire mesh was developed shown in figure 2.15(b) with more defined structure since the freestanding wire mesh may move during contact with skin changing electrode distance. Insulating wires was interweaved onto a nylon wire mesh with ~200 µm spacing which acted as frame for the woven wire mesh. The skin-contact

conjunction points was polished similar to the freestanding wire mesh to act as electrodes.

2.6.1.2 Chemicals and experimental methods

Calcein was selected as the test molecule for measurement of electroporation efficiency with wire mesh electrode array. Calcein is a fluorescent molecule with MW of 622.55, -4 charge, and solubility in water at low concentrations. At pH=7.4, 1mM concentration calcein solution appeared yellow-green, with the excitation wavelength and emission wavelength being 495/515 nm, respectively. Calcein was selected for this study because it crosses intact skin in very small amounts under passive diffusion conditions and was used commonly in electroporation studies for its simplicity of detection. The donor solution is 1mM calcein mixed with 0.9% saline, with pH was adjusted to 7. The receptor solution is 0.9% saline. MCNTs and SWCNTs were bought from cheaptubes.com.

Fresh porcine pig ear skin was obtained from a local abattoir. Front and back side ear skin was dermatomed to 250-300 µm thick pieces and kept in -20°C refrigerator until use. Before conducting an experiment the skin is taken out and thawed in 0.9% saline under room temperature. Skin with resistance below 6kohms/cm^2 is discarded because the low electric resistance indicated a damaged skin and another piece of skin is tried.

Pulses were delivered by a Keithley 2430 potentiostat. In this study 180-360 pulses of 100-150 V were delivered at 1-5 ms duration and 1 Hz, which were the electric parameters which electroporated the stratum corneum with high electrical efficiency according to a previous report.[73] Pulses from Keithley 2430 were checked by an oscilloscope to ensure that pulses with desired voltage and duration were obtained from the potentiostat.

A flow cell setup was used to measure calcein flux enhancement from wire mesh electroporation which is shown in figure 2.17. Upstream of the sample chamber is a syringe pump with the injection speed set to 400 µL/h. The diffused calcein through skin is carried by the flow of saline into the autosampler, which was set to rotate every 30-60 min so samples were collected every 30-60 minutes, depending on the needs of the specific experiment. The calcein concentration from collected samples was measured on a Fluorospectrometer with the calibrated detection limit to be 10^{-4} µg/L.

2.7 Electroporation results and discussion

2.7.1 Electroporated skin resistance recovery

Transverse skin resistance was routinely used to gauge the integrity of the barrier function of the stratum corneum, so a U-tube setup was used to measure transverse skin resistance with the skin clamped between 2 U-tube half-cell. 0.1M KCl solution

filled both sides of the U-tube and 2 Ag/AgCl electrodes were used as working and reference electrode, with the working electrode on one side of the U-tube and the reference electrode on the other side of the U-tube. Under this setup, intact fresh dermatomed skin measured 11-22 kΩ/cm^2, which agreed well with previous publications. Electroporation was applied to the skin with electric parameters of 5ms duration, 180 pulses, and 100V using the wire mesh array as electrodes, after which the electroporated skin was quickly mounted in the U-tube setup in order to measure transverse skin resistance. Skin resistance measured 3-4 kΩ/cm^2 immediately following electroporation. This drop in resistance was associated with the creation of new aqueous pathways and enlargement of existing conduits, which allowed increased ionic current through the skin resulting in decreased skin resistance. In a time span of 2-4 hours resistance of the skin recovered to70-80% of its original value of 11-22 kΩ/cm^2, with the final value dependent on the voltage used. It is generally accepted that resistance recovery time is related to flux enhancement duration and the resistance recovery percentage indicating reversibility of electroporation, as extremely high voltages of up to 300+ volts have been used to electroporate the skin and have shown low reversibility with the end skin resistance covering to 20-30% of its initial value. In this case not only aqueous pathways were created but also permanent changes to the stratum corneum structure.

2.7.2 Electroporation enhanced calcein flux

Dermatomed skin pieces with intact stratum corneum structure were electroporated by the wire mesh electrode with the setup shown in figure 2.17. Typical flux enhancement plot as measured by fluorospectrometry is shown in figure 2.18. It can be seen that after electroporation of the skin at start of hour 2, calcein flux continued to increase from hour 2 to hour 6 until it stabilized at ~$1*10^{-3}$ μg/(cm^2*h), which is ~10 fold enhancement compared to initial flux. This enhancement ratio understands well with similar lateral electroporation device reports, but is smaller compared to transverse electroporation enhancement which can yield enhancement factors up to 1-3 orders of magnitude.[68,70,71] As shown in figure 2.13, lateral electroporation sacrificed some of the enhancement efficiency for a more practical lateral geometry which can be exploited in building compact electroporation devices. Conventional electroporation devices were designed to clamp the skin or "pinch" the skin in order to partially transverse the skin, which is impractical for long-term transdermal drug delivery and cumbersome. Lateral electroporation by means of either wire mesh or electrode array could be easily coupled with transdermal patches/ CNT membrane on one single piece of device. Both freestanding wire meshes and nylon mesh supported wire meshes have successfully shown the ability to electroporate the skin to increase calcein diffusion flux through the skin, yet the nylon mesh supported wire mesh is probably preferred in future experiments due to its robustness.

2.7.3 Outlook of electroporation enhanced CNT membrane transdermal drug delivery

The combination of CNT membrane and electroporation may be the solution to a key practical problem with transdermal drug delivery: the need for a programmable rate controlling device that can deliver beyond a small set of drugs, limited by low diffusion flux. CNT membranes have shown their ability to programmably deliver nicotine and other molecules. It is planned that coupled with an electroporation device to disrupt the skin barrier, CNT membranes may be able to programmably deliver a variety of drug molecules at an enhanced rate. Although a series of electroporation experiments with wire mesh have been shown to greatly enhance calcein test molecule flux, the results were inconsistent through a series of repetitions. In some trials the enhancements were only 2-3 fold and in some experiments enhancement was not noticeable. Upon scrutiny of wire mesh contact with skin, the main problem was identified to be insufficient wire mesh electrode contact with skin: although initially the skin was rigid and firm at the start of experiment when it topped the sampling chamber, after 4-6 hours it became loose and bent due to solution flow hydration, which meant the loss of contact between the skin and the wire mesh. The second problem identified was the mediocre quality of wire mesh and the polishing process: even though wire meshes were home-made to the highest standard, over-polishing occurred in some of the junction points which meant electric field was not only confined to the skin but also being released into the donor solution, dissipating electric energy. This did not have adverse effects in previous reports as in their practices the skin was first dry electroporated, the electroporation device removed from skin, and then the donor solution being applied so no contact of donor solution and electrodes existed during electroporation.[73] In our system where a

continuous electroporation setup the contact between donor solution and electrodes was necessary, electric field confinement became a serious problem.

A possible solution was to measure electroporation enhancement flux by the microdialysis setup which was discussed in the previous section. The removal of a solution flow filled sample chamber meant the wire mesh is in firm contact with skin, ensuring the confinement of electric field to the stratum corneum so the entirety of electric energy would be released on the skin. Another possible solution would be the use of a confined electrode array as reported by J.C. Weaver et al,[74] where an insulation disc was used to completely surround disc shaped electrode on all sides except the side that was in contact with skin to force electric field through skin instead of dissipated in donor solution. This approach however requires sophisticated micro-fabrication, which at the present stage seemed hard to be combined with a CNT membrane.

2.8 Conclusions

In this chapter CNT membranes were utilized for its abilities to programmably deliver molecules. The research was divided into two related sections: 1) The use of CNT membranes to transdermally deliver nicotine with switchable rates and the use of microdialysis to accurately map time dependent delivery profile; preparation of nylon mesh supported CNT membranes for safe animal studies. 2) The use of electroporation

combined with CNT membranes to expand the types of deliverable drugs and enable delivery with switchable rates. For the first section promising *in vitro* results showed that microdialysis could accurately map nicotine delivery profiles under skin and following *in vivo* hairness guinea pig experiments were expected in the future. In the second section results were not so promising, the major setback being insufficient wire mesh electrode contact with skin which resulted in inconsistent results. Either a microdialysis setup that removes the sampling chamber to ensure electrode-skin contact or micro-fabricated insulated disc electrode was suggested to solve the problem. Only after wire mesh electrodes could electroporate the skin with good repetition rates and high enhancement ratio can we combine it with CNT membranes to show programmable transdermal delivery of a variety of drugs in the future.

The eventual vision was a portable transdermal device that could safely and programmably deliver a variety of drugs under remote counseling, as in addiction treatments of nicotine it is most effective to administer psychological counseling, although currently prohibitive due to high costs.[75] By using smartphones which can be designed to programmably control CNT membrane delivery rates by simply a change in voltage bias, remote counseling could be achieved over the phone or by internet. The patient can receive doctor administered delivery profiles at home and conveniently use smartphones to control drug flux without making visits to the hospital.

Table 2.1 List of transdermal patches and characteristics

Active ingredient	Product name	Dose and size Of patch	Dose delivered	Clinical indication
Clonidine	Catapres-TTS	2.5–7.5 mg in 3.5–10.5 cm^2	0.7–2.1 mg in 7d	Hypertension
Ethinyl oestradiol (EO)	Ortho-Evra	0.75 mg EO and 6 mg N in 20 cm^2	0.14 mg EO and 1.05 mg N in 7 d	Birth control
Fentanyl	Duragesic	2.5–10 mg in cm^2	1.8–7.2 mg in 3 d	Analgesia
Nicotine	Habitrol Nicoderm-CQ Nicotrol	8.3–114 mg in 3.5–30 cm^2	5–22 mg in 16–24 h	Smoking cessation
Nitroglycerin	Nitro-Dur Transderm-Nitro	12.5–160 mg in 5–40 cm^2	1.2–11.2 mg in 12–14 h	Angina
17β-oestradiol	Alora, Climara Esclim, Estraderm FemPatch, Vivelle	0.39–20 mg in 2.5–44 cm^2	0.075–0.7 mg in 3–7 d	Hormone Replacement
Oestradiol (O), norethindrone (N)	*CombiPatch*	0.51–0.62 mg O and 2.7–4.8 mg N in 9–16 cm^2	0.15–0.20 mg O and 0.42–1.0 mg N in 3–4 d	Hormone Replacement
Oxybutynin	Oxytrol	36 mg in 39cm^2	11.7–15.6 mg in 3–4 d	Overactive bladder
Scopolamine	Transderm Scop	1.5 mg in 2.5 cm^2	1.0 mg in 3 d	Motion sickness
Testosterone	Androderm Testoderm TTS	10–328 mg in 37–60 cm^2	2.5–6 mg in 1 d	Hypogonadism

Data reproduced from ref.45

Table 2.2 KCl screening current and nicotine ON/OFF ratios of Porifera membranes; comparison with microtome-cut CNT membranes

Membrane	CNT Inner Diameter (nm)	0.1 M KCl screening Current (μA)	Nicotine flux in flow cell setup w/o skin OFF state (μmole/h*cm^2)	Nicotine flux in flow cell setup w/o skin ON state (μmole/h*cm^2)	ON/OFF ratio of nicotine flux
13 batch Porifera	3	0.3-0.4	0.25	1.6	6.40
16 batch Porifera	6	1-2	0.40	1.98	4.95
25 batch Porifera	3	0.6-0.8	0.028	0.13	4.64
46 batch Porifera	2	40-50	0.08	0.04	0.50
47 batch Porifera	2	45-50	0.09	0.05	0.56
50 batch Porifera	6	3-7	0.04	0.04	1.00
Microtome cut CNT membrane (2.5%)	1.6	8-10	0.17	1.35	7.94

Table 2.3 Effects of electroporation on the skin and analysis methods. Reproduced from ref. 69

Investigation method	Observations
Visual aspect	Mild reversible erythema
Impedance	↓ Resistance (up to three orders of magnitude on a time scale of microsecond)
FTIR	=fluidity of the lipid alkyl chain, ↑ hydration
DTA	=T° (T2 and T3+4), ↓ in enthalpy→disordering
Xray scattering	↓ lamellar ordering, ↓ intralamellar packing
FFEM	Spherical deformations, rough surfaces disorganization of the lamellae, appearance in a network-like structure
TEWL	Mild reversible increase (impairment in barrier function)
LDV	Mild reversible increase in blood circulation, no significant modification in blood flow
LDI	Reversible (10 min) decrease in blood circulation
Chromameter	Mild reversible erythema, no erythema
Clinical evaluation	No skin irritation, Electrical sensation well tolerated by most patients

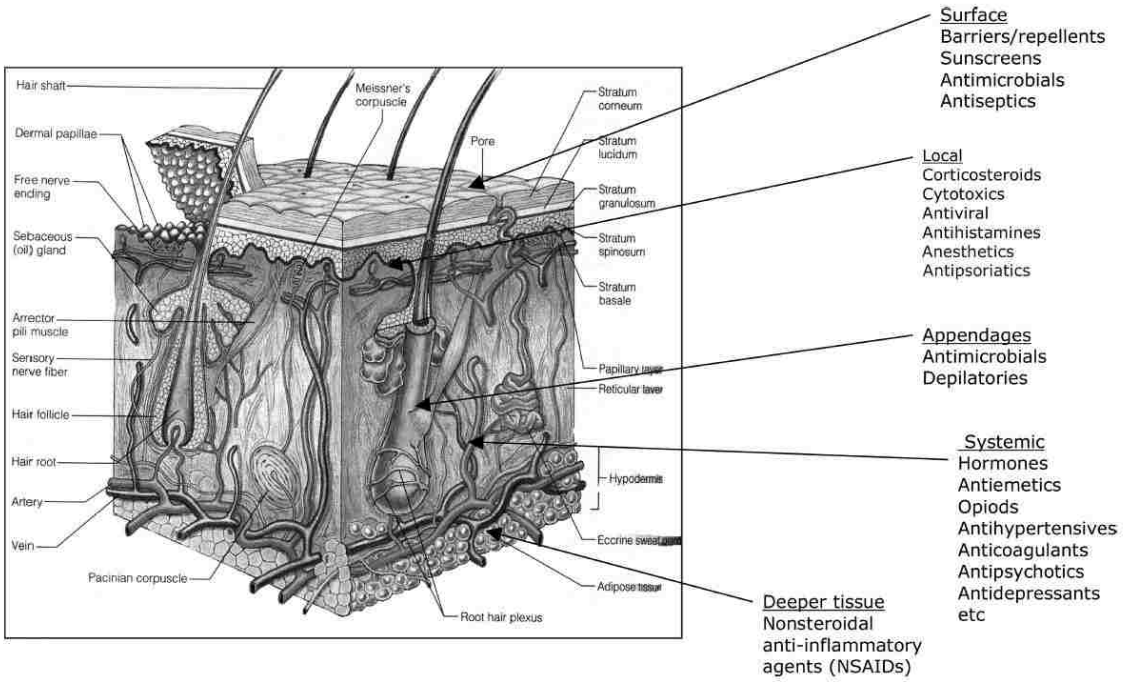

Figure 2.1 Detailed structure of the skin. Reproduced from ref.44

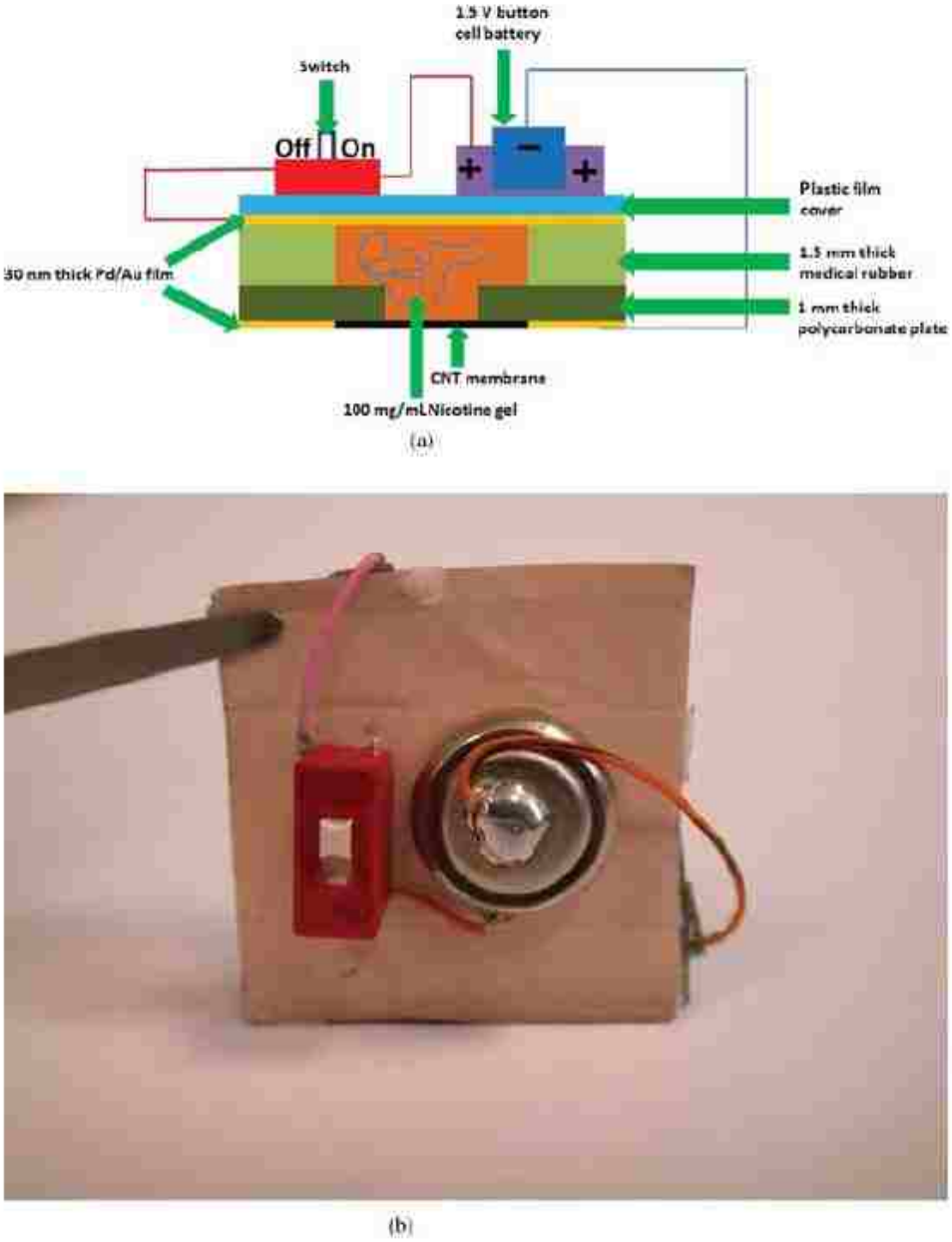

Figure 2.2 (a) Schematic of the CNT membrane for the in vivo transdermal drug delivery of nicotine in hairness guinea pigs. (b) Optical image of the top of the device. Reproduced from ref.42

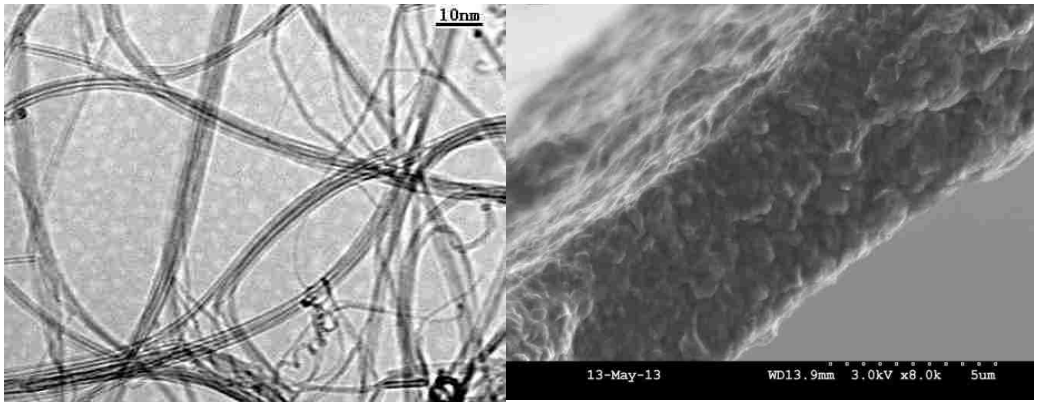

Figure 2.3 (a) TEM of the DWCNT as purchased (cheaptubes.com). (b) SEM Cross section of the as-microtomed DWCNT membrane (Model S-3200-N Hitachi SEM). (c) Top view of as-microtomed DWCNT membrane.

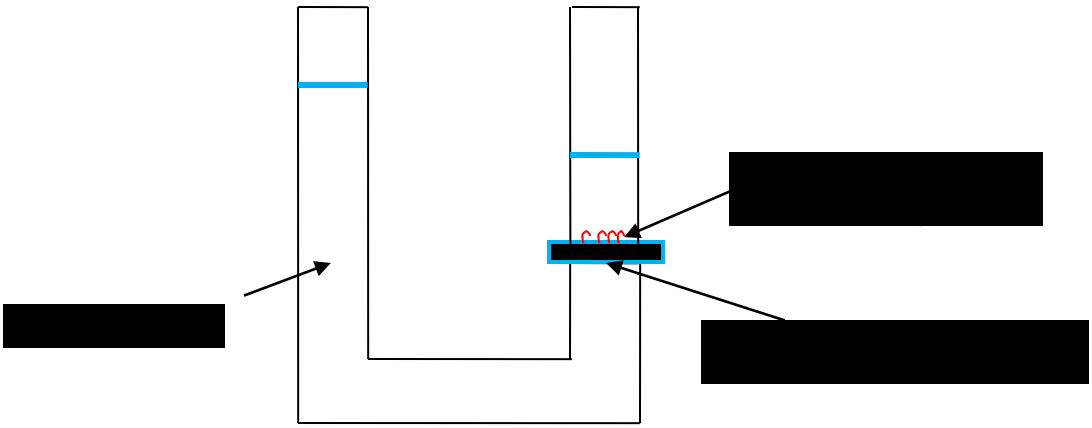

Figure 2.4 Schematic of U-tube setup for CNT membrane functionalization. The top side of the membrane is immersed in either diazonium solution or direct blue solution with EDC and sulfo-NHS. 2cm DI water pressure column is maintained to confine functionalization to the tip of the membrane. The average membrane area is approximately 0.07 cm^2.

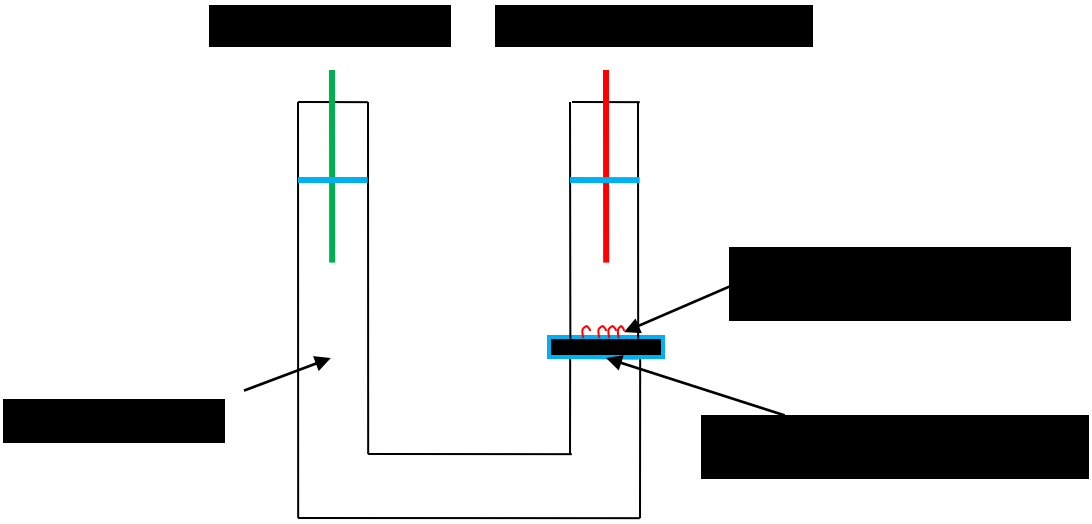

Figure 2.5 Schematic of U-tube setup for KCl screening of CNT membranes.

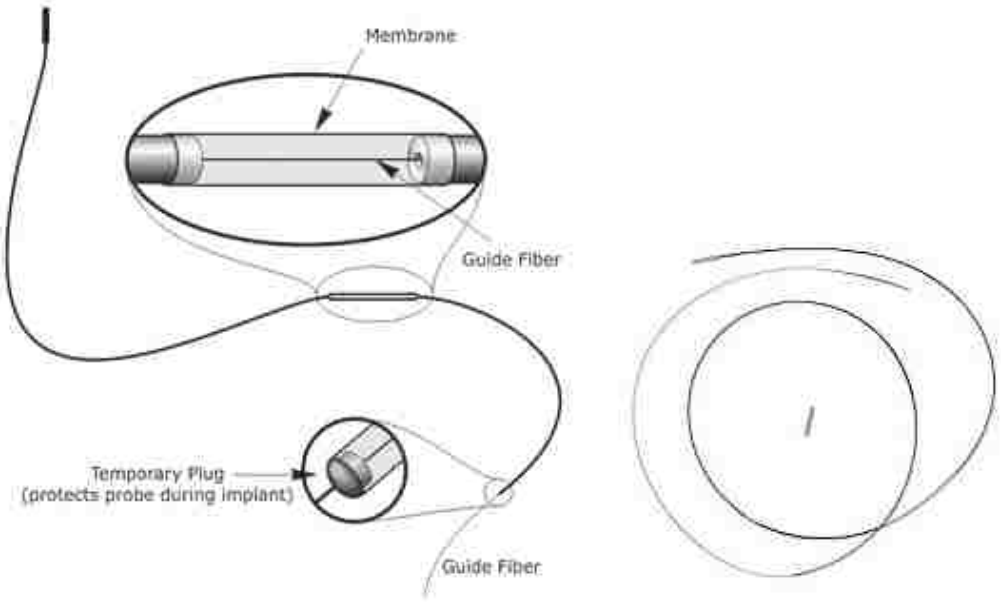

Figure 2.6 Schematic of microdialysis probe. Reproduced from BASi, the manufacturer.

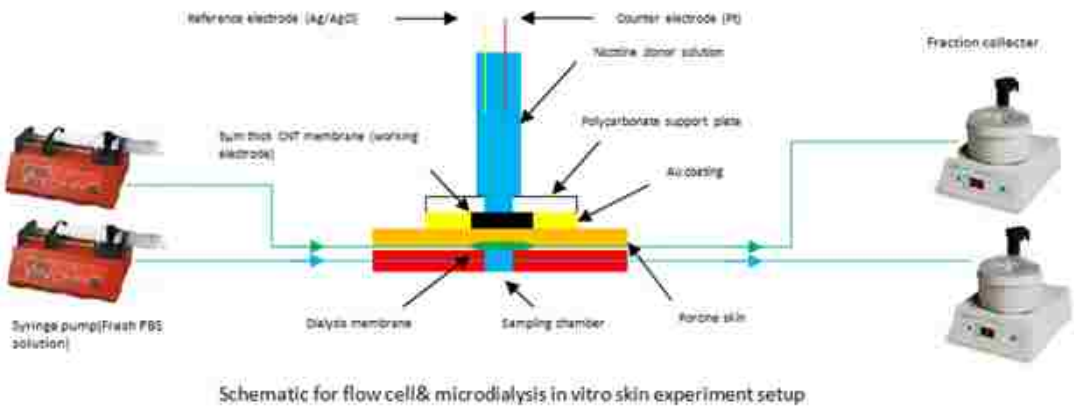

Figure 2.7 Schematic of microdialysis& flow cell setup.

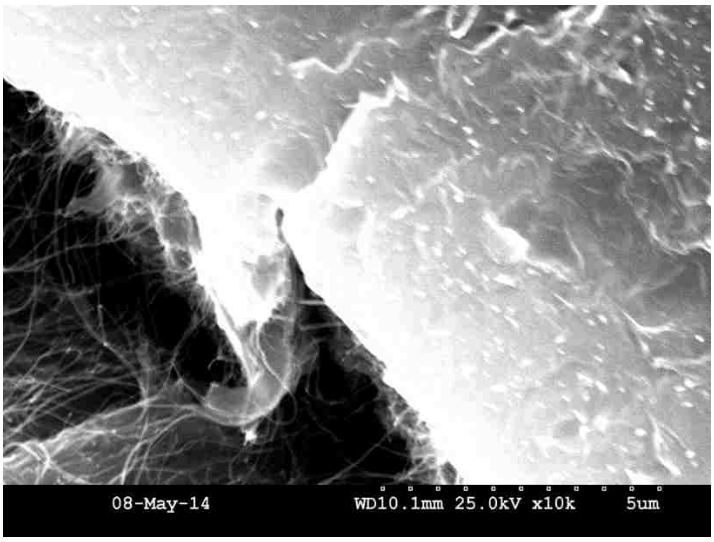

Figure 2.8 SEM images of batch 16 Porifera membranes. (a) Top view of CNT membrane surface. The white dots are CNT tips which protrude out of embedding polymer. (b) Top and cross section view of the membrane. The top surface can be seen with protruding CNTs, while many CNTs can be seen protruding out from the cross section.

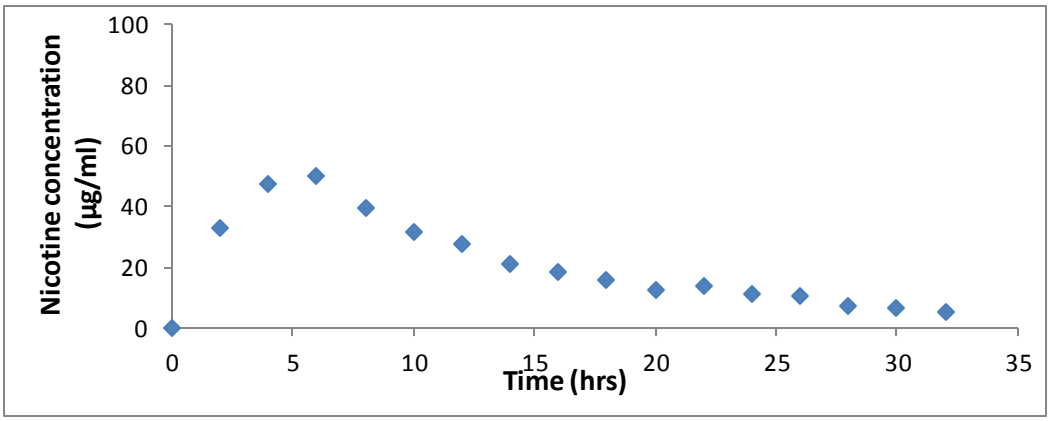

Figure 2.9 Nicotine flux measured by microdialysis membrane implanted in complete thickness porcine skin with Nicoderm application (0-6h) and removal (6-32h).

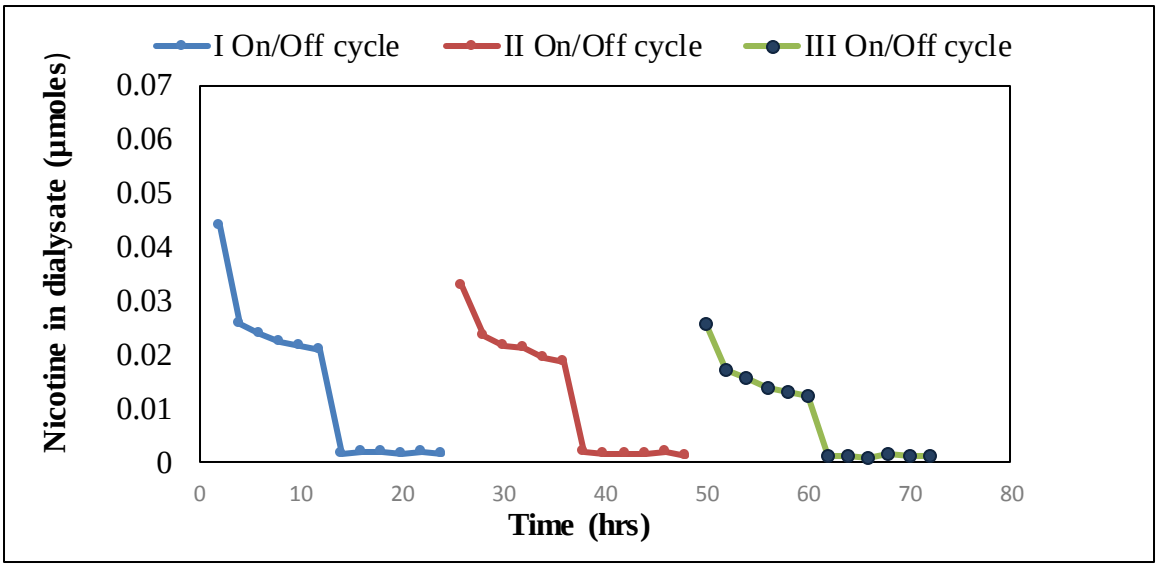

Figure 2.10 Nicotine flux measured by microdialysis membrane below 200-300 µm thin skin. Nicotine was administered by a 0.07 cm^2 Nicoderm patch (cut to the same size as CNT membrane for comparison) during 0-12h and removal 12-24h. Three cycles of ON/OFF with 12h ON and 12h OFF were used.

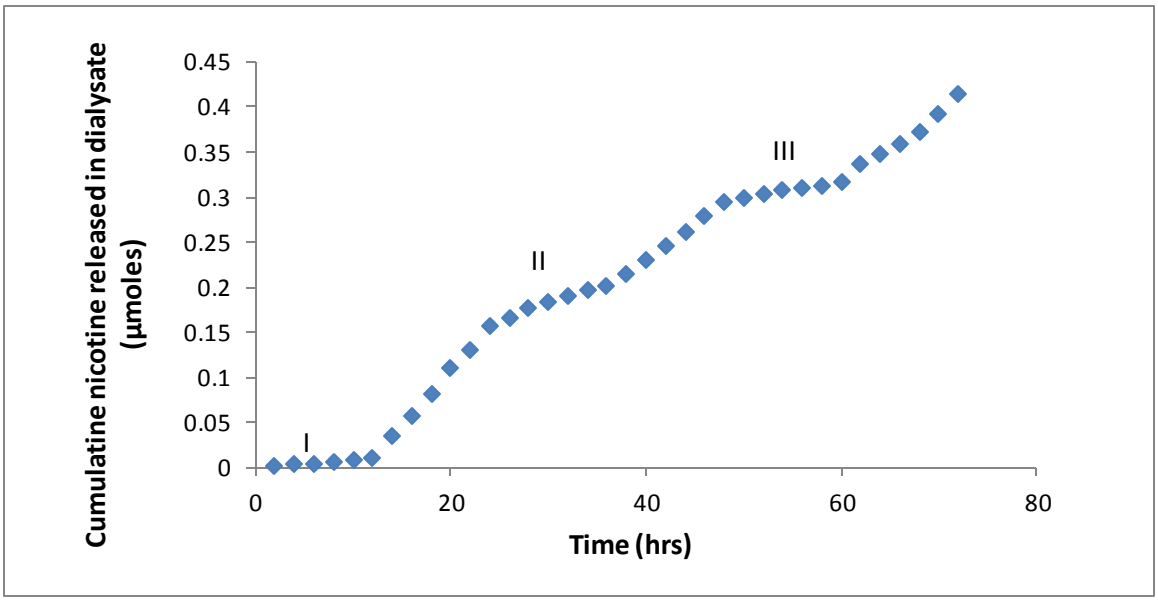

Figure 2.11 Switchable nicotine delivery of CNT membrane measured by microdialysis. Shown with 3 cycles of ON/OFF.

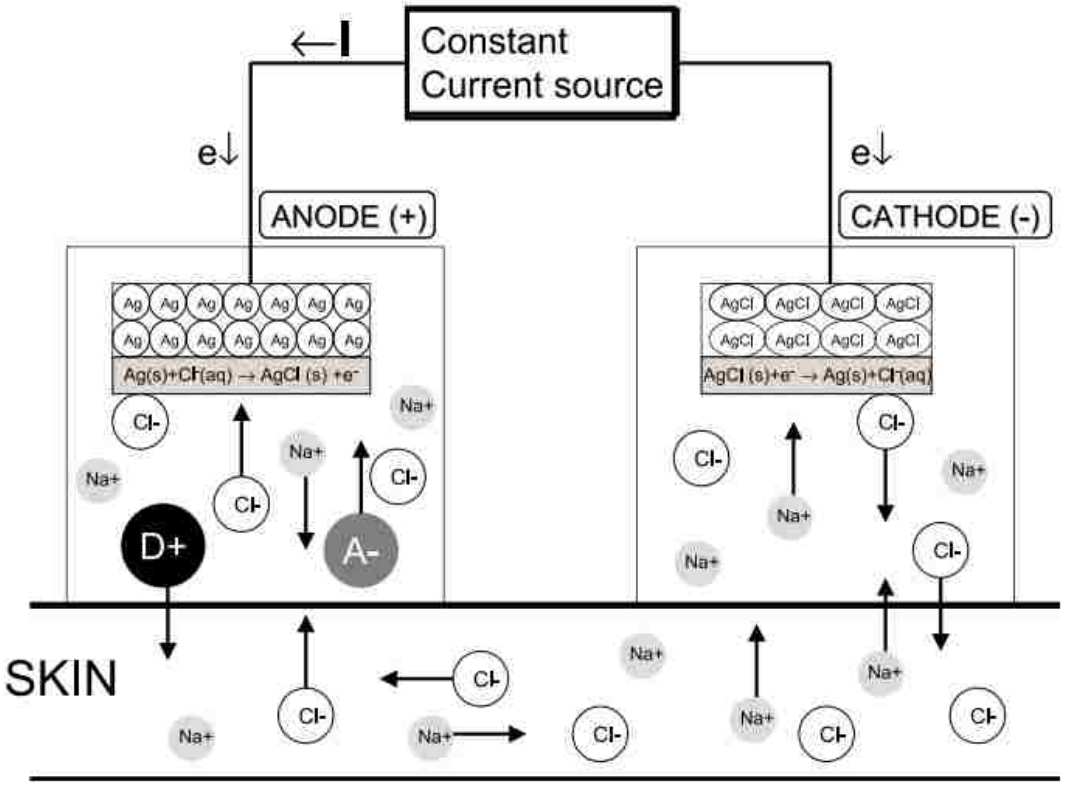

Figure 2.12 Iontophoresis using Ag/AgCl electrodes. The ionizable drug D^+ with its counter ion A^- is placed within anode compartment. Application of current flows within the iontophoresis system. Electromigration transports the cations D^+ into the skin. The flow of drug ions is counterbalanced by transport of endogenous Cl^- ion movement. Reproduced from ref.61

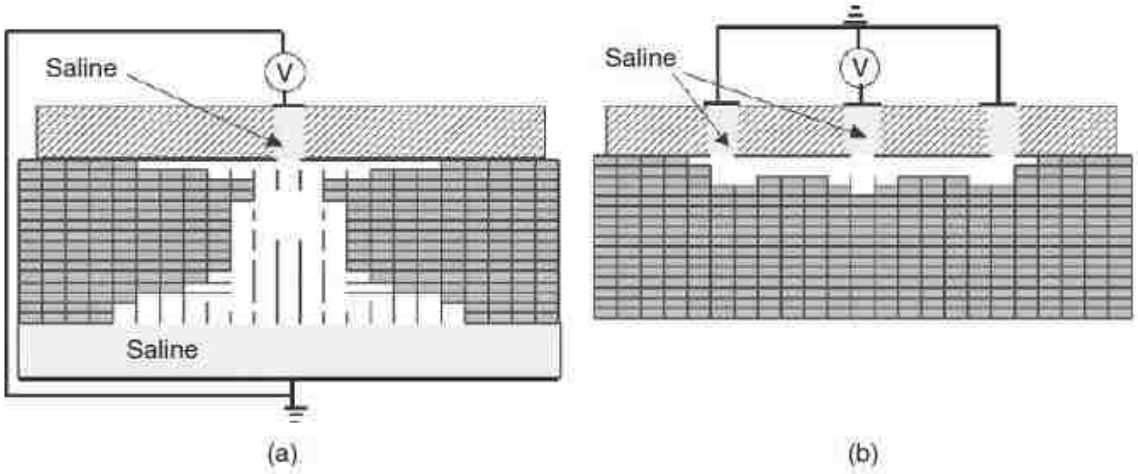

Figure 2.13 Illustration of (a) transverse and (b) lateral electroporation. The array of rectangles represent the brick and mortar structure of the stratum corneum. Reproduced from ref.70

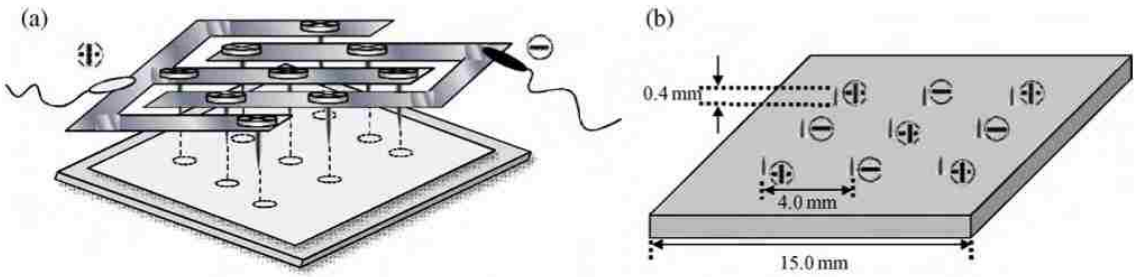

Figure 2.14 In-skin electroporation device built on a microneedle array. (a) The microneedles were separated into two groups with one group being applied positive bias and the other group being applied negative bias. (b) Upon contact with the skin, lateral electric field will electroporated the skin in the stratum corneum layer. The distance between electrodes vertically aligned are 0.4 mm, and horizontally aligned 4.0 mm. Reproduced from ref.72

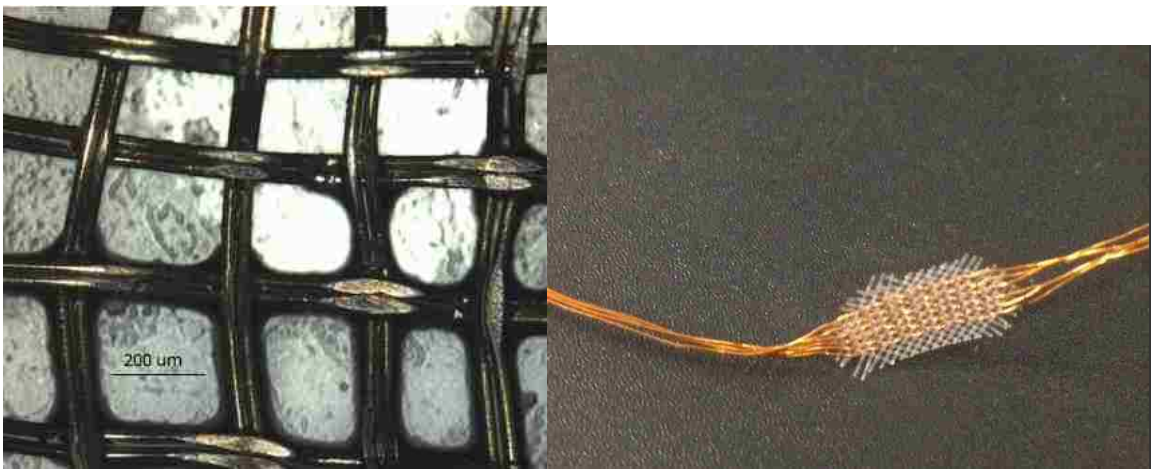

Figure 2.15 (a) freestanding type wire mesh after polishing out metal contacts viewed under microscope. It is stained orange/green of the calcein. (b) Optical image of nylon mesh supported wire mesh.

Figure 2.16 Side view of polished wire mesh in contact with skin. In unpolished areas aluminum is insulated by PAC coating so electric discharge is confined to the bottom plane. The silver segments show exposed aluminum acting as electrodes for electroporation.

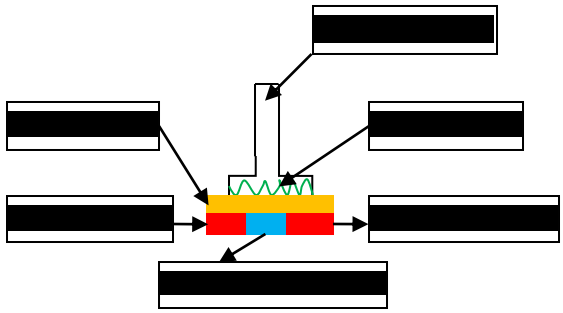

Figure 2.17 Flow cell setup of wire mesh electroporation. The syringe pump supplies PBS at set rate which flows into the sampling chamber and carry out permeated calcein. The fraction sampler collector collect samples at set intervals which was examined by fluorescence spectroscopy.

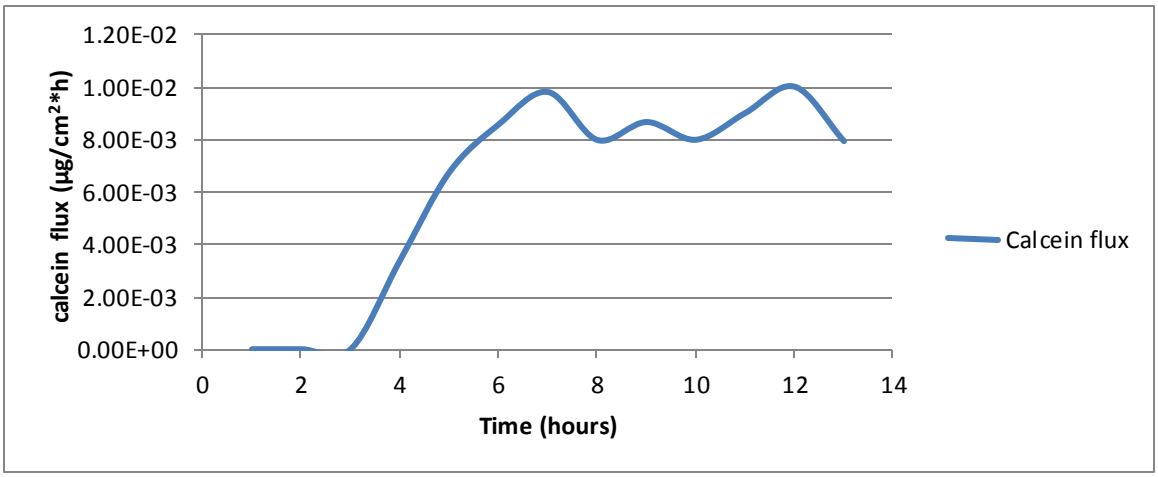

Figure 2.18 Calcein flux after electroporation. Electroporation using wire mesh electrode was applied at start of hour 2 with 180 pulses of 100V, 5 ms duration.

Chapter 3 Aptamer based gating of ionic transport through CNT membranes

3.1 Introduction

Due to their remarkable properties carbon nanotubes were fabricated into carbon nanotube membranes and previously utilized for programmable delivery of nicotine. However the smooth frictionless inner sidewall, small diameter, high conductivity, and unique geometry of carbon nanotubes make them equally ideal for studying ionic flow phenomenon in nano-sized tunnels. A series of studies by various groups was performed to explore mass flow inside carbon nanotubes and through CNT membranes. L. Sun, R.M. Crooks studied mass transport in a single carbon nanotube membrane, though due to the large 150 nm diameter of the carbon nanotube no significant deviation from conventional continuum model was observed.[32] F. Fornasiero, O. Bakajin et al. observed fast single profile water flow in sub-2-nm CNT membrane and ion rejection due to steric hindrance and charge repulsion at CNT tip. Later H. Liu, S. Linday, C. Nuckolls et al. successfully translocated single stranded DNA through single-walled carbon nanotubes, using ionic current change during DNA blocking of carbon nanotubes during translocation for detection.[76] J. Wu, B.J. Hinds et al found that as the mobile cation diameter matched the inner diameter of single walled carbon nanotubes, nearly ideal electroosmostic flow rate of 0.16 cm s^{-1} V^{-1}could be achieved, which is 25-110 fold improvement compared to conventional nanoporous materials.[41] J. Wu, B.J. Hinds et al also studied electrophoretically induced aqueous flow through small diameter single

walled carbon nanotubes,[77] where under low ionic concentrations the observed electrophoretic mobility of K^+ was three times higher than that of bulk electrophoretic mobility. A potential explanation given for the efficient electroosmosis is that at sufficiently low concentrations, the anionic carboxylate groups at CNT tips can reject anions allowing only cations to flow through CNT core resulting in net enhanced electroosmosis flow. An interesting ionic flow rectifying diode effect based on ionic size was also observed for the first time, while a similar previous observation of rectification was primarily based on surface charge exclusion.[78]

Basing on these interesting studies on ionic flow phenomenon in carbon nanotube core, in this chapter we utilize the special attributes of carbon nanotube membranes to study the reversible aptamer gating of CNT membrane and enhanced electroosmosis effect of CNT membranes for water pumping.

3.2 Aptamer Introduction

Aptamers are short (15-70 nucleotides) synthetic DNA or RNA strands that can specifically bind to non-nucleic acid targets, such as peptides, proteins, drugs, organic and inorganic molecules with high affinity.[79,80,81,82] Since the first reports in 1990 that short RNA and ssDNA with high binding affinity could be screened from a large randomized library, potential application of aptamers was quickly explored, especially in

the field of therapeutics and diagnostics.[83] There are several advantages that make aptamers ideal for use in analytics. Firstly, aptamers could be screened and mass replicated *in vitro* via SELEX (Systematic Evolution of Ligands by EXponential enrichment) technique without the need of animal hosts or expensive cell culturing facilities.[84] The schematic flow chart of SELEX method is shown in figure 3.1,[85] where a large pool of single stranded oligonucleic acid sequences (>10^{10}) were contacted with the target molecule under certain conditions during which some would specifically bind to the target. The sequences that specifically binded to the target are isolated and repeatedly contacted with the target again for refining the selection process, and only the most adequate sequences were finally isolated and amplified by PCR, yielding the final aptamer sequence. It should be noted that multiple aptamer sequences may rise for a single target but only the one with highest affinity and specificality was usually chosen for further applications.

Aptamers have also shown remarkable specificality and affinity comparable to traditional bio-recognition agents and anti-bodies. R.D. Jenison et al. reported theophylline binding RNA with K_d values in the picomolar range which was superior to their anti-body counterparts.[86] They also found that the dissociation constant for theophylline is 10,000 fold greater than the RNA's affinity for caffeine, even though caffeine differs from theophylline only by a methyl group at nitrogen atom N-7. These results show that aptamers hold great potential in target recognition and discrimination.

Finally aptamers have shown to be versatile and robust molecules that could be functionalized with various linkers and immobilized on an array of substrate surface to exert their recognizing capabilities while preserving its natural structure. Fluorophores, enzymes, and other functional molecules such as carbon linkers, amines, biotin, cyanine, and thiols could be attached to aptamers during their synthesis process, making them viable for further functionalization and grafting.

Due to these desirable properties aptamers have been used in development of aptasensors,[87] for bioanalysis,[88] drug delivery,[89] and molecular beacons. A molecular beacon is a modified aptamer sequence that consisted of the original sequence and a complementary base sequence which allowed the formation of a hairpin structure. As shown in figure 3.2, before binding to the target no fluorescence is emitted from the aptamer because the fluorophore is close to the quencher. Upon binding to the target, the conformation of the aptamer dramatically changes, opening up into single profile which separates the quencher and fluorophore, as the result fluorescence is emitted from the aptamer and detected. Molecular beacon type hairpin aptamers are of special interest to us because their ability to dramatically change configuration upon binding of a target. Shown in figure 3.3(a) is an original ATP binding aptamer which exhibited minimal conformation change upon binding to 2 AMP molecules; in 3.3(b) considerable conformation change was displayed by a modified hairpin type ATP binding aptamer. Upon binding to 2 AMP target molecules, the added hairpin sequence dissociated from

its complementary section of the original aptamer, leaving a single strand behind. The ability of the molecular beacon type aptamer to change conformation upon target identification and binding is ideal for the gating of CNT membranes pores to exert a switch mechanism between high and low flux.

3.3 Hypothesis of reversible CNT membrane gating by ATP hairpin aptamer

Carbon nanotube (CNT) membrane is a robust platform that mimics natural cell membranes with the advantages of fast flow and selectivity. Crooks et al. reported the flow of polystyrene through a membrane containing only a single 150 nm diameter carbon nanotube, which was the first quantitative study of mass transport through carbon nanotubes.[32] B.J. Hinds et al later reported a CNT membrane fabricated by embedding vertically aligned MWCNT array in polystyrene which made possible macro-scale studies of fluid/gas flow and ionic transport in carbon nanotubes.[33] Carbon nanotube membranes offer unique attributes which make them desirable for acting as artificial biomimetic membranes: (1) an amazing 4-5 orders of magnitude higher enhanced fluid/gas flow compared to conventional polymeric membranes. (2) High conductivity allowing electrochemical grafting and electrophoretic/ electroosmosis transport. In previous pursuits to mimic biological membranes, gatekeeper molecules were placed at the tip of carbon nanotubes of CNT membranes to allow to an extent ion flux control and selectivity. Majumder et al. studied the gate keeping effects of CNT membranes with respect to ion transport selectivity and flux by functionalizing the CNT

tips with negative dyes, observing 4 times cationic molecule flux increase over as-made membranes.[34] By the combination of tip functionalization coulombic attraction and efficient electrophoresis& electro-osmosis, J. Wu, B.J. Hinds et al. achieved the controllable delivery of nicotine by CNT membranes *in vitro* and *in vivo*.[40,42] In this regard remarkable flux control and selectivity were realized on CNT membranes either through passive reactions induced by functionalization or combined electrophoresis& electro-osmosis effects by applying an electric bias. However to our knowledge stimuli responsive gating of CNT membranes by aptamers have not been reported before, even though the use of aptamers in nanopore gating have been reported previously: Abelow et al. modified 20 or 65 nm glass nanopores with cocaine aptamers to control ion transport upon reversible binding of the aptamer with cocaine molecules[90]. Zhu et al. showed that controlled release of Ibuprofen from mesoporous silica nanoparticles could be achieved by deploying aptamer-gold nanoparticle as a molecular gate.[91] Similarly, V. C. Ozalp et al. used molecular beacon type ATP aptamer to gate mesoporous silica nanoparticles and regulate the release of fluorescein upon reversible binding to ATP target in the environment.[92,93]

We herein report the first case of gating CNT membranes with molecular beacon type ATP aptamers to allow ionic flux control through the core of CNTs, using the ATP/adenosine binding sequence originally selected by Huizenga et al.[94] The original ATP binding aptamer was transformed into a molecular beacon type aptamer by adding

an additional hairpin sequence (figure 3.3a, b) which gave the aptamer pronounced conformation change upon binding to the target, allowing more efficient gating.[85] The aptamer was grafted on to the tip of single-walled carbon nanotubes in the CNT membrane, in its natural state resuming a hairpin double helix configuration at the nanotube tip with a width of ~2nm. The small inner diameter of SWCNT (average inner diameter 1.5 nm) meant that this double helix structure could spatially limit the flux of ions through the carbon nanotube core and acts as a molecular gate. Upon binding to the target molecule (AMP), the hairpin-like structure breaks down leaving in the proximity of the carbon nanotube tip a single-stranded region, allowing higher flux of ions to transport through the carbon nanotube core thus opening the gate. The changes in ionic flux could quantitatively be determined by applying potentiostatic bias to the CNT membrane system and measuring current, which in turn confirms the conformation change of the aptamer. This stimuli responsive CNT membrane gating mechanism represents a new direction in development of smart biomimetic artificial membranes.

3.4 Experimental

3.4.1 Materials

SWCNT with an average core diameter of 1.5 nm was purchased from cheaptubes.com. MHHPA(hexahydro-4-methylphtalic-anhydride, mixture of cis and trans), catalyst (2-ethyl-4-methyl-1H-imidazole-1-propanenitrile, MES(2-[N-morpholino]ethane sulfonic

acid), AMP(adenosine 5' monophosphate), EDC(ethyl-(N',N'-dimethylamino)propylcarbodiimide hydrochloride), sulfo-NHS(N-hydroxysulfosuccinimide), Direct blue 71 dye, Dowex monosphere 650C cation resin, Dowex monosphere 550A anion resin was purchased from Sigma Aldrich. Note that AMP was used for binding experiments instead of ATP because the aptamer binds to both ATP and AMP, however AMP is more stable than ATP in solution, so it is frequently chosen for binding experiments. The hairpin type ATP aptamer with the sequence 5'-CAC CTG GGG GAG TAT TGC GGA GGA AGG TTC CAG GTG-NH_2-3' was synthesized by Sigma Aldrich. Filter membranes with pore size 1 µm and 20 µm PTFE unlaminated was purchased from Sterlitech. $[Ru(bpy)_3]_3[Fe(CN)_6]_2$ solution was obtained by first ion exchanging $K_3Fe(CN)_6$ into $H_3Fe(CN)_6$ and $Ru(bpy)_3Cl_2$ into $Ru(bpy)_3(OH)_2$, then mixing of the two solutions.

3.4.2 Membrane fabrication

SWCNT with 2% loading was fabricated with modifications from a previous method.[32] To describe it briefly 0.1g DWCNTs were first dispersed in 1L DI water with 2g SDS under tip sonication at 10W, 20% magnitude for 2h (Qsonica, Model S-4000, tip size of 1/8 inch). The solution was then filtered through 20 µm PTFE membrane to remove CNT bundles and impurities, after which SWCNTs were gathered from the filtered solution on a 1 µm PTFE membrane. The purified SWCNTs are then retrieved and mixed with Epon 862,

MHHPA, surfactant Triton X-100, and catalyst by a Thinky^{TM} centrifugal shear Mixer. The mixed CNT-epoxy is degassed through vacuum (Welch 1400B pump) to remove bubbles and cured under 85^{O}C to appropriate hardness for cutting into 5µm thick membranes with a Reichert-Jung microtome. The cut membranes (0.6 cm x 0.6 cm) were glued over a 3mm hole in polycarbonate plate to act as mechanical support, where the top side of the membrane is in the recess of the hole and the bottom side of the membrane is designated on the bottom plane of the polycarbonate plate. Both sides of the as-prepared SWCNT membrane were treated with water plasma oxidation for 1min to remove extra polymer at CNT tip.

3.4.3 SWCNT membrane functionalization

To activate the membrane surface, the SWCNT membranes were first flow-grafted (FG) with benzoic acid by immersing the top of the membrane in 100 mM 4-carboxy phenyl diazonium tetrafluoroborate and under 2 cm DI water pressure at the bottom of the membrane for 12 h using U-tube fitting setup. Following diazonium grafting, aptamers were grafted onto the tip of carbon nanotubes by an EDC/sulfo-NHS coupling reaction between the diazonium carboxylate groups on the CNT and amine groups on the 3' end of aptamers. It should be noted that flow grafting with 2 cm DI water pressure limited diazonium and subsequent aptamer functionalization to the tip of the carbon nanotubes, protecting the inner sidewalls of carbon nanotubes from undesired

reactions. Several buffers and solutions were prepared for the functionalization process: 1) 50 mM MES (2-(N-morpholino) ethanesulfonic acid) pH 5, PBS (phosphate buffered saline) pH 7.4, and PBS (phosphate buffered saline) pH 8.0.

To describe it briefly, the CNT membrane surface is first rinsed with 50 mM MES buffer pH 5. Immediately before use, a solution containing 50 mg/mL ethyl-(N',N'dimethylamino) propylcarbodiimide hydrochloride (EDC) and 50 mg/mL sulfo N-hydroxyl succinimide ester (Sulfo-NHS) in 50 mM MES buffer at pH 5 were added to the membrane surface in the hole recess (CNT membrane top side) for 15 min incubation to activate the carboxylate groups. The supernatant was removed quickly after 15 min and 100 µM aptamer solution (12.5 nmoles of aptamer was dissolved in 125 µL PBS pH 7.4 to make 100 µM aptamer stock solution) was added onto the top of the membrane for grafting for 2 hours under mixing conditions. Rigorous pipetting of the aptamer solution was maintained throughout the grafting process as a means of mixing due to the small size of the 3mm hole. The membrane surface was rinsed afterwards with PBS after grafting and incubated with 50 mM ethanolamine in PBS 8.0 for 60 minutes to deactivate unreacted moieties.

3.4.4 Experimental setup and methods

An U-tube fitting setup shown in figure 3.5 was used to measure ionic current through the CNT membrane. The two electrode system was used with the working electrode (W.E.) being Ag/AgCl electrode and Reference electrode (R.E.) being Ag/AgCl electrode, the distance was 10 cm between the two electrodes. An Edaq potentiostat provided constant bias and ionic current was recorded and analyzed using E-chem software.

3.5 Results and Discussion

3.5.1 Membrane pore area calculation

Membrane pore area was calculated by ionic current in a U-tube fitting setup with 0.1 M KCl as the probe ions using Ag/AgCl electrodes as both the working and reference/counter electrode using the following equations[95]:

$$A_p = \frac{M * l}{\mu_{EM} * C * E} \qquad 3.1(1)$$

$$M = I * \frac{t^+}{e * N} \qquad 3.2\ (2)$$

Where A_p is membrane pore area; M is the electrophoretic molar flow rate of K^+ ions through SWCNT membrane; l is the thickness of the membrane(5 µm); μ_{EM} is the the experimentally measured K^+ electrophoretic mobility of 0.1 M in SWCNTs (~8x-10^{-08} m^2/s-V)[41]; C is the concentration of KCl solution (100mM); E is the applied bias(-0.6V); I is ionic current measured; t^+ is K^+ transport number(0.5); e is the elementary charge

and N is the Avogadro constant. For a typical 2% loading SWCNT membrane used in the following experiments, the trans-membrane ionic current in 0.1 M KCl under -0.6 V bias is 1.5 μA, which gives a pore area of 8.7×10^{-12} m^2. It is important to note that the pore area of different membranes are not exactly the same, likely due to varying carbon nanotube dispersion and opening of nanotube tips.

3.5.2 Ionic current reduction with diazonium chemistry functionalization

It has been shown previously by J. Wu, B.J. Hinds that the grafting of diazonium and dye on the tips of carbon nanotubes in CNT membranes cause small molecule ionic current rectification,[95] where ionic rectification factor is defined as the ratio of maximum current applying a negative bias (-0.6V) divided by the maximum current applying a positive bias (0.6V). Ratios of 2.18-2.3 on 2% SWCNT membranes were obtained by us after diazonium grafting, which is close to 2.3 as reported by J. Wu, B.J. Hinds et al. Figure 3.6 compares 0.1 M KCl ionic current of a SWCNT membrane in the as-made condition and after diazonium grafting, yielding the rectification ratio of 2.18. The rectification is likely due to carboxylate groups covalently grafted on carbon nanotube tips drawn toward the pore entrance under positive bias which causes charge repulsion and hinders ionic transport, while no such hindrance existed under negative applied bias.

The rectification observed by us shows agreement with literature and proves that diazonium carboxylate was successfully functionalized onto the SWCNT membrane. The abundance of diazonium chemistry generated carboxylate groups were key to subsequent high yield grafting of aptamer onto SWCNT membranes. In membranes with defect or low diazonium grafting density no ionic current rectification was observed.

3.5.3 Aptamer gating causing ionic current reduction

Potentiostatic ionic current measurements traversing a CNT membrane could be used to probe the opening and closing of CNT pores similar to the measurement of DNA translocation in solution, based on the fact that ionic flux is directly related to available pore area. When the carbon nanotube pores are gated by the ATP aptamer (the "closed" state), ionic current is subject to decrease due to the steric hindrance of the aptamer spatially limiting the flow of ions into the carbon nanotube core.

As can be seen in figure 3.7, under negative applied bias, transmembrane ionic current after aptamer grafting was substantially decreased compared to the current before grafting, which proves aptamers was successful grafted onto carbon nanotube tips. Specifically in this case where 0.1 M KCl solution was used for probing, the ionic current reduction after aptamer grafting reduction was 39.6%. This reduction percentage may be compared to a previous report where 20 nm and 65 nm diameter glass nanopores

were functionalized on the sidewalls with cocaine-binding aptamers and approximately 15-35% current reduction was achievd.[90] In their case the size of the aptamer was substantially smaller compared to the large pore diameter (20 nm and 65 nm), therefore only partial blocking of the pores was achieved and thus a smaller reduction in ionic current.

Under positive applied bias rectification ratio of ~2 was observed in the SWCNT membrane both before and after aptamer grafting, presumably because negatively charged groups caused weak charge repulsion which led to the rectification effect. Higher rectification ratio after the grafting of aptamers was initially expected because the phosphate groups on aptamers which replaced diazonium carboxylate groups was more negatively charged, which should in turn cause stronger charge repulsion& rectification. We proposed two explanations for the fact that observed rectification was almost identical in both cases: 1) The Debye screening length is less than 1 nm in 0.1M KCl which is smaller than the dimensions of the CNT core and DNA double helix, thus charge repulsion would be dramatically reduced even if the CNT tip was functionalized with aptamers[41]; 2)The long relaxed geometry of the aptamer means that not all negative charges were concentrated at the pore entrance, which means weaker charge repulsion of ions& rectification effect.

3.5.4 Big anion/cation ionic current with aptamer gating

$[Ru(bpy)_3]_3[Fe(CN)_6]_2$ solution was used to examine the effect of ion size on the blocking efficiency of CNT membranes by aptamers, as $[Ru(bpy)_3]^{2+}$ and $[Fe(CN)_6]^{3-}$ are respectively larger than K+ and Cl-. The ionic diameter of $[Ru(bpy)_3]^{2+}$ and $[Fe(CN)_6]^{3-}$ is close to the CNT core diameter of 1.5 nm which should result in noticeable ionic current reduction due to spatial confinement, both at the core entrance and through the length of carbon nanotubes. Transmembrane ionic current measured in 1mM $[Ru(bpy)_3]_3[Fe(CN)_6]_2$ is shown in Figure 3.8. As can be seen, the maximum current measured under the negative bias of -0.6 V dropped 2 orders of magnitude from ~$1x10^{-6}$ A using 0.1M KCl to ~$3x10^{-8}$ A when measured with the large cation/anion $[Ru(bpy)_3]_3[Fe(CN)_6]_2$ solution. This result is expected because the magnitude of ionic current is directly related to per area ionic molar flow rate, which was substantially decreased due to the larger size of $[Ru(bpy)_3]^{2+}$ and $[Fe(CN)_6]^{3-}$. The decrease in the number of ions flowing across the membrane also resulted in the observed fuzziness of the potentiostatic plot as ionic current dropped near residue current value. Current reduction percent increased from 39.6% using 0.1 M KCl to 70.1% in 1mM $[Ru(bpy)_3]_3[Fe(CN)_6]_2$, which shows that while using large cation/anions for probing the aptamer more efficiently blocked carbon nanotube pores and hindered ion flow.

Rectification of $[Ru(bpy)_3]_3$ $[Fe(CN)_6]_2$ solution ionic current under positive bias was not observed in both before and after aptamer grafting, likely due to the carbon nanotube pore steric hindrance effect outweighing the charge repulsion effect under positive bias: it is equally difficult for the large ions to enter the CNT core under either positive or negative bias, so the rectification effect related to charge repulsion is negligible.

3.5.5 The reversibility of CNT membrane gating

Reversibility of aptamer gating measured by ionic current is important not only to show that the ionic current reduction is truly due to aptamer acting as gating molecules hindering ion flow, but also to show that the gating of CNT pores is reversible. In order to demonstrate the reversibility of aptamer gating, the transmembrane ionic current was measured after each step of membrane functionalization: 1) H_2O plasma oxidized (the as-made membrane); 2) after diazonium grafting (attachment of carboxylate groups to CNT tips); 3) after aptamer grafting (which spatially gates the CNT membrane), 4) after AMP binding to the ATP aptamer. For the H_2O plasma oxidized, diazonium grafted, and after aptamer grafted state phosphate buffer solution without AMP addition was used for ionic current measurements. For the AMP binding case phosphate buffer solution with AMP target molecule addition was used.

As can be seen in figure 3.9, the as-made H_2O plasma etched membrane potentiostatic bias-current plot is linear because a minimum amount of charged molecules existed on the membrane and also blocking of carbon nanotubes pores was non-existent, resulting in a perfect curve following equation 3.1. After diazonium grafting, rectification effect with a ratio of ~2 was seen due to weak charge repulsion because diazonium functionalization introduced negatively charged carboxylate groups onto tips of carbon nanotubes. After aptamers are grafted onto carbon nanotube tips via linkage with carboxylates, large ionic current reduction was seen under negative applied bias presumably due to the steric hindrance of the grafted aptamers. Specifically, ionic current after aptamer grafting under negative applied bias decreased 50.2% when compared to the as-made membrane due to the large double helix hairpin size of the aptamer in the natural state(2nm) blocking SWCNT pores tips(0.8-1.6 nm inner diameter). A schematic of the ATP aptamer gating the CNT membrane is shown in figure 3.4(a).

When PBS solution without addition of AMP was replaced with PBS+10mM AMP solution, each aptamer binds to 2 AMP molecules and changes their conformation as depicted in figure 3.4(b) (c). The aptamer resumes a more linear and relaxed conformation by releasing the hairpin upon binding to AMP and leaves only a single strand at the carbon nanotube tip, thus the membrane enters an “open state” and ionic current is greatly increased, partially recovering up to ~88% of the as-made membrane

value. During this process ionic current under positive applied bias showed little change, as described previously rectification already existed after diazonium grafting. It should be noted that the positive bias rectification ratio may differ from membrane to membrane due to the broad distribution of carbon nanotube diameter and functional density variance between membranes. Diazonium grafted membranes have shown rectification ratios ranging from 1.5 to 2.2.

To show the multiple cycle reversible switching of aptamer gating, the binding/unbinding of AMP to the aptamer was conducted for three full cycles. Specifically, after the transmembrane ionic current was measured with PBS with no AMP addition, the solution is removed and the U-tube refilled with PBS with 10mM AMP addition on the aptamer grafted side of the membrane (top side) and the ionic current measured. For removing AMP we simply replaced PBS with 10mM AMP addition with fresh PBS, and this process was repeated 3 times. 5 minutes was allowed each cycle for the full binding of AMP molecules to the aptamer before taking any measurements. 10mM AMP was well above the saturation concentration required to ensure the full binding of aptamers.[94] The stable ionic current under AMP binded and unbinded state was recorded under -0.6 V negative bias and shown in figure 3.10. Ionic current change corresponded well to the binding and unbinding of AMP molecules to aptamer.

For comparison the ionic current reduction before/after aptamer grafting is shown with three different probe solutions in table 3.1. The ions are of different sizes thus resulting in varying degrees of spatial hindrance caused by aptamer gating. Using 0.1 M KCl as the probe solution the smallest ionic current reduction was observed, which is expected as KCl solution has the smallest ions when compared to phosphate buffer solution and $[Ru(bpy)_3]_3$ $[Fe(CN)_6]_2$. Using $[Ru(bpy)_3]_3$ $[Fe(CN)_6]_2$ as the probe solution ionic current reduction of 70.1% was observed which is moderate considering the gating system is not yet utilized, because multiple facing of grafted aptamers exists which will lower the gating efficiency; only the upright aptamers gate pores with the highest efficiency.

3.5.6 Conclusions

We have shown that aptamers at the tip of CNT membrane may act as gatekeepers and regulate ionic flux passing through the membrane. We also showed that this CNT membrane-aptamer gating system is reversible over multiple AMP binding and unbinding cycles as measured by ionic current. The gating efficiency is closely related to the size of the probe ion, underlining the spatial blocking ability of the aptamer. Overall the reversible aptamer gated CNT membranes herein reported may have significant impact on active membrane design, drug delivery, and molecular sensing. By utilizing aptamers at CNT membrane surface, we closely mimics how nature's ion channels works

by binding to signal molecules and regulate flux. Further work in the future may be in the direction to enhance the efficiency of membrane pore gating by increasing aptamer grafting density and improving grafting design. Target molecules beyond ATP/AMP may be sensed by grafting their respective recognition aptamers at CNT membrane surface. Aptamers may also be coupled with other chemistry at the CNT membrane surface to perform not only gating, but other functions such as active pumping, sensing, and separation.

3.6 Enhanced Electroosmosis of CNT Membrane

3.6.1 Introduction

Electroosmosis refers to the bulk motion of electrolyte induced by an applied potential across a fluid conduit. Electroosmosis flow can be the primary method to control fluid flux in small scale systems such as microfluidics, medical implants, drug delivery and chemical separations.[40,96,97,98] It is commonly used for pumping or removal of liquids across interfaces and in and out of micro compartments. For example, proton exchange membrane fuel cells (PEMFCs) have been developed for electric power generation for portable hand held devices, however cathode flooding with water occurs during normal exchange operations which greatly reduces its performance and robustness. C. R. Buie et al used porous glass electroosmostic pump to remove hydration from the cathode and resulted in increased PEMFC power density and

current density.[99] As shown in figure 3.11, typical electroosmosis efficiency depended heavily on charge density of the microchannels where the fluid contacts. By proper functionalization and surface chemistry treatment, J. Miao et al. fabricated micropumps which was based on enhanced electroosmotic effect in AAO membranes.[100] A. Brask et al. developed an efficient low operating voltage electroosmosis based on ion exchange membranes packed with dense charged groups. Despite the amount of interest and work in electroosmosis, it is still a relatively inefficient process which have so far shown promising but limited applications.

Although electroosmosis was first extensively researched in porous glass pumps, C.R. Martin et al. studied electroosmosis flow in CNT membranes with large diameter (200 nm) and found that by functionalizing charged (positive or negative) groups inside core of CNTs the direction of electroosmosis could be altered.[101] The attributes of functionalized CNT meets well the requirements for efficient electroosmosis: 1) high surface charge 2) small diameter 3) slippery interface. Sun and Crooks found that no enhanced fluid flux or electroosmosis velocity was observed in a single carbon nanotube embedded polymer membrane because of the large diameter of their carbon nanotube (500 nm). Later efficient electroosmosis was observed in carbon nanotube based membranes by J. Wu, B.J. Hinds et al, where electroosmosis velocity of ions was compared in single-walled, multi-walled, and conventional polymeric membranes.[41] Electroosmosis flow up to 1-3 orders of magnitude faster was observed in SWCNTs and

MWCNTs compared to conventional AAO membrane with larger diameter. A neutral molecule caffeine was efficiently pumped through CNT core by electroosmosis, where the steady state flux was increased by ~4 times. Because of the absence of J_{ep} from electrophoresis for the neutral caffeine molecule, applying the below equations the flux increase could be entirely attributed to electroosmosis flow J_{eo}. Applying -300 mV bias, electroosmosis velocity as high as 0.054 cms^{-1}(0.018 s^{-1} V^{-1}) was obtained by J. Wu, B.J. Hinds et al. which should the promising electroosmosis applications based on carbon nanotubes.

$$J(x) = J_{ep} + J_{eo} \qquad (1)$$

$$v_{eo} = J_{eo}/C \qquad (2)$$

3.6.2 Hypothesis of highly efficient CNT membrane electroosmotic pump

It is suggested here that highly efficient electroosmosis could be achieved by functionalized high porosity vertically aligned CNT membranes. We also plan to directly observe water movement as a result of electroosmosis, where in previous reports concerning carbon nanotube electroosmosis ionic current was primarily used to determine electrolyte transfer. We based the study on the following assumptions: 1) High porosity vertically aligned CNT membranes could be fabricated. Although in J. Wu, B.J. Hinds' earlier report a remarkable $1.8*10^{-1}$ cm s^{-1} V^{-1} electroosmosis velocity was observed in SWCNTs, the small membrane area of 0.07 cm^2 and low porosity of 0.0027%

in microtome fabricated CNT membranes meant electroosmosis could only be used in micro-scale applications. Porifera is a company which fabricates vertically aligned CNT membranes via CVD method, where CNT membrane discs with area up to ~80 cm^2 could be synthesized. With the earlier reported electroosmosis velocity of $1.8*10^{-1}$ cm s^{-1} V^{-1}, possible aligned CNT membrane porosity of 0.1%, 1.22 L water could be electroosmotically pumped under 1V bias in 24h if the whole CNT membrane area was utilized, which greatly surpasses that of "microscale". 2) Both sides of the carbon nanotube membrane could be functionalized with negatively charged dye molecules which serves two purposes as shown in figure 3.12. Dye functionalization with carboxylate groups functionalized on the positive (donor) side would attract positive ions close to the tip which preferentially flows into CNT core. This increases the feed of positive ions in the CNT core which is the active pumping ions under the forward bias direction and also repel negative ions although they generally flow in the opposite direction. On the receptor side, the functionalized carboxylate groups would greatly repel negatively charged ions from entering the CNT core under the current direction and thus maintain the dominance of forward pumping ions in the CNT core. Since SWCNTs and DWCNTs with diameter close to positive ions would be used for the study, efficient electroosmosis pumping can be expected with the "ratchet" type functionalization on both sides of the CNT membrane.

To directly observe electroosmosis flow visually, a glass capillary can be used to determine small volume liquid changes by the movement of water meniscus against time, which in turn yields electroosmosis velocity. It can be estimated that by using a 1mm inner diameter glass capillary, a 0.07 cm^2 area CNT membrane with 0.01% porosity could pump 0.0252 cm^2 under 1V pumping bias in 1 hour, which translates into 3.21 cm meniscus level rise, well observable by water level marking or photography.

3.6.3 Experimental setup and outlook

A proof of concept electroosmosis setup for CNT membrane is shown in figure 3.13. The CNT membrane was functionalized with dye groups on both sides according to steps given in chapter 2 and 3. The functionalized CNT membrane is clamped between two glass tubes, separating the donor and receptor compartment. Depending on the study, either 5 mM KCl solution or 5mM $K_3Fe(CN)_4$ solution filled both side of the donor and receptor solution. A two electrode setup was used, with Ag/AgCl as the working electrode in the L shape donor compartment and Ag/AgCl as the reference electrode in the straight receptor compartment. The receptor compartment was filled in such a way that no bubble was present and water transport from the donor compartment would entirely be contributed to meniscus rise in the receptor compartment capillary. The experiment was performed in constant temperature room to rid of temperature related water volume expansion.

Water meniscus level rise was seen in a few electroosmosis experiments, however results was not consistent through a series of repetitions. This could be attributed to a few possibilities: 1) Electroosmosis velocity depends heavily on the quality of the CNT membrane, and currently Porifera and microtomed CNT membranes showed porosity which was lower than expected. 2) Electrolysis of water would generate hydrogen ions and hydroxide ions which likely occurs due to positive ion movement. These ions would change pH of the compartments limiting further electroosmosis beyond the initial pumping phase. 3) Absolute levelness between the donor and receptor compartments is extremely important in order to rid of gravity related water flow artifacts. Under current experimental conditions this was hard to achieve and we hope in the future more sophisticated setups could be utilized to solve this problem.

Table 3.1 Potentiostatic ionic current reduction comparison between three probe solutions with varying ion size.

Probe solution	Potentiostatic current reduction after aptamer functionalization
0.1M KCl	39.6%
1mM $[Ru(bpy)_3]_3[Fe(CN)_6]_2$	70.1%
1x 5M PBS	50.2%

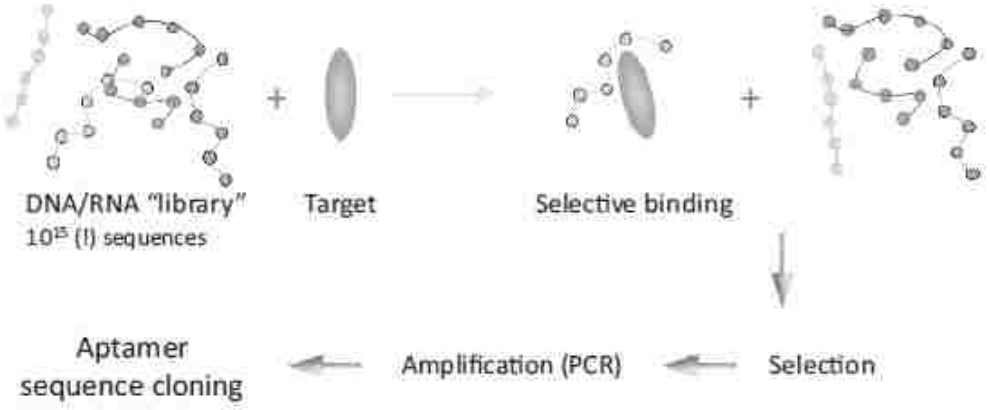

Figure 3.1 Principle of the "systematic evolution of ligands by Exponential enrichment", SELEX, for identification of aptamers that binded to a specific target. Reproduced from ref. [88]

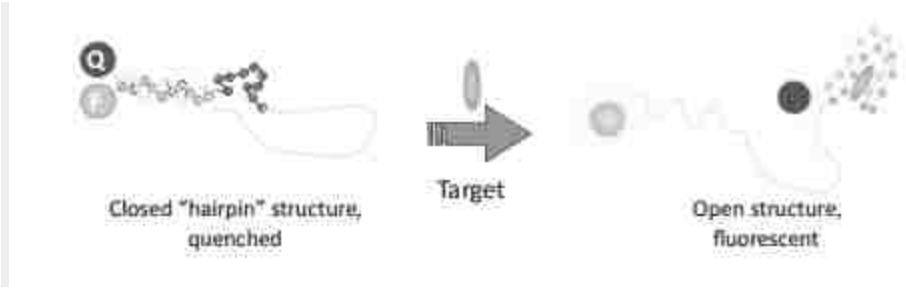

Figure 3.2 Schematic of a hairpin aptamer. Stringed circles indicate the aptamer sequence which binded to the target, the straight line the linker. Q: Quencher. F: Fluorophore. Reproduced from ref. [88]

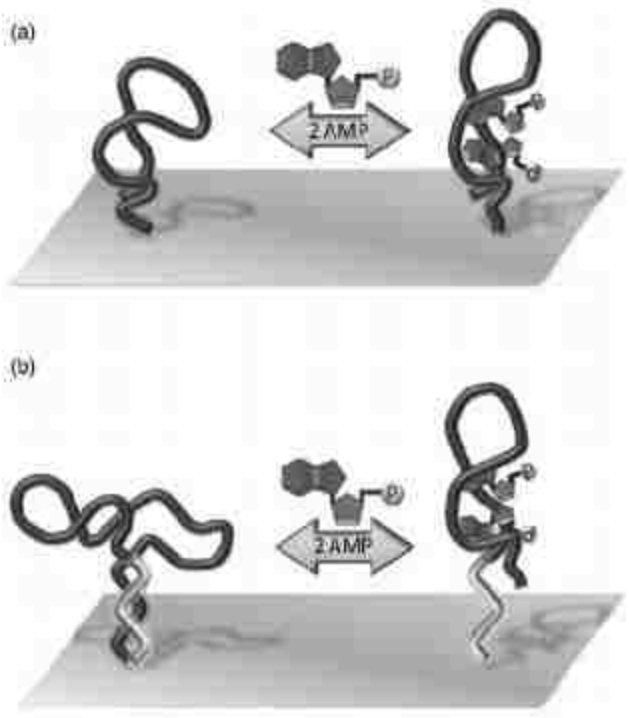

Figure 3.3 (a) the original ATP binding aptamer, a single 27-mer oligonucleotide. (b) The hairpin (molecular beacon) form of the ATP binding aptamer, which was created by adding 7 hairpin forming nucleotide sequence at its 3' end. Reproduced from ref. [88]

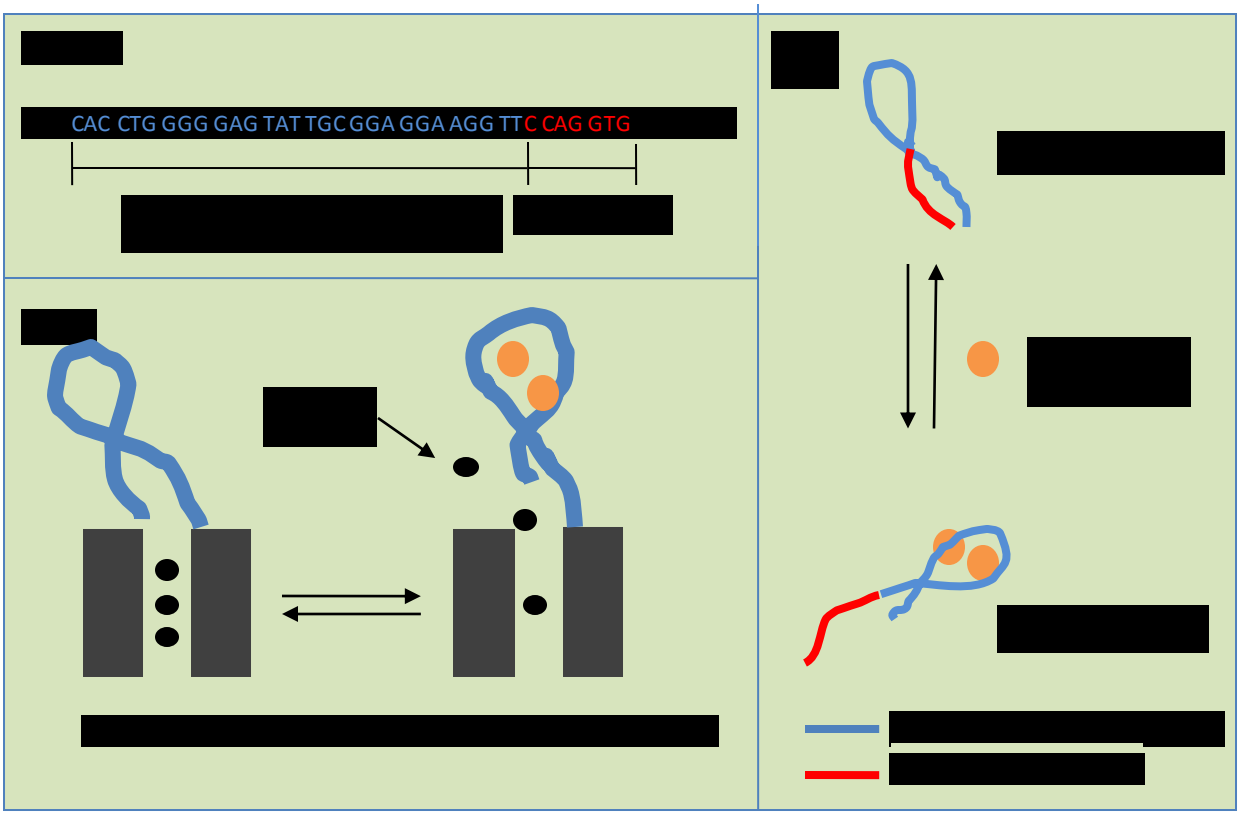

Figure 3.4 Aptamer grafting on CNT membrane. A) The sequence of the ATP-binding hairpin. The blue sequence is the ATP/adenosine binding aptamer sequence originally selected by Huizenga et al. [97] the red sequence is the hairpin forming sequence. B) Conformational change of the ATP hairpin upon binding 2 AMP molecules, going from the closed state to the open state. C) Schematic of the ATP hairpin functionalized at the tip of a SWCNT that exhibits gating function and regulates ionic flow. Representation of the ATP hairpin with references from V.C. Ozalp et al. [96]

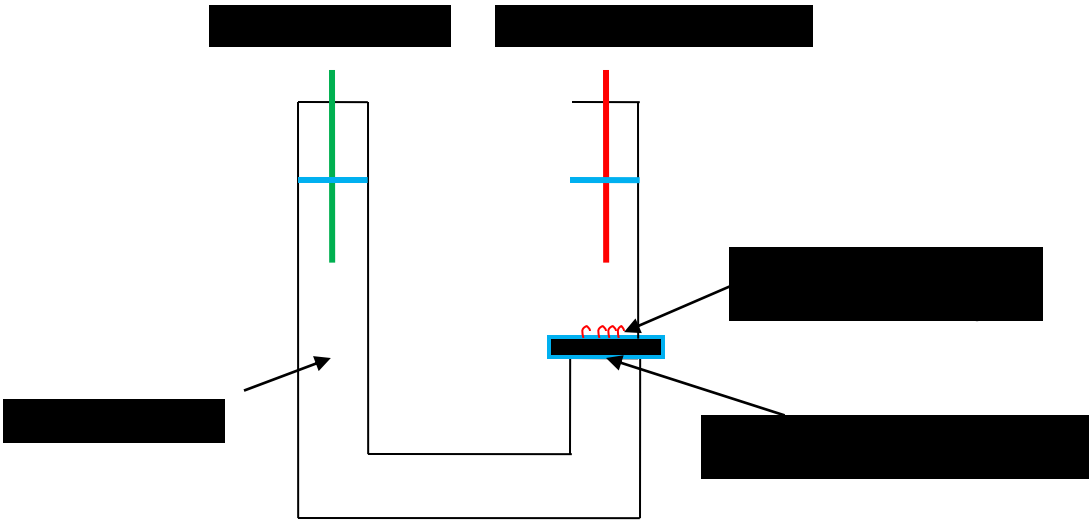

Figure 3.5 Schematic of I-V current measurement setup. For ionic current measurements, Working electrode(W.E.) is a Ag/AgCl electrode. Reference electrode(R.E.) is Ag/AgCl electrode. Constant potential is provided with Edaq potentiostat. Counter electrode(C.E.) is a sintered Ag/AgCl electrode from IVM company. The membrane area is approximately 0.07 cm^2. The distance between the electrodes is 10 cm and kept constant in all experiments.

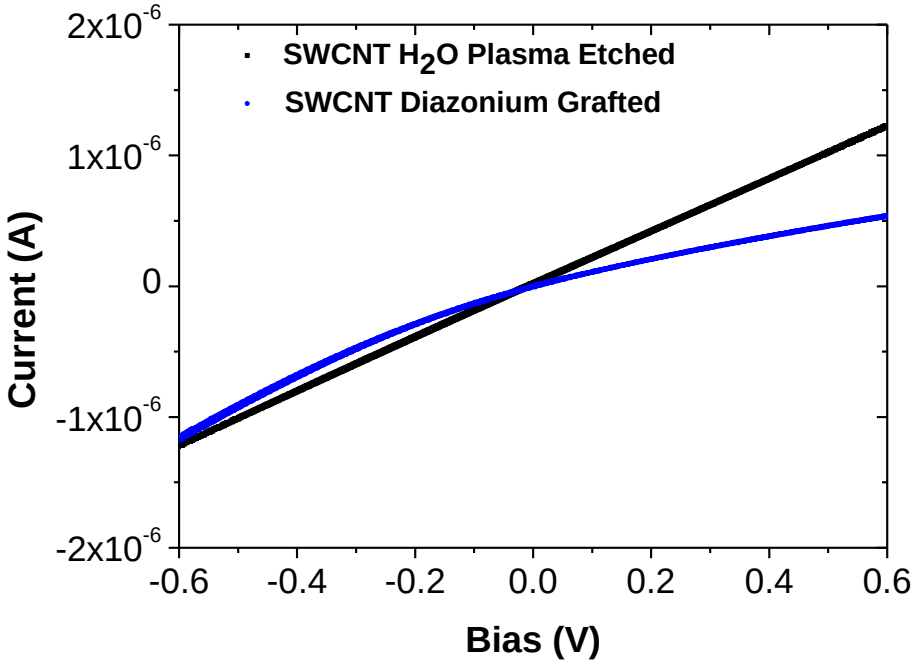

Figure 3.6 Rectification effect of diazonium chemistry on tip of SWCNTs. Ionic rectification of as-made membrane was compared to SWCNT membrane after diazonium grafting chemistry. Both sides of the U-tube cell was filled with 0.1 M KCl, working and counter/reference electrode is both Ag/AgCl.

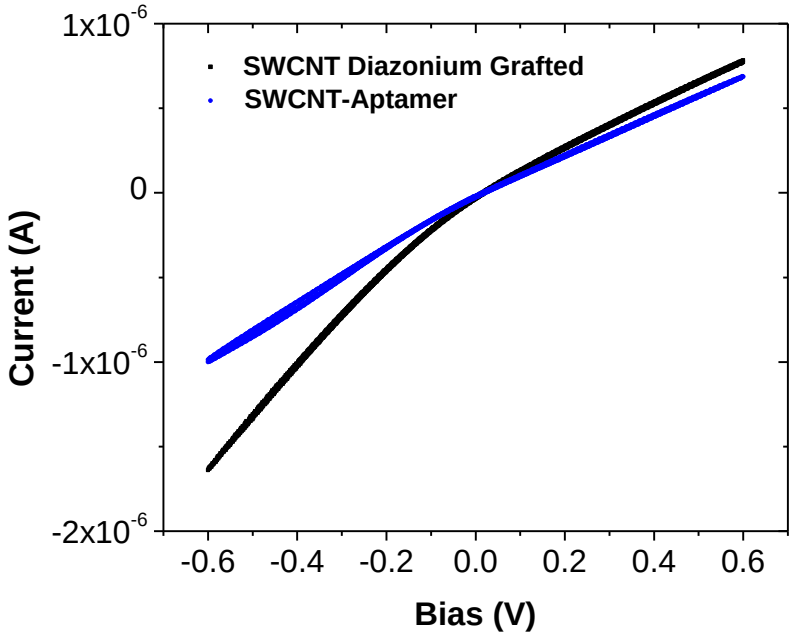

Figure 3.7 Ionic current reduction due to aptamer grafting gating the CNT membrane. 0.1M KCl was used on both side of u-tube cell. The working electrode is Ag/AgCl on the bottom side of membrane, and the Counter/reference electrode is Ag/AgCl on the top side of the membrane where aptamer was grafted.

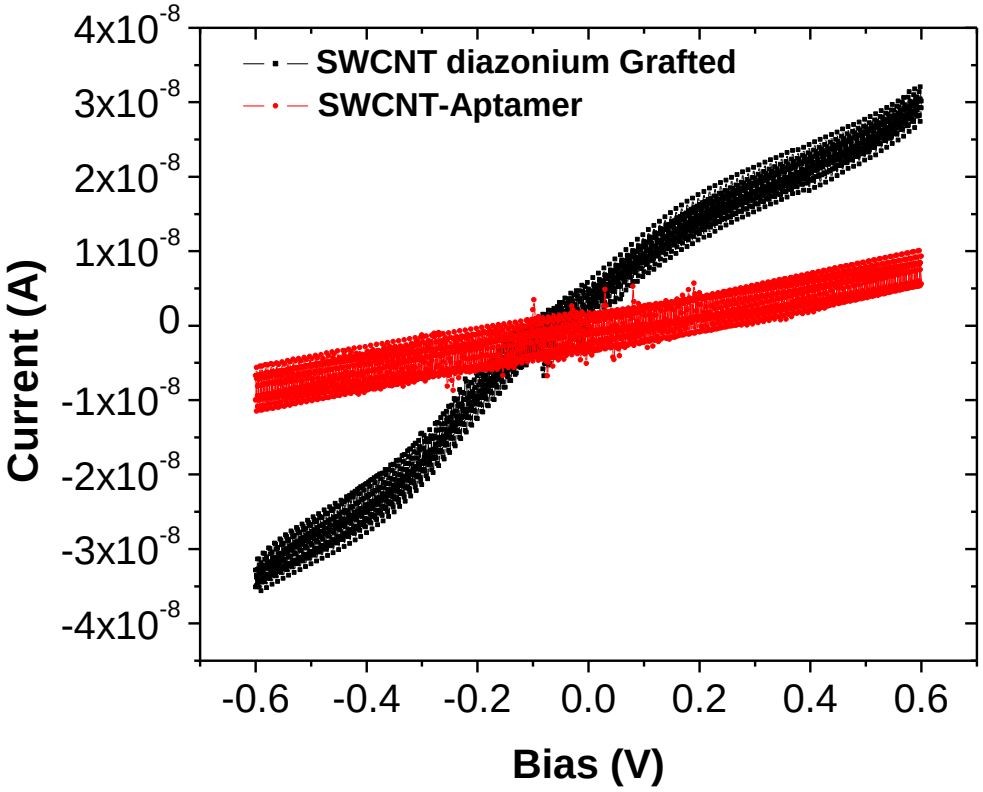

Figure 3.8 Ionic current before and after aptamer grafting using a big cation/anion probe solution. 1mM $[Ru(bpy)_3]_3$ $[Fe(CN)_6]_2$ was used on both sides of U-tube setup. The working electrode is Ag/AgCl on the bottom side of the membrane, and the Counter/reference electrode is Ag/AgCl on the top side of membrane where aptamer is grafted.

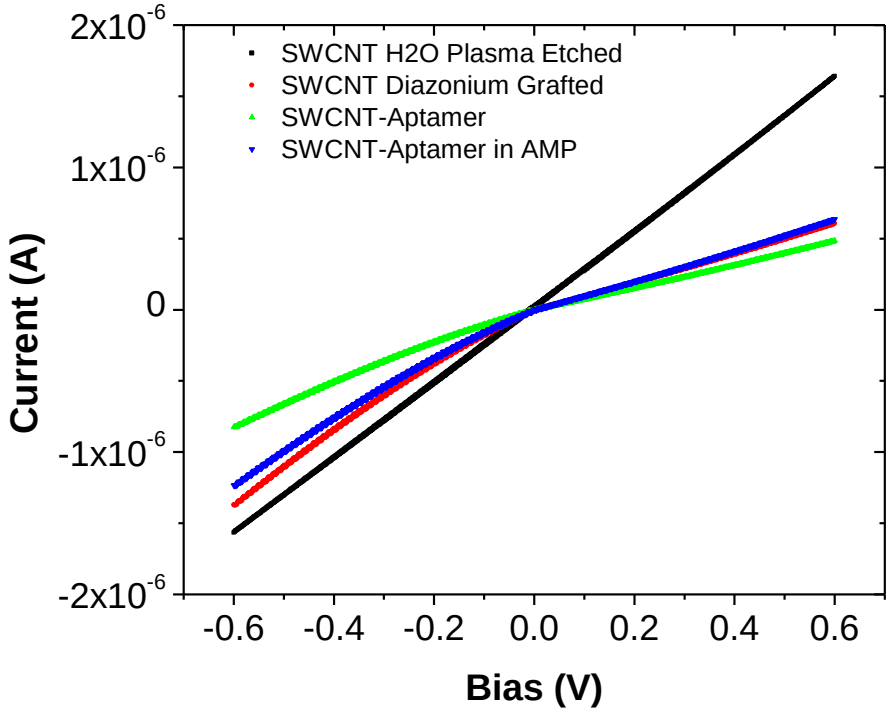

Figure 3.9 Ionic current changes due to aptamer grafting and AMP binding. 1x5M PBS solution was used for SWCNT H2O plasma etched, SWCNT diazonium grafted, and SWCNT-Aptamer measurement. For the SWCNT-Aptamer in AMP case a 1x5M PBS with 20mM dissolved AMP solution is used. The working electrode is Ag/AgCl on the bottom side of the membrane, and the Counter/Reference is Ag/AgCl on the top side where the aptamer is grafted.

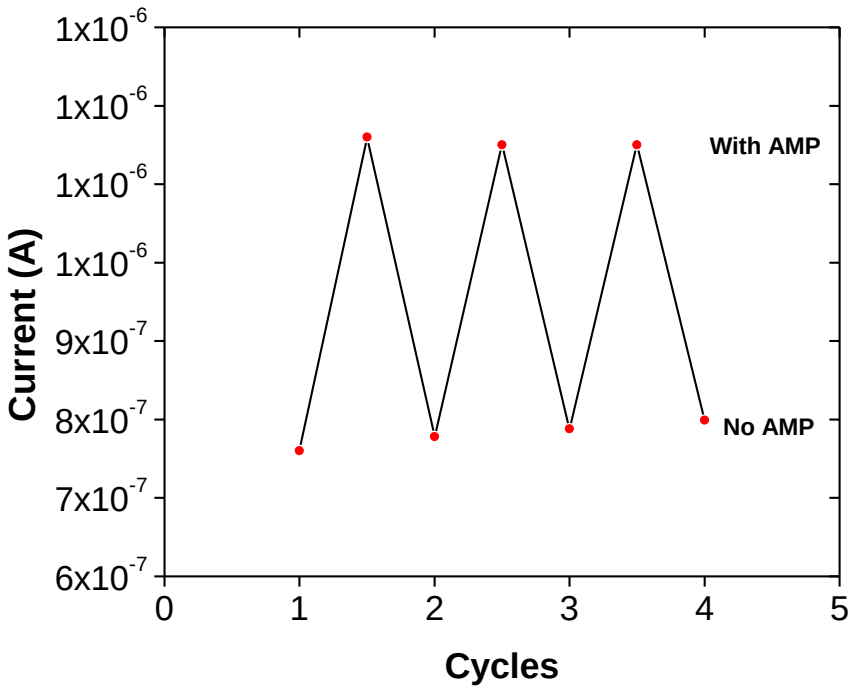

Figure 3.10 Reversibility of AMP target binding to ATP aptamer and unbinding as measured by transmembrane ionic current. The plot is shown with three cycles of binding and unbinding.

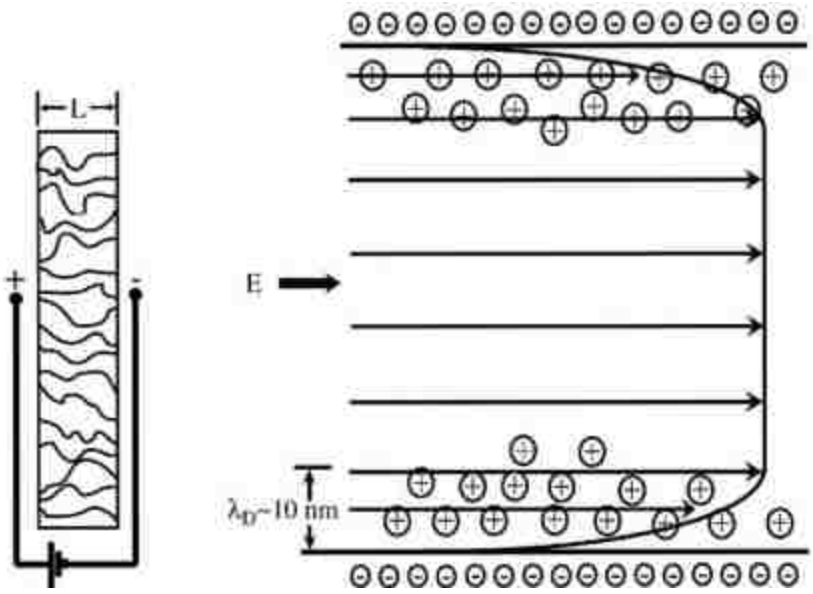

Figure 3.11 Schematic of electroosmosis pumping of liquids

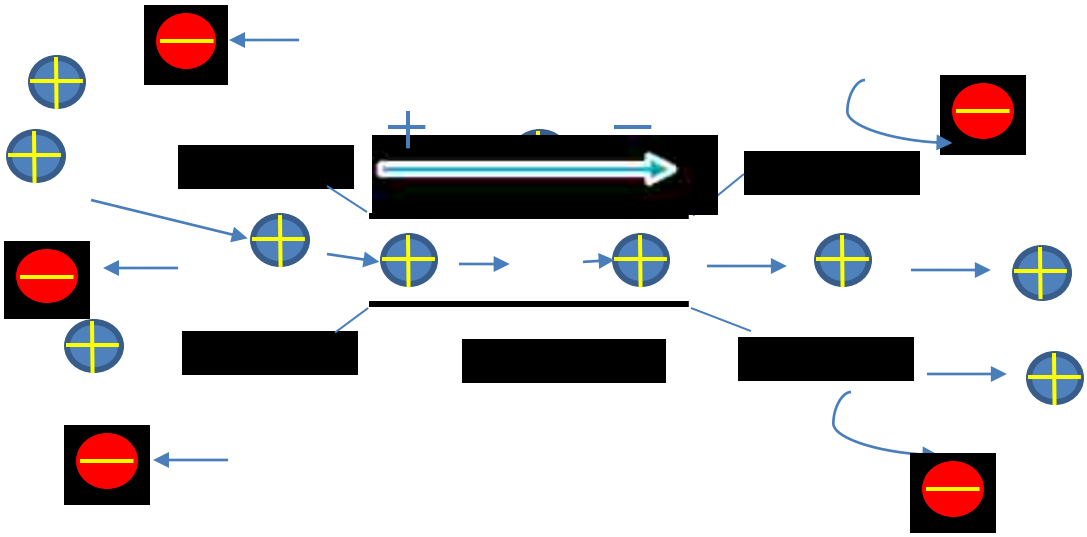

Figure 3.12 Schematic of double dye functionalization at tip of CNTs on CNT membrane

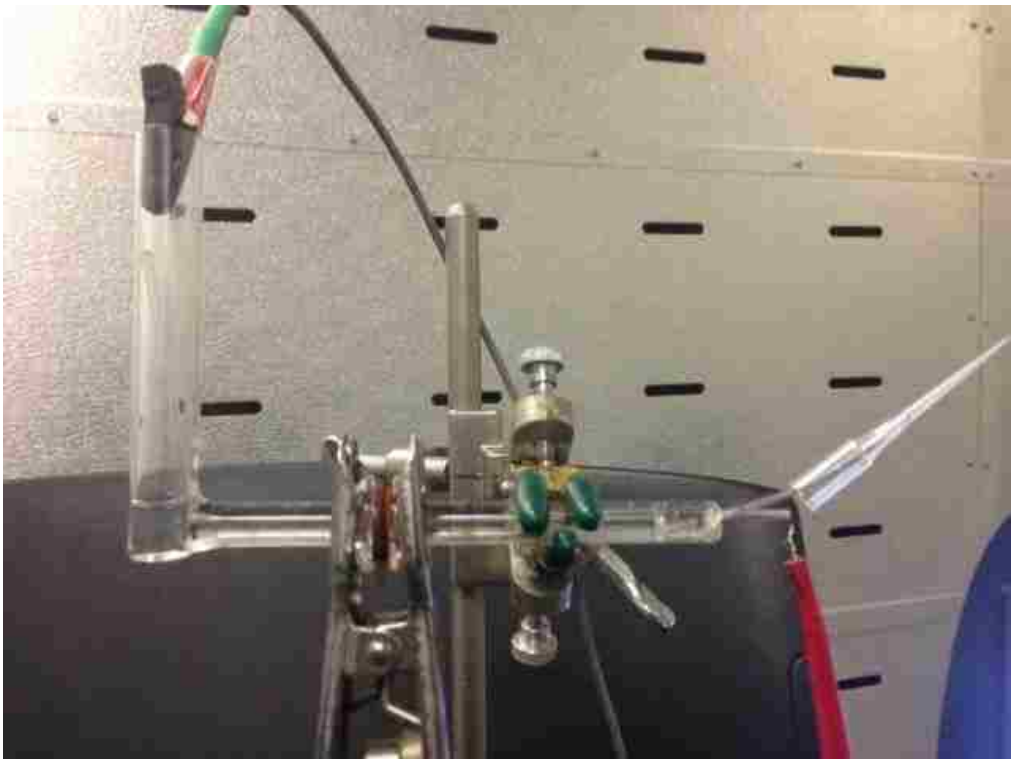

Figure 3.13 CNT membrane electroosmosis setup

Chapter 4 Conclusions and future work

Carbon nanotubes are allotropes of carbon with fascinating attributes which was extensively studied and applications continues to be explored. Through the hard work of researchers carbon nanotubes have been used in various fields of science, shining in the physics sciences, chemistry, materials, and medical fields. The current group under Dr. Hinds first synthesized aligned CNT membranes which bridged the gap between nano-sized carbon nanotubes and the macro-scale. They continued to show that carbon nanotubes could be efficiently functionalized for enhanced electroosmosis/ electrophoresis and gatekeeping, which saw switchable transdermal nicotine delivery realized as a practical application. More work will be done from the group utilizing carbon nanotubes to for discovery of interesting new phenomenon and concepts as well as working current results into applications.

As described in chapter 2, microdialysis sampling will be used to accurately map nicotine delivery profiles of CNT membrane *in vivo* to show the potential of CNT membrane ON/OFF and examine existing shortcomings. With sufficient experience and proof of concept, the final vision would be portable and rate switchable transdermal devices which could be administered via phone or internet counseling. This would revolutionize and expand the current transdermal market. To expand the range of drugs compatible with transdermal drug delivery, electroporation device that reliably weakens the

stratum corneum skin barrier would be developed and coupled with CNT membrane to programmably deliver. This would be a great advancement in nicotine replacement therapy and addiction drug treatments where dosage is sensitive.

Active gating and functionalization of carbon nanotube membranes would be continued to further mimic natural membranes to show potential beyond molecular detection, discrimination, but also separation of ions and proteins, fluid transport, catalysis and possibly development of a multi-functional membrane.

However the basis of these new phenomenon and applications would be a truly robust, fast flow, and easy to synthesis carbon nanotube membrane. Remarkable advances in the fabrication of carbon nanotube membranes have been made in the past, but will still be needed in the future. We truly would like to see carbon nanotubes being used to improve our everyday life.

References

[1] C.A.M. Mihail C. Roco, Mark C. Hersam, Nanotechnology Research Directions for Societal Needs in 2020: Retrospective and outlook, Springer, 2011.

[2] S. Iijima, Helical microtubules of graphitic carbon, Nature 354 (1991) 56-58.

[3] N. Saifuddin, A. Z. Raziah, and A. R. Junizah, Carbon Nanotubes: A Review on Structure and Their Interaction with Proteins, Journal of Chemistry, vol. 2013, Article ID 676815, 18 pages, 2013.

[4] J. Prasek, J. Drbohlavova, J. Chomoucka, J. Hubalek, O. Jasek, V. Adam, and R. Kizek, Methods for carbon nanotubes synthesis—review, Journal of Materials Chemistry, 2011, 21, 15872.

[5] Hong, Seunghun; Myung, S (2007). Nanotube Electronics: A flexible approach to mobility, Nature Nanotechnology 2 (4): 207–208.

[6] M. Yu, O. Lourie, M.J. Dyer, T.F. Kelly, R.S. Ruoff, Strength and breaking mechanism of multiwalled carbon nanotubes under tensile load, Science, 287 (2000), pp. 637-640.

[7] A. Peigney, C. Laurent, E. Flahaut, R.R. Bacsa, A. Rousset, Specific surface area of carbon nanotubes and bundles of carbon nanotubes, Carbon 39 (2001) 507-514.

[8] M.F. Islam, E. Rojas, D.M. Bergey, A.T. Johnson, and A.G. Yodh, High Weight Fraction Surfactant Solubilization of Single-Wall Carbon Nanotubes in Water, Nano Letters, 2003, 3 (2), pp 269-273.

[9] H.-C. Wu, X. Chang, L. Liu, F. Zhao, Y. Zhao, Chemistry of carbon nanotubes in biomedical applications, Journal of Materials Chemistry 20 (2010) 1036-1052.

[10] J. Liu, A.G. Rinzler, H. Dai, J.H. Hafner, R.K. Bradley, P.J. Boul, A. Lu, T. Iverson, K. Shelimov, C.B. Huffman, F. Rodriguez-Macias, Y.-S. Shon, T.R. Lee, D.T. Colbert, R.E. Smalley, Fullerene Pipes, Science 280 (1998) 1253-1256.

[11] S.S. Wong, E. Joselevich, A.T. Woolley, C.L. Cheung, C.M. Lieber, Covalently functionalized nanotubes as nanometre- sized probes in chemistry and biology, Nature 394 (1998) 52-55.

[12] S. Baranton, D. Bélanger, Electrochemical Derivatization of Carbon Surface by Reduction of in Situ Generated Diazonium Cations, The Journal of Physical Chemistry B 109 (2005) 24401-24410.

[13] D.M. Shewchuk, M.T. McDermott, Comparison of Diazonium Salt Derived and Thiol Derived Nitrobenzene Layers on Gold, Langmuir 25 (2009) 4556-4563.

[14] T. Lin, V. Bajpai, T. Ji, L.M. Dai, Chemistry of carbon nanotubes, Australian Journal of Chemistry 56 (2003) 635-651.

[15] R.J. Chen, Y.G. Zhang, D.W. Wang, H.J. Dai, Noncovalent sidewall functionalization of single-walled carbon nanotubes for protein immobilization, Journal of the American Chemical Society 123 (2001) 3838-3839.

[16] J.M. Schnorr, T.M. Swager, Emerging Applications of Carbon Nanotubes, Chemistry of Materials 23 (2010) 646-657.

[17] Zhang, M.; Atkinson, K. R.; Baughman, Multifunctional Carbon Nanotube Yarns by Downsizing an Ancient Technology, R. H. Science 2004, 306, 1358.

[18] Banks, C. E.; Crossley, A.; Salter, C.; Wilkins, S. J.; Compton, R. G., Carbon Nanotubes Contain Metal Impurities Which Are Responsible for the "Electrocatalysis" Seen at Some Nanotube-Modified Electrodes, Angew. Chem., Int. Ed. 2006, 45, 2533.

[19] B.Fang, N.K. Chaudhari, M. Kim, J.H. Kim, J.S. Yu, Homogeneous Deposition of Platinum Nanoparticles on Carbon Black for Proton Exchange Membrane Fuel Cell, J. Am. Chem. Soc., 2009, 131 (42), pp 15330–15338.

[20] Hull RV, Li L, Xing YC, Chusuei CC. Pt nanoparticle binding on functionalized multiwalled carbon nanotubes, Chem Mater 2006;18(7):1780–8.

[21] Li ZJ, Yan WF, Dai S., Surface functionalization of ordered mesoporous carbons – a comparative study. Langmuir 2005;21(25):11999–2006.

[22] X.Su, J. Wu, B.J. Hinds., Catalytic activity of ultrathin Pt films on aligned carbon nanotube arrays, Carbon 49 (2011) 1145-1150.

[23] V. Lordi, N. Yao, J. Wei, Method for Supporting Platinum on Single-Walled Carbon Nanotubes for a Selective Hydrogenation Catalyst, Chem. Mater., 2001, 13 (3), pp 733–737.

[24] J. Kong, et al., Nanotube Molecular Wires as Chemical Sensors, Science 287, 622 (2000).

[25] T.W. Tombler et al., Nature 405, 769 (2000).

[26] Y. Zhang, Y. Bai, B. Yan, Functionalized carbon nanotubes for potential medicinal applications, Drug Discovery Today 15 (2010) 428-435.

[27] A. Bianco, K. Kostarelos, C.D. Partidos, M. Prato, Biomedical applications of functionalised carbon nanotubes, Chemical Communications (2005) 571-577.

[28] Z. Liu, S. Tabakman, K. Welsher, H. Dai, Carbon nanotubes in biology and medicine: In vitro and in vivo detection, imaging and drug delivery, Nano Research 2 (2009) 85-120.

[29] Z. Liu, K. Chen, C. Davis, S. Sherlock, Q. Cao, X. Chen, H. Dai, Drug Delivery with Carbon Nanotubes for In vivo Cancer Treatment, Cancer Research 68 (2008) 6652-6660.

[30] D.A. Doyle, J.M. Cabral, R.A. Pfuetzner, A. Kuo, J.M. Gulbis, S.L. Cohen, B.T. Chait, R. MacKinnon, The Structure of the Potassium Channel: Molecular Basis of K+ Conduction and Selectivity, Science 280 (1998) 69-77.

[31] G. Hummer, J.C. Rasaiah, J.P. Noworyta, Water conduction through the hydrophobic channel of a carbon nanotube, Nature 414 (2001) 188-190.

[32] L. Sun, R.M. Crooks, Single Carbon Nanotube Membranes: A Well-Defined Model for Studying Mass Transport through Nanoporous Materials, Journal of the American Chemical Society 122 (2000) 12340-12345.

[33] B.J. Hinds, N. Chopra, T. Rantell, R. Andrews, V. Gavalas, L.G. Bachas, Aligned multiwalled carbon nanotube membranes, Science 303 (2004) 62-65.

[34] M. Majumder, N. Chopra, B.J. Hinds, Effect of Tip Functionalization on Transport through Vertically Oriented Carbon Nanotube Membranes, Journal of the American Chemical Society 127 (2005) 9062-9070.

[35] M. Majumder, N. Chopra, R. Andrews, B.J. Hinds, Nanoscale hydrodynamics: Enhanced flow in carbon nanotubes (vol 438, pg 44, 2005), Nature 438 (2005) 930-930.

[36] J.K. Holt, H.G. Park, Y. Wang, M. Stadermann, A.B. Artyukhin, C.P. Grigoropoulos, A. Noy, O. Bakajin, Fast Mass Transport Through Sub-2-Nanometer Carbon Nanotubes, Science 312 (2006) 1034-1037.

[37] M. Majumder, N. Chopra, B.J. Hinds, Effect of Tip Functionalization on Transport through Vertically Oriented Carbon Nanotube Membranes, Journal of the American Chemical Society 127 (2005) 9062-9070.

[38] M. Majumder, X. Zhan, R. Andrews, B.J. Hinds, Voltage Gated Carbon Nanotube Membranes, Langmuir 23 (2007) 8624-8631.

[39] M. Majumder, B. Corry, Anomalous decline of water transport in covalently modified carbon nanotube membranes, Chemical Communications 47 (2011) 7683-7685.

[40] J. Wu, K.S. Paudel, C. Strasinger, D. Hammell, A.L. Stinchcomb, B.J. Hinds, Programmable transdermal drug delivery of nicotine using carbon nanotube membranes, Proceedings of the National Academy of Sciences (2010).

[41] J. Wu, K. Gerstandt, M. Majumder, X. Zhan, B.J. Hinds, Highly efficient electroosmotic flow through functionalized carbon nanotube membranes, Nanoscale 3 (2011) 3321-3328.

[42] K.S. Paudel, J. Wu, B.J. Hinds, A.L. Stinchcomb, J. Pharm. Sci., 2012 101(10) 3823-32.

[43] M.R. Prausnitz, R. Langer, Transdermal drug delivery, Nat Biotechnol. 2008 November; 26(11): 1261–1268.

[44] M.B. Brown, G.P. Martin, S.A. Jones, F.K. Akomeah, Dermal and transdermal drug delivery systems: current and future prospects, Drug Delivery, 13:175–187, 2006.

[45] M.R. Prausnitz, S. Mitragotri, R. Langer, Current status and future potential of transdermal drug delivery, Nature Reviews Drug Discovery 3, 115-124 (February 2004).

[46] D. W. Sifton, (ed.) Physicians' Desk Reference (Thomson PDR, Montvale, 2003).

[47] Cramer, M. P. & Saks, S. R. Translating safety, efficacy and compliance into economic value for controlled release dosage forms. Pharmacoeconomics 5, 482–504 (1994).

[48] Henningfield, J. E. Nicotine medications for smoking cessation. N. Engl. J. Med. 333, 1196–1203 (1995).

[49] R.J. Scheuplein, I.H. Blank, Permeability of the skin, Physiological reviews, Vol. 51, No. 4, October 1971, 702-747.

[50] M.R. Prausnitz, The effects of electric current applied to skin: a review for transdermal drug delivery, advanced drug delivery reviews, 18, (1996), 395-425.

[51] C.E. Burton, R.M. David, W.M. Portnoy, and L.A. Akers, The application of Bode analysis to skin impedance, (1974) Psychophysiology II. 517-525.

[52] R. Darlenski, J.W. Fluhr, Clinics in dermatology, Volume 30, Issue 3, May-June 2012, Pages 269-273.

[53] Manchikanti L (2007) National drug control policy and prescription drug abuse: Facts and fallacies. Pain Physician 10:399–424.

[54] R.D. Gordon, T.A. Peterson. Four myths about transdermal drug delivery. Drug Delivery Technology 3(4), June 2003.

[55] D.H. Malin (2001) Nicotine dependence: Studies with a laboratory model. Pharmacol Biochem Behav 70:551–559.

[56] F.J. Verbaan, SM Bal, D.J. Van den Berg, J.A. Bouwstra. Assembled microneedle arrays enhance the transport of compounds varying over a large range of molecular weight across human dermatomed skin, Journal of Controlled Release. Volume 117, Issue 2, 12 February 2007, Pages 238-245.

[57] Y.B. Bannon, J. Corish, O.I. Corrigan, J.G. Devane, M. Kavanagh, S. Mulligan, Transdermal delivery of nicotine in normal human volunteers: a single dose and multiple dose study, European Journal of Clinical Pharmacology, 1989, Volume 37, Issue 3, pp 285-290.

[58] R. Borland, C.J. Segan, P.M. Livingston, N. Owen, The effectiveness of callback counselling for smoking cessation: a randomized trial, Addiction, 96 (2001) 881-889.

[59] A.C. Williams, B.W. Barry, Penetration enhancers. Adv Drug Deliv Rev 2004;56:603–618.

[60] P. Karande, A. Jain, Ergun K, V. Kispersky, S. Mitragotri. Design principles of chemical penetration enhancers for transdermal drug delivery. Proc Natl Acad Sci USA 2005;102:4688–4693.

[61] Y. N. Kalia, A. Naik, J. Garrison, R.H. Guy, Iontophoretic drug delivery, Advanced drug delivery reviews, 56 (2004), 619-658.

[62] D. Marro, Y.N. Kalia, M.B. Delgado-Charro, R.H. Guy, Contributions of electromigration and electroosmosis to iontophoretic drug delivery, Pharm. Res. 18 (2001) 1701 – 1708.

[63] S.K. Gupta, M. Southam, G. Sathyan, M. Klausner, Effect of current density on pharmacokinetics following continuous or intermittent input from a fentanyl electrotransport system, J. Pharm. Sci. 87 (1998) 976 – 981.

[64] C.L. Gay, P.G. Green, R.H. Guy, M.L. Francoeur, Ionotophoretic delivery of piroxicam across the skin in vitro, J. Control. Release 22 (1992) 57 – 68.

[65] Sivamani RK, Liepmann D, Maibach HI. Microneedles and transdermal applications. Expert Opin Drug Deliv 2007;4:19–25.

[66] Prausnitz, MR.; Gill, HS.; Park, JH. Modified Release Drug Delivery. In: Rathbone, MJ.; Hadgraft, J.; Roberts, MS.; Lane, ME., editors. New York: Informa Healthcare; 2008.

[67] Denet AR, Vanbever R, Preat V. Skin electroporation for transdermal and topical delivery. Adv Drug Deliv Rev 2004;56:659–674.

[68] M.R. Prausnitz, V.G. Bose, R. Langer, J.C. Weaver, electroporation of mammalian skin: a mechanism to enhance transdermal drug delivery, PNAS, Vol. 90, pp 10504-10508.

[69] V. Preat, R. Vanbever, Skin electroporation for transdermal and topical drug delivery, in: R.H. Guy, J. Hadgraft (Eds.), Transdermal Drug Delivery, vol. 123, Marcel Dekker, New York, 2002, pp. 227 – 254.

[70] T.R. Gorishankar,T.O. Hernadon, and J.C. Weaver. Transdermal Drug Delivery by Localized Intervention. IEEE Engineering in Medicine and Biology Magazine. JANUARY/FEBRUARY 2009 55-63.

[71] K. Yan, H. Todo, K. Sugibayashi. Transdermal drug delivery by in-skin electroporation using microneedle array. International journal of pharmaceutics, 397 (2010), 77-83.

[72] T.W. Wong, C.H. Chen, C.C. Huang, C.D. Lin, S.W. Hui, Painless electroporation with a new needle-free microelectrode array to enhance transdermal drug delivery, Journal of Controlled Release 110 (2006) 557 – 565.)

[73] U. Pliquett, R. Langer, J.C. Weaver. Changes in the passive electrical properties of human stratum corneum due to electroporation. Biochimica et Biophysica Acta 1239 (1995) 111-121

[74] T.R. Gowrishankar, T.O. Hernadon, T.E. Vaughan, J.C. Weaver, Spatially constrained localized transport regions due to skin electroporation, Journal of controlled release 60 (1999) 101-110.

[75] Fagerström, K.O. A comparison of psychological and pharmacological treatment in smoking cessation, Journal of behavioral medicine 5, 343-351 (1982).

[76] H.Liu, J. He, J. Tang, H. Liu, P. Pang, D. Cao, P. Krstic, S. Joseph, S. Lindsay, C. Nuckolls, Translocation of single-stranded DNA through single-walled carbon nanotubes, Science, vol 327, 64-67.

[77] J. Wu, K. Gerstandt, H. Zhang, J. Liu, B.J. Hinds, Electrophoretically induced aqueous flow through single-walled carbon nanotubes, Nature Nanotechnology, Vol 7, February, 133-139.

[78] Scruggs, N. R., Robertson, J.W. F., Kasianowicz, J. J. & Migler, K. B. Rectification of the ionic current through carbon nanotubes by electrostatic assembly of polyelectrolytes. Nano Lett. 9, 3853-3859 (2009).

[79] DJ Patel, AK Suri, F Jiang, L Jiang, P Fan, RA Kumar, S Nonin, Structure, recognition and adaptive binding in RNA aptamer complexes, J Mol Biol 1997, 272(5):645-664.

[80] T Mairal,V.C. Özalp,P.L. Sánchez,M. Mir,I Katakis,C. K. O'Sullivan, Aptamers: molecular tools for analytical applications, Analytical and Bioanalytical Chemistry, February 2008, Volume 390, Issue 4, pp 989-1007.

[81] SL Clark, VT Remcho, Aptamers as analytical reagents, Electrophoresis 23(9):1335-1340.

[82] E Luzi, M Minunni, S Tombelli, M Mascini, New trends in affinity sensing: aptamers for ligand binding, Trends Anal Chem, 2003, 22(11):810-818

[83] C. Tuerk and L. Gold, Systematic evolution of ligands by exponential enrichment: RNA ligands to bacteriophage T4 DNA polymerase, Science, 1990, 249, 505-510.

[84] A. D. Ellington and J. W. Szostak, In vitro selection of RNA molecules that bind specific ligands, Nature, 1990, 346, 818-822.

[85] V.C. Ozalp, M.B. Serrano-Santos, T. Shaefer, oligonucleic acids("aptamers") for designing stimuli-responsive membranes, Responsive Membranes and Materials, DOI: 10.1002/9781118389553.

[86] R.D. Jenison, S.C. Gill, A. Pardi, B. Polisky, High-resolution molecular discrimination by RNA, Science 11 March 1994: Vol. 263 no. 5152 pp. 1425-1429.

[87] B. K. Das, C. Tlili, S. Badhulika, L. N. Cella, W Chena, A. Mulchandani, Single-walled carbon nanotubes chemiresistor aptasensors for small molecules: picomolar level detection of adenosine triphosphate, Chem. Commun., 2011, 47, 3793–3795.

[88] DW Drolet, L Moon-McDermott, TS Romig, An enzyme-linked oligonucleotide assay. , Nat Biotechnol 1996 14(8):1021-1027.

[89] Min, K.; Jo, H.; Song, K.M.; Cho, M.; Chun, Y.S.; Jon, S.; Kim, W.J.; Ban, C. Dual-aptamer-based delivery vehicle of doxorubicin to both PSMA (+) and PSMA (−) prostate cancers, Biomaterial 2011, 32, 2124–2132.

[90] A. E. Abelow, O. Schepelina, R. J. White, A. Vallee-Belisle, K. W. Plaxco, I. Zharov, Chem. Commun. 2010, 46, 7984 – 7986.

[91] C. L. Zhu, C. H. Lu, X. Y. Song, H. H. Yang, X. R. Wang, J. Am. Chem. Soc. 2011, 133, 1278 –1281.

[92] V. C. Ozalp, T Schafer, Aptamer-Based Switchable Nanovalves for Stimuli-Responsive Drug Delivery, Chem. Eur. J. 2011, 17, 9893-9896.

[93] V.C. Özalp , A. Pinto , E. Nikulina , A.Chuvilin ,T. Schäfer, In Situ Monitoring of DNA-Aptavalve Gating Function on Mesoporous Silica Nanoparticles, Part. Part. Syst. Charact. 2014, 31, 161–167.

[94] D. E. Huizenga , J. W. Szostak , Biochemistry 1995 , 34 , 656.

[95] J Wu, X Zhan, B.J. Hinds, Ionic rectification by electrostatically actuated tethers on single walled carbon nanotube membranes, Chem. Commun., 2012, 48, 7979–7981.

[96] J.W. Hong, V. Studer, G. Hang, W.F. Anderson, S.R. Quake, A nano-liter nucleic acid processor with parallel architecture, Nature Biotechnology 22, 435 - 439 (2004).

[97] R. Qiao and N. R. Aluru, Atypical Dependence of Electroosmotic Transport on Surface Charge in a Single-wall Carbon Nanotube, Nano Letters, 2003, 3 (8), pp 1013–1017.

[98] A Manz, C S Effenhauser, N Burggraf, D J Harrison, K Seiler and K Fluri, Electroosmotic pumping and electrophoretic separations for miniaturized chemical analysis systems, 1994 J. Micromech. Microeng. 4 257.

[99] C.R. Buie, J.D. Posner, T. Fabian, S.W. Cha, D. Kim, F.B. Prinz, J.K. Eaton, J.G. Santiago, Water management in proton exchange membrane fuel cells using integrated electroosmotic pumping, Journal of Power Sources 161 (2006) 191–202.

[100] J. Miao, Z. Xu, Xinyi Zhang, N. Wang, Z. Yang, P. Sheng, Micropumps Based on the Enhanced Electroosmotic Effect of Aluminum Oxide Membranes, Adv. Mater. 2007, 19, 4234 – 4237.

[101] S.A. Miller, C.R. Martin, Controlling the rate and direction of electroosmotic flow in template-prepared carbon nanotube membranes, Journal of Electroanalytical Chemistry 522 (2002) 66–69.

Vita

Author's name – Tao Chen

Birth place – Changsha, Hunan, China

Education

Bachelor of Science in Materials Physics
Tianjin University of Technology
June 2011

Research Experience

University of Kentucky
Lexington, KY
August 2011- Present
Graduate Research Assistant

Tianjin University of Technology
Tianjin
May 2009-June 2011
Undergraduate Research Assistant

Peer Reviewed Publications

Zhiqiang Chen, **Tao Chen**, Xinghua Sun, Bruce Hinds, Dynamic Electrochemical Membranes for Continuous Affinity Protein Separation, Advanced Functional Materials, Volume 24, Issue 27, pages 4317-4323, July 16, 2014.

Juan Wang, Hongfu Luo, **Tao Chen**, and Zhihao Yuan, A facile shape-selective growth of ZnO nanotips and graded nanowires from its oriented nanorods in a saturated ZnS Solution, Nanotechnology, Volume 21 (2010) 505603.

Society Memberships

- The Electrochemical Society (ECS), ECS University of Kentucky Chapter
- Materials Research Society